FINAL TECHNICAL REPORT

PREPARED FOR

THE NATIONAL SCIENCE FOUNDATION
EARTHQUAKE HAZARD AND MITIGATION PROGRAM

RESEARCH INITIATION GRANT
NSF CONTRACT NO. PFR-7823098

NONLINEAR VISCOELASTIC BEHAVIOR OF A COHESIVE SOIL
UNDER UNIAXIAL LOADING CONDITIONS

BY

SAEED RAFIE AND M.G. SHARMA

THE PENNSYLVANIA STATE UNIVERSITY
UNIVERSITY PARK, PENNSYLVANIA   16802

SEPTEMBER 1980

EAS INFORMATION RESOURCES
NATIONAL SCIENCE FOUNDATION

ABSTRACT

The nonlinear viscoelastic behavior of a cohesive soil under uniaxial loading conditions has been studied. A constitutive relationship based upon a multiple integral representation has been developed. The time dependent parameters of this relation (kernel functions) have been determined, performing uniaxial single-step creep tests on a specially developed test apparatus. The constitutive relationship has been generalized for multi-step loading, as well as dynamic sinusoidal loading conditions. It has been shown that the behavior of the material for multi-step loading conditions can be predicted by the results of the single-step tests. In addition, the behavior of the soil under uniaxial compressive cyclic loading has also been studied, using an apparatus specially developed for the purpose. The energy dissipation in a given cycle of loading has been evaluated. The effect of frequency on the energy loss has been studied.

TABLE OF CONTENTS

LIST OF TABLES

LIST OF FIGURES

LIST OF SYMBOLS

Symbol

$D(t,\sigma)$	Creep compliance
$D_i(t_1,t_2,\ldots,t_i)$	i^{th} order kernel function
$\hat{D}_i(\omega,\omega,\ldots)$	i^{th} order Fourier cosine integral
$D_i(\omega,\omega,\ldots)$	i^{th} order Fourier sine integral
F	Function
$H(t)$	Heaviside step function
N, K_i, λ_i	Constants
t	Time
t_i	Time interval for application of ith step
σ_i	Uniaxial stress magnitude for i^{th} step loading
σ_o	Maximum dynamic stress amplitude
$\varepsilon(t)$	Uniaxial strain magnitude
ε_{oo}	Instantaneous time independent strain
ε_{oi}	Overall instantaneous time independent strain for i step loading
ω	Frequency (Hz)
W_ω	Weight of water
W_S	Weight of dry soil
$\overset{o}{\omega}/_o$	Water content

CHAPTER I

INTRODUCTION

1.1 General Remarks

The design and analysis of soil-structure systems subjected to vibratory and impulsive forces have attracted considerable attention in recent years. It is known that ground motions due to the transient forces impose severe inertia forces on structures. These inertia forces may influence the load bearing capacity of the soil underneath the structures. This mutual influence between the structure and soil is usually known as the soil-structure interaction. The study of this problem requires a knowledge of dynamic soil properties. Designers are concerned with the soil behavior under dynamic loading conditions, but there has been no attempt to develop a rational and analytical method to represent the behavior of this material.

The soil-structure interaction has been studied by numerous investigators. To date most of the soil-interaction work has been done assuming the soil mass underneath a foundation as elastic (1,2). This assumption has been used in three different methods to represent the behavior of a soil mass:

    (1) Elastic half-space theory;

    (2) Lumped parametric representation; and

    (3) Finite elements analysis.

Although in recent years some attempts have been made to analyze the stresses and strains in the soil mass assuming the material as linear viscoelastic (3), very little work has been done to determine the realistic properties of this material.

Generally soils are rheological in nature. They display time-

dependent creep behavior under steady loading conditions. A study on creep and relaxation behavior (4) shows, soils behave as a nonlinear viscoelastic material. Recently, much attention has been given to represent the behavior of a nonlinear viscoelastic material by using the multiple integral theory. According to this theory, the nonlinear viscoelastic behavior of a material is specified in the form of a series of kernel functions which are assumed to be symmetric. These kernel functions that are time dependent only have to be determined from a series of tests involving step loading. It is generally known that a large number of tests are necessary to determine the kernel functions (5).

In this thesis, multiple integral representation theory has been used for characterizing the nonlinear viscoeleastic behavior of a cohesive soil. The work describes a comprehensive experimental program for determination of kernel functions. It is shown that if certain symmetry properties are assumed, the kernel functions can be determined from relatively few tests.

1.2 Statement of the Problem

Although rheological behavior of soils has been studied extensively for the last three decades, much of the literature deals with the development of laboratory techniques for studying the behavior under creep, stress relaxation, and dynamic sinusoidal loading conditions. Very few attempts have been made to analyze the data from rational mechanistic principles. Even those investigators (6,7,8,9,10), who have attempted to describe the behavior of soils from mechanistic principles, have assumed the cohesive soils as

(1) Elastic;

(2) Elastic-plastic; and

(3) Linear viscoelastic.

It is well-known that soils display appreciable nonlinear stress-time dependent behavior (5). There is a great need for the development of constitutive relations that reflect these properties of soils.

The thesis describes an experimental program, as well as the theoretical development for the one-dimensional constitutive relationship that represents the nonlinear viscoelastic behavior of a cohesive soil. The constitutive relationship has been developed from creep tests. The generality of the developed constitutive relationship is verified by predicting the behavior of the material under other stress histories. The predicted values have been correlated with the observed values for the same stress histories.

1.3 Objectives

The objectives of this investigation are as follows:

(1) To study the creep behavior of a cohesive soil under various uniaxial compressive loadings at a given moisture content and to develop a one-dimensional constitutive relation that reflects the viscoelastic and nonlinear effects.

(2) To study the rheological behavior of the cohesive soil under other stress histories such as the multi-step and sinusoidal stress histories.

(3) To correlate the observed behavior of the material for stress histories that are studied under item (2) with the predicted behavior based upon the developed constitutive relationship.

1.4 Scope and Limitation of the Thesis

The work reported in this thesis is primarily concerned with the experimental investigation for the creep and dynamic mechanical behavior of unconfined cylindrical specimens of a cohesive soil subjected to uniaxial stresses varying from 5 to 38 psi. The deformation was measured for a short time interval (500 seconds). Creep tests have also been conducted for other stress histories such as two-and three-step histories. Two-step loading tests were performed for three stress levels, whereas, three-step loading tests were performed for only one stress level. Also tests under sinusoidal loading for a frequency range from 9 to 22 Hz were conducted as part of this study. The particular soil used in this investigation is a remolded soil from the test track area of the Pennsylvania Transportation Facility. The soil specimens were tested at room temperature (75°F), and for a moisture content of 18.9% water under a constant compaction effort.

The background for the proposed investigation including the related literature has been presented at the end of this Chapter. Chapter II describes a review of the nonlinear theory of viscoelasticity leading to a one-dimensional constitutive relationship for characterizing the stress-strain-time behavior of a given rheological material. The one-dimensional constitutive relationship for dynamic sinusoidal loading is also discussed in this Chapter. The details on soil specimen preparation, test apparatus, and experimental procedures are given in Chapter III. In Chapter IV, the experimental results and complete determination of the stress-strain-time behavior of a cohesive soil are presented. The application of this relation is discussed for two- and three-step loading conditions. The correlation of the creep test results, with the dynamic

sinusoidal test results,is also given in this Chapter. Summary and conclusions are given in Chapter V.

1.5 Literature Survey

Soils can be considered as one of the oldest and the most complex materials of construction. It is generally understood that the stability and durability of a structure will largely depend upon the behavior of the soil upon which it is built.

Mechanical behavior of soils primarily has been studied by considering soil as an elastic or elastic-plastic material. Among the investigators, Wilson and Dietrich (6) have studied the elastic strain response of a cohesive soil by performing incremental and repeated loading tests. Elastic-plastic behavior of soil was studied by Mitchell and McConnell (7). They discussed a possible approach for separation of elastic and plastic deformation by performing the creep-recovery tests. They found the elastic deformation is nonlinear with respect to the stress level.

In early 1960, several investigators (8,9,10) have studied the time-dependent behavior, by conducting creep and stress relaxation tests. Their results show soils are rheological in nature, and their mechanical response depends on both the loading path, as well as the history of loading. Murayama and Shibata (8) by assuming a rheological model for clays, derived a relationship for strain response of the material with respect to stress and time. Vialov and Skibitsky (9,10) have studied the rheological properties of soil by considering a Kelvin model. The viscous element in this model was replaced by an elasto-plastic viscous element. The results show that the model is suitable for describing the stress relaxation of dense clay. Folque (11) and Barden (12)

performed creep and relaxation tests. The results from these tests were represented by models consisting of linear springs and dash-pots. Comparison of the results from experimental data and differential laws based on the model indicate the existance of nonlinear effects in cohesive soils. Drescher (4), has done a comprehensive work for characterization of soil behavior. On the basis of experimental results under various loading programs, he found that the response of soil under creep loading for a short duration is markedly nonlinear. He also observed that the nonlinearity of soil increases with the value of applied stress and time.

During the last decade, some attempts have been made to analyze stresses and strains in the soil mass assuming the material as linear viscoelastic. In most of these investigations, the principle of superposition proposed by Boltzmann was the basis for describing the linear viscoelastic behavior of soils. Kondner and Krizek (13), presented a creep compliance function for the creep response of a cohesive soil under uniaxial compression. They obtained an explicit form for the creep compliance, that included the nonlinear effects of the material. Veletros and Verbic (3), studied the effects of soil damping on steady-state response of harmonically excited foundation. They represented the dynamic viscoelastic behavior of a soil by two models that consisted of a standard Voigt model in series with a constant hysteretic element. Kondner (14), studied a soil-structure system subjected to a vertical sinusoidal loading. His experimental results indicate that the soil-foundation system behaves nonlinearly. Kondner (15), and Krizek (16), by performing creep and dynamic sinusoidal loading tests represented the time and rate effects on the

stress-strain response of a cohesive soil in terms of a compliance-time function. Their experimental data showed that the stress-strain time response from the creep and dynamic sinusoidal loading is definitely nonlinear. The nonlinearity was handled by reducing the response to a constant level which can be approximated by linear theory of viscoelasticity. Kondner (15) also found that the experimental results from blast pulse loading correlate quite well with those obtained from dynamic steady-state loading tests.

The energy storage and energy dissipation characteristics of soils have been specially considered in the design and analysis of soil-structure systems subjected to transient loadings such as earthquake phenomena. There has been a considerable effort to characterize the dynamic behavior of soils. Krizek (17) suggested the use of one-sided Fourier transform techniques to transform the results from the time-dependent creep tests for a remolded clay into the frequency domain. He obtained approximate expressions for the storage and loss compliance functions. The use of this technique was limited for a linear viscoelastic material. The energy storage and energy dissipation characteristic of a cohesive soil was studied experimentally by Kondner and Ho (18) and Kondner and Krizek (19). They performed strain-controlled vibratory uniaxial compression tests, and obtained the response of the material in terms of conventional viscoelastic parameters such as storage modulus, loss modulus, and the loss tangent. Dynamic stress-strain response showed that nonlinearity existed even at very small values of dynamic strain. Their experimental results indicate that the phase angles between sinusoidally applied strains and the resulting stresses are small (a few degrees). Also they found for

the linear range, the applied stress level has little effect on the dynamic response. The results of the dynamic testing show that storage loss, and loss tangent decrease with dynamic strain amplitude. Krizek and Franklin (20), studied the energy dissipation characteristics of soft kaolin clay. They obtained the hysteresis loops produced by subjecting a clay specimen to a harmonically varying torsional shear strain. The energy losses were determined by using the phase angle between the stress and strain combination with linear theory of viscoelasticity. The results show that the energy losses are slightly higher than those measured from the hysteresis loops. The difference can be attributed to the nonlinearity of the soils behavior. They also found that the energy dissipation is relatively independent of frequency for frequencies ranging from .1 to 30 cps.

In order to study the dynamic stress-strain response of a cohesive soil for short time (0.2 m sec.), Kondner and Forrest (21), performed compression tests for duration of approximately 3.0 m sec., by explosion of a rifle cartridge. The stress-strain response of soil under a short time impulsive loading was found to be nonlinear. They represented the nonlinear stress-strain effect in terms of a two-constant hyperbolic relationship. The volumetric stress-strain behavior of soils was investigated by Klausner (22). He showed that the mechanical analogy of volumetric behavior can be represented either by Kelvin elements coupled in series, or by Maxwell elements coupled in parallel. The results show that linear viscoelasticity is not suitable to represent a volumetric constitutive relationship.

A more comprehensive experimental study on soils has been reported by Drnevich (23), and Drnevich, Hardin, and Shippy (24). They

used the resonant-column method to obtain modules and damping of solid cylindrical soil specimens. In their method, shear or compressional waves were propagated by applying a sinusoidal torque, or a sinusoidal axial compression to the specimens. The frequency of the applied torque or force was adjusted until resonance occurred. The resonant frequency plus the magnitude of the applied torque or force and the magnitude of the resulting motions have been used to calculate the modulus, damping, and strain amplitude.

CHAPTER II

THEORETICAL CONSIDERATION

2.1 Introduction

In order to obtain a general constitutive relationship for a cohesive soil under uniaxial loading conditions, a nonlinear theory of viscoelasticity based upon the multiple integral representation is discussed. The nonlinear representation has been determined by using the experimental data from the uniaxial creep tests on the cohesive soil specimens. As the experimental results (see Chapter IV) indicated nonlinear response, attempts have been made to model this behavior in terms of a nonlinear theory of viscoelasticity. For a linear viscoelastic material, the creep compliance, which is defined as the strain per unit of applied stress, is independent of the stress level and is a function of time only, whereas, for a nonlinear viscoelastic material, the creep compliance is dependent upon the stress level, as well as the time of loading.

The nonlinear theory of viscoelasticity has other features in common with the linear theory, which is the memory hypothesis. This hypothesis, in terms of a stress-strain relationship, simply means that the current value of strain is determined not only by the current value of stress, but also by the complete past history of stress.

In the following, a general one dimensional constitutive relationship for a nonlinear viscoelastic material under uniaxial loading condition has been given. A multiple integral functional relationship has been employed to obtain the constitutive relationship. Application of this relationship for different loading

histories consisting of one, two, and three steps loading has also

been discussed. Finally, expressions for the sinusoidal behavior

of a nonlinear viscoelastic material in terms of dynamic kernel

functions are obtained, using the kernel functions from creep loading.

2.2 One Dimensional Constitutive Relationship

The most general uniaxial constitutive relationship for a

nonlinear viscoelastic material may be expressed as:

$$\varepsilon(t) = F \left[\frac{d\sigma(t')}{dt'} \right]_{t' = -\infty}^{t} \tag{1}$$

According to equation (1), the strain depends upon the entire past

history of stress. When the function F is linear, equation (1) re-

presents the Boltzmann superposition integral that is, the basis

of the linear theory of viscoelasticity:

$$\varepsilon(t) = \int_{-\infty}^{t} D(t-t') \frac{d\sigma(t')}{dt'} dt' \tag{2}$$

where D(t) is the creep compliance function that is a function of

time only.

By assuming the nonlinearity and continuity of the functional

F in equation (1), and utilizing a Fréchet series, Green, Rivlin,

and Spencer (25,26,27), have shown that the functional can be re-

presented by an infinite series of multiple integrals as follows:

$$\varepsilon(t) = \int_{-\infty}^{t} D_1(t-t_1) \frac{d\sigma(t_1)}{dt_1} dt_1 + \int_{-\infty}^{t}\int_{-\infty}^{t} D_2 (t-t_1,t-t_2) \frac{d\sigma(t_1)}{dt_1}$$

$$\frac{d\sigma(t_2)}{dt_2} \ dt_1 dt_2 + \int_{-\infty}^{t}\int_{-\infty}^{t}\int_{-\infty}^{t} D_3 \ (t-t_1, t-t_2, t-t_3) \ \frac{d\sigma(t_1)}{dt_1}$$

$$\frac{d\sigma(t_2)}{dt_2} \cdot \frac{d\sigma(t_3)}{dt_3} \ dt_1 dt_2 dt_3 + \dots \tag{3}$$

where $D_1(t)$, $D_2(t,t)$, $D_3(t,t,t)$, ... are Kernel functions which are symmetric with respect to their arguments. These kernel functions are completely determined when their values are known for the following situations:

$$D_1(t) \qquad\qquad t \geq 0$$

$$D_2(t_1, t_2) \qquad\quad t_1 \geq t_2 \geq 0 \tag{4}$$

$$D_3(t_1, t_2, t_3) \qquad t_1 \geq t_2 \geq t_3 \geq 0$$

The first order kernel function $D_1(t)$ is described in terms of a single time parameter t and may be illustrated by a plane curve as shown in Figure 1, whereas the determination of the nonlinear kernel fucntions such as $D_2(t,t)$ and $D_3(t,t,t)$ require more than one time parameter. The second order Kernel function $D_2(t,t-t_1)$ may be illustrated by a surface P as shown in Figure 2.

The type of input stresses $\sigma(t)$ that may be used to determine the kernel functions is arbitrary. The form of the equation (3) is particularly suited to step loading inputs, for example, for single step creep loading:

$$\sigma(t) = \sigma H(t) \tag{5}$$
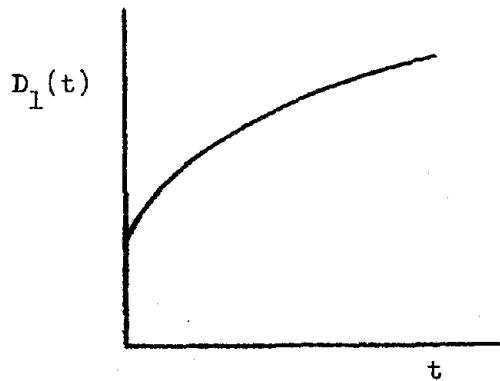
Figure 1. First Order Kernel Function vs. time
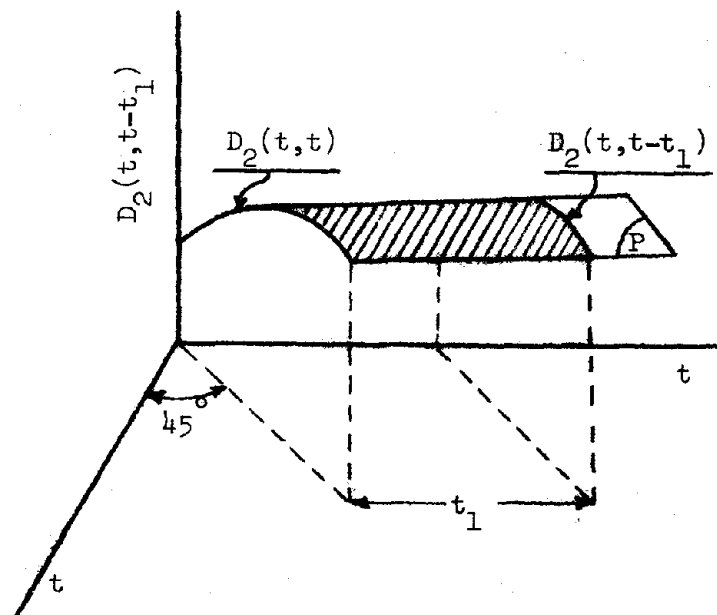
Figure 2. Second Order Kernel Function vs. t,t

where $H(t)$ represents the Heaviside step function. Subsituting equation (5) in equation (3), it can be shown:

$$\varepsilon(t) = \sigma D_1(t) + \sigma^2 D_2(t,t) + \sigma^3 D_3(t,t,t) + \ldots \qquad (6)$$

or

$$D(t,\sigma) = \frac{\varepsilon(t)}{\sigma} = D_1(t) + \sigma D_2(t,t) + \sigma^2 D_3(t,t,t) + \ldots \qquad (7)$$

where $D(t,\sigma)$ is the creep compliance function which for a nonlinear viscoelastic material is both stress and time dependent.

A number of investigators have proposed methods for the experimental determination of the kernel functions. In most of these investigations, the representation corresponding to equation (1), has been terminated after a finite number of terms and then the tacit assumption is made that this finite-order expansion represents the system exactly.

The representation of the uniaxial nonlinear constitutive relation can be extended to a multi-axial stress state by considering all the possible combinations of stress tensors and stress invariants, which is beyond the scope of this thesis.

2.3 Uniaxial Multi-Step Loading

2.3.1 Two-Step Loading

In order to develop the constitutive relationship for two-step loading history, the load levels during the two steps will be given arbitrary values. In most of the existing experimental data have been obtained from the cases where the load is doubled or removed in the second step (recovery). The two-step stress history

as shown in Figure 3 can be formulated as followings:

$$\sigma(t) = 0 \qquad t < 0$$

$$\sigma(t) = \sigma_1 \qquad 0 \le t < t_1 \qquad (8)$$

$$\sigma(t) = \sigma_1 + \sigma_2 \qquad t \ge t_1$$

An examination of the experimental data indicates that three terms in the infinite series integral equation (equation (3)), are sufficient to describe the creep behavior of the test material.

$$\varepsilon(t) = \int_o^t D_1(t-t_1) \frac{d\sigma(t_1)}{dt_1} dt_1 + \int_o^t \int_o^t D_2(t-t_1, t-t_2) \frac{d\sigma(t_1)}{dt_1} \cdot$$

$$\frac{d\sigma(t_2)}{dt_2} dt_1 dt_2 + \int_o^t \int_o^t \int_o^t D_3(t-t_1, t-t_2, t-t_3) \frac{d\sigma(t_1)}{dt_1} \cdot \frac{d\sigma(t_2)}{dt_2} \cdot$$

$$\frac{d\sigma(t_3)}{dt_3} dt_1 \cdot dt_2 \cdot dt_3 \qquad (9)$$

By substituting equation (8) in (9), the single integral for two-step loading can be shown as following:

$$\int_o^t D_1(t-t_1) \frac{d\sigma(t_1)}{dt_1} dt_1 = D_1(t)\sigma_1 + D_1(t-t_1)\sigma_2 \qquad (10)$$

The double and triple integrals of equation (9) can be evaluated as follows:

$$\int_o^t \int_o^t D_2(t-t_1, t-t_2) \frac{d\sigma(t_1)}{dt_1} \frac{d\sigma(t_2)}{dt_2} dt_1 dt_2 = \sigma_1[D_2(t,t)\sigma_1 +$$
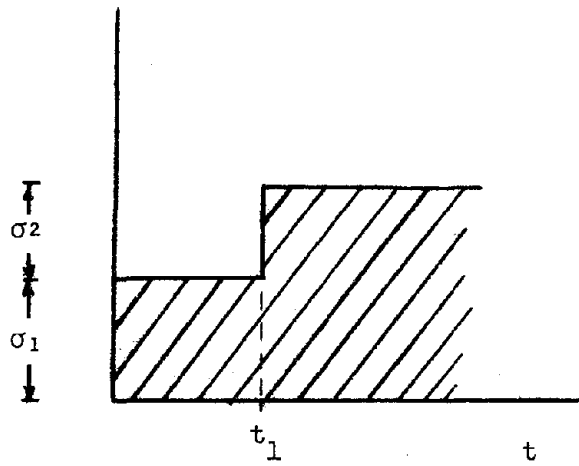
Figure 3. Two-Step Stress History
vs. Time
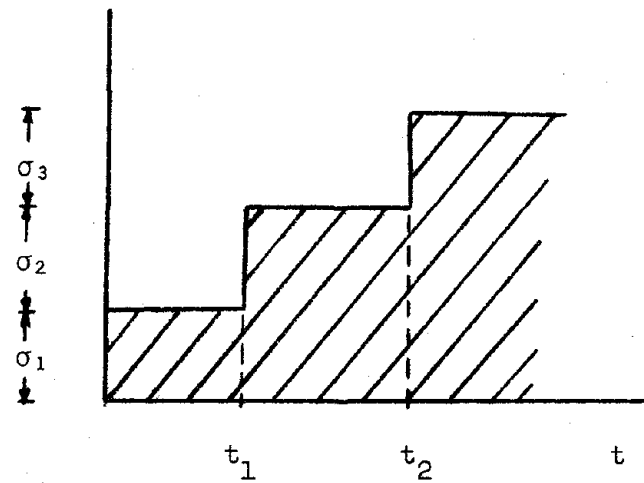
Figure 4. Three-Step History
vs. Time

$$+ D_2(t,t-t_1)\sigma_2] + \sigma_2[D_2(t-t_1,t)\sigma_1 + D_2(t-t_1,t-t_1)\sigma_2] =$$

$$= D_2(t,t)\sigma_1^2 + D_2(t-t_1,t-t_1)\sigma_2^2 + 2\sigma_1\sigma_2 D_2(t,t-t_1) \tag{11}$$

and

$$\int_o^t \int_o^t \int_o^t D_3(t-t_1,t-t_2,t-t_3) \; \frac{d\sigma(t_1)}{dt_1} \cdot \frac{d\sigma(t_2)}{dt_2} \cdot \frac{d\sigma(t_3)}{dt_3} \; dt_1 dt_2 dt_3 =$$

$$= \sigma_1[D_3(t,t,t)\sigma_1^2 + D_3(t,t-t_1,t-t_1)\sigma_2^2 + 2\sigma_1\sigma_2 D_3(t,t,t-t_1)]$$

$$+ \sigma_2[D_3(t-t_1,t,t)\sigma_1^2 + D_3(t-t_1,t-t_1,t-t_1)\sigma_2^2 + 2\sigma_1\sigma_2 D_3(t-t_1,t,t-t_1) =$$

$$= D_3(t,t,t)\sigma_1^3 + D_3(t-t_1,t-t_1,t-t_1)\sigma_2^3 + 3\sigma_1\sigma_2[\sigma_1 D_3(t,t,t-t_1) +$$

$$+ \sigma_2 D_3(t,t-t_1,t-t_1)] \tag{12}$$

Therefore, the creep response for two-step loading history can be expressed by the following equation:

$$\varepsilon(t,t_1,\sigma_1,\sigma_2) = D_1(t)\sigma_1 + D_1(t-t_1)\sigma_2 + D_2(t,t)\sigma_1^2 + D_2(t-t_1,t-t_1)$$

$$\sigma_2^2 + 2\sigma_1\sigma_2 D_2(t,t-t_1) + D_3(t,t,t)\sigma_1^3 + D_3(t-t_1,t-t_1,t-t_1)\sigma_2^3 +$$

$$3\sigma_1\sigma_2[\sigma_1 D_3(t,t,t-t_1) + \sigma_2 D_3(t,t-t_1,t-t_1)] \tag{13}$$

2.3.2 Three-Step Loading

Three-step loading history as shown in Figure 4, can be formulated as followings:

$$\sigma(t) = 0 \qquad t<0$$

$$\sigma(t) = \sigma_1 \qquad 0 \leq t < t_1$$

$$\sigma(t) = \sigma_1 + \sigma_2 \qquad t_1 \le t < t_2$$

$$\sigma(t) = \sigma_1 + \sigma_2 + \sigma_3 \qquad t_2 \le t \le t_3 \qquad (14)$$

By expanding the results from the two-step loading history, the strain response under a three-step loading can be expressed as following:

$$\varepsilon(t, t_1, t_2, \sigma_1, \sigma_2, \sigma_3) = D_1(t)\sigma_1 + D_1(t-t_1)\sigma_2 + D_1(t-t_2)\sigma_3 +$$

$$+ \sigma_1^2 D_2(t,t) + \sigma_2^2 D_2(t-t_1, t-t_1) + \sigma_3^2 D_2(t-t_2, t-t_1) + 2[\sigma, \sigma_2 D_2$$

$$(t, t-t_1) + \sigma_1 \sigma_3 D_2(t, t-t_2) + \sigma_2 \sigma_3 D_2(t-t_1, t-t_2)] + \sigma_1^3 D_3(t,t,t) +$$

$$+ \sigma_2^3 D_3(t-t_1, t-t_1, t-t_1) + \sigma_3^3 D_3(t-t_2, t-t_2, t-t_2) + 3[\sigma_1^2 \sigma_2 D_3$$

$$(t, t, t-t_1) + \sigma_1^2 \sigma_3 D_3(t, t, t-t_2) + \sigma_1 \sigma_2^2 D_3(t, t-t_1, t-t_2) + \sigma_1 \sigma_3^2 D_3$$

$$(t, t-t_2, t-t_2) + \sigma_2^2 \sigma_3 D_3(t-t_1, t-t_1, t-t_2) + \sigma_2 \sigma_3^2 D_3(t-t_1, t-t_2, t-t_2)] +$$

$$+ 6\sigma_1 \sigma_2 \sigma_3 D_3(t, t-t_1, t-t_2) \qquad (15)$$

2.4 Determination of Kernel Functions

Equations (6), (13), and (15) indicate that a large number of tests are required to determine the kernel functions completely. Several methods for determination of kernel functions based upon results from multi-step history loading have been suggested in recent years (5,28). In this thesis, a method has been developed for the determination of kernel functions from creep tests.

2.4.1 Multiple-Step Creep Tests

The first order kernel function, $D_1(t)$ can be determined experimentally by performing single-step creep tests at several stress

levels. The experimental data from these creep tests can provide three equations for determining $D_1(t)$, $D_2(t,t)$, and $D_3(t,t,t)$. From the creep tests, the second and third order kernel functions can be only known for the same arguments.

To obtain a complete determination of the second order kernel functions, it is necessary to perform several combinations of different time and stress levels of two-step loading tests. The two-step stress history can be formulated as follows:

$$\sigma(t) = \sigma_1 H(t) + \sigma_2 H(t-t_1) \tag{16}$$

The experimental results from three different loading conditions as represented by equation (16) can be used to determine $D_2(t,t-t_1)$, $D_3(t,t,t-t_1)$, and $D_3(t,t-t_1,t-t_1)$.

To obtain the third order kernel functions with different values of arguments, it is necessary to perform several three-step loading tests as follows:

$$\sigma(t) = \sigma_1 H(t) + \sigma_2 H(t-t_1) + \sigma_3 H(t,t-t_1,t-t_2) \tag{17}$$

The total number of experimental tests required for complete determination of kernels are presented in Table 1 on the following page. The number N is related to the number of spatial lines on which the second and third order kernel functions must be known in order to satisfactorily specify these functions.

Table 1. Experimental Tests Required for Complete Determination of Kernel Functions(5)

loading program	number of tests
$\sigma(t) = \sigma_1 H(t)$	1
$\sigma(t) = \sigma_2 H(t)$	1
$\sigma(t) = \sigma_3 H(t)$	1
$\sigma(t) = \sigma_4 H(t) + \sigma_5 H(t-t_1)$	N
$\sigma(t) = \sigma_4 H(t) + \sigma_6 H(t-t_1)$	N
$\sigma(t) = \sigma_7 H(t) + \sigma_5 H(t-t_1)$	N
$\sigma(t) = \sigma_8 H(t) + \sigma_9 H(t-t_1) + \sigma_{10} H(t-t_2)$	$1/2 \ N^2$
Total number of tests	$1/2 \ N^2 + 3N + 3$

2.4.2 Exponential Representation of Kernel Functions

A general and simple approximation method for determining the kernel functions, has been suggested by Nakada (29). He derived a general constitutive relationship for a nonlinear viscoelastic material by considering three assumptions of causality, convergence, and stationariness.

$$\varepsilon(t) = \int_{-\infty}^{+\infty} D_1(t_1) \frac{d\sigma(t-t_1)}{dt_1} \ dt_1 + \int_{-\infty}^{+\infty}\int_{-\infty}^{+\infty} D_2(t_1,t_2) \frac{d\sigma(t-t_1)}{dt_1}$$

$$\frac{d\sigma(t-t_2)}{dt_2} \ dt_1 dt_2 + \int_{-\infty}^{+\infty}\int_{-\infty}^{+\infty}\int_{-\infty}^{+\infty} D_3(t_1,t_2,t_3) \frac{d\sigma(t-t_1)}{dt_1} \ \frac{d\sigma(t-t_2)}{dt_2}$$

$$\frac{d\ (t-t_3)}{dt_3}\ dt_1 dt_2 dt_3 + \ldots \tag{18}$$

A most simple and convenient approximation for kernel functions, for single-step excitation, can be expressed by exponential functions as follows:

$$D_1(t) = K_1 \lambda_1 (1-e^{-t/\lambda_1})$$

$$D_2(t,t) = K_2 \lambda_2^2 (1-e^{-t/\lambda_2})^2$$

$$D_3(t,t,t) = K_3 \lambda_3^3 (1-e^{-t/\lambda_3})^3 \tag{19}$$

In order to determine the three kernel functions, the experimental data should be fitted to equations (19), or any other exponential functions that fit the test results well.

2.5 Dynamic Behavior of a Nonlinear Viscoelastic Material

A uniaxial constitutive relationship that describes the dynamic mechanical behavior of a nonlinear viscoelastic material can be obtained extending the multiple integral representation (equation 3). Assuming the dynamic excitation as follows:

$$\sigma(t) = \sigma_o \cos \omega t \tag{20}$$

Substituting equation(20)in equation(9), we have

$$\varepsilon(t) = \int_{-\infty}^{t} D_1(t-t_1)(-\sigma_o \omega \sin \omega t_1)dt_1 + \int_{-\infty}^{t}\int_{-\infty}^{t} D_2(t-t_1,t-t_2)$$

$$(-\sigma_o \omega \sin \omega t_1)(-\sigma_o \omega \sin \omega t_2) \, dt_1 dt_2 + \int_{-\infty}^{t} \int_{-\infty}^{t} \int_{-\infty}^{t} D_3(t-t_1,$$

$$t-t_2, t-t_3)(-\sigma_o \omega \sin \omega t_1)(-\sigma_o \omega \sin \omega t_2)(-\sigma_o \omega \sin \omega t_3)$$

$$dt_1 dt_2 dt_3 \tag{21}$$

Assuming $t-t_i = \theta_i$, the above equation leads to:

$$\varepsilon(t) = \sigma_o \omega [D''_1(\omega_1) \cos \omega t - D'_1(\omega_1) \sin \omega t] - 1/2 \, \sigma_o^2 \, \omega^2$$

$$[D'_2(\omega_1, \omega_2) \cos 2 \omega t + D''_2(\omega_1, \omega_2) \sin 2 \omega t - D'_2(\omega_1, -\omega)] +$$

$$+ 1/4 \, \sigma_o^3 \, \omega^3 [D'_3(\omega_1, \omega_2, \omega_3) \sin 3 \omega t - D''_3(\omega_1, \omega_2, \omega_3) \cos 3 \omega t$$

$$- D'_3(\omega_1, \omega_2, -\omega_3) \sin \omega t - D''_3(\omega_1, \omega_2, -\omega_3) \cos \omega t - 2 \sin \omega t$$

$$\int_o^\infty \int_o^\infty \int_o^\infty D_3(\theta_1, \theta_2, \theta_3) \cos \omega (\theta_1 - \theta_2) \cos \omega \, \theta_3 d\theta_1 d\theta_2 d\theta_3 + 2 \cos \omega t$$

$$\int_o^\infty \int_o^\infty \int_o^\infty D_3(\theta_1, \theta_2, \theta_3) \cos \omega (\theta_1 - \theta_2) \sin \omega \, \theta_3 \, d\theta_1 d\theta_2 d\theta_3] \tag{22}$$

where

$$D'_1(\omega_1) = \int_o^\infty D_1(\theta_1) \cos \omega \, \theta_1 d\theta_1$$

$$D''_1(\omega_1) = \int_o^\infty D_1(\theta_1) \sin \omega \, \theta_1 d\theta_1$$

$$D'_2(\omega_1, \omega_2) = \int_o^\infty \int_o^\infty D_2(\theta_1, \theta_2) \cos \omega (\theta_1 + \theta_2) d\theta_1 d\theta_2$$

$$D''_2(\omega_1,\omega_2) = \int_0^\infty \int_0^\infty D_2(\theta_1,\theta_2) \, \sin \omega(\theta_1+\theta_2) d\theta_1 d\theta_2$$

$$D'_2(\omega_1,-\omega_2) = \int_0^\infty \int_0^\infty D_2(\theta_1,\theta_2) \, \cos \omega(\theta_1-\theta_2) d\theta_1 d\theta_2$$

$$D'_3(\omega_1,\omega_2,\omega_3) = \int_0^\infty \int_0^\infty \int_0^\infty D_3(\theta_1,\theta_2,\theta_3) \, \cos \omega(\theta_1+\theta_2+\theta_3) d\theta_1 d\theta_2 d\theta_3$$

$$D''_3(\omega_1,\omega_2,\omega_3) = \int_0^\infty \int_0^\infty \int_0^\infty D_3(\theta_1,\theta_2,\theta_3) \, \sin \omega(\theta_1+\theta_2+\theta_3) d\theta_1 d\theta_2 d\theta_3$$

$$D'_3(\omega_1,\omega_2,-\omega_3) = \int_0^\infty \int_0^\infty \int_0^\infty D_3(\theta_1,\theta_2,\theta_3) \, \cos \omega(\theta_1+\theta_2+\theta_3) d\theta_1 d\theta_2 d\theta_3$$

$$D''_3(\omega_1,\omega_2,-\omega_3) = \int_0^\infty \int_0^\infty \int_0^\infty D_3(\theta_1,\theta_2,\theta_3) \, \sin \omega(\theta_1+\theta_2+\theta_3) d\theta_1 d\theta_2 d\theta_3 \quad (23)$$

The dynamic constitutive relationship can be obtained by substituting equation (23) in equation (22), and assuming $\omega_1=\omega_2=\omega_3=\omega$.

$$\varepsilon(t) = \sigma_0 \omega[D''_1(\omega) \cos \omega t - D'_1(\omega) \sin \omega t] - 1/2 \, \sigma_0^2 \, \omega^2$$

$$[D'_2(\omega,\omega) \cos 2 \omega t + D''_2(\omega,\omega) \sin 2 \omega t - D'_2(\omega,-\omega)] - 1/4 \, \sigma_0^3 \, \omega^3$$

$$[D'_3(\omega,\omega;\omega) \sin 3 \omega t - D''_3(\omega,\omega,\omega) \cos 3 \omega t - 3D'_3(\omega,\omega,-\omega) \sin \omega t$$

$$- 3D''_3(\omega,\omega,-\omega) \cos \omega t] \quad (24)$$

CHAPTER III

EXPERIMENTAL ARRANGEMENT AND PROCEDURES

3.1 Testing Apparatus

3.1.1 Single and Multi-Step Test Apparatus

The uniaxial creep tests were conducted by using a specially developed apparatus. A schematic diagram of the experimental set up is shown in Figure 5. The soil specimens were subjected to axial compression loads by means of dead weights in a pan hung from one end of the lever arm. The other end was connected to the upper platen of the testing frame using a Thompson bearing. In order to eliminate the force due to the weight of the lever on a specimen, a counter-balance weight was attached to one end of the lever arm. The lever arm ratio was such that the load in the pan was magnified five times. A Thompson bearing was also used to connect the loading shaft to the lever arm. To produce a uniform load on the specimen, a 3/4 in. in diameter of a solid steel ball was used between the main shaft and the connecting loading shaft to the lever arm. The specimens were enclosed in a plexiglas triaxial cell that can impose a desired confined pressure range 0 to 5 psi (Figure 6). A Thompson ball bushing was built in the upper platen of the triaxial cell. This enabled the main shaft to transfer the applied load vertically with less friction to the top of specimen. A photograph of the test apparatus is shown in Figure 7.

The axial deformation of specimen was measured by two linear variable differential transformers (LVDT) of Schavitz model 250 MHR. The deformation observed from each different transformer (LVDT) were different. The difference could be due to bending effects from the
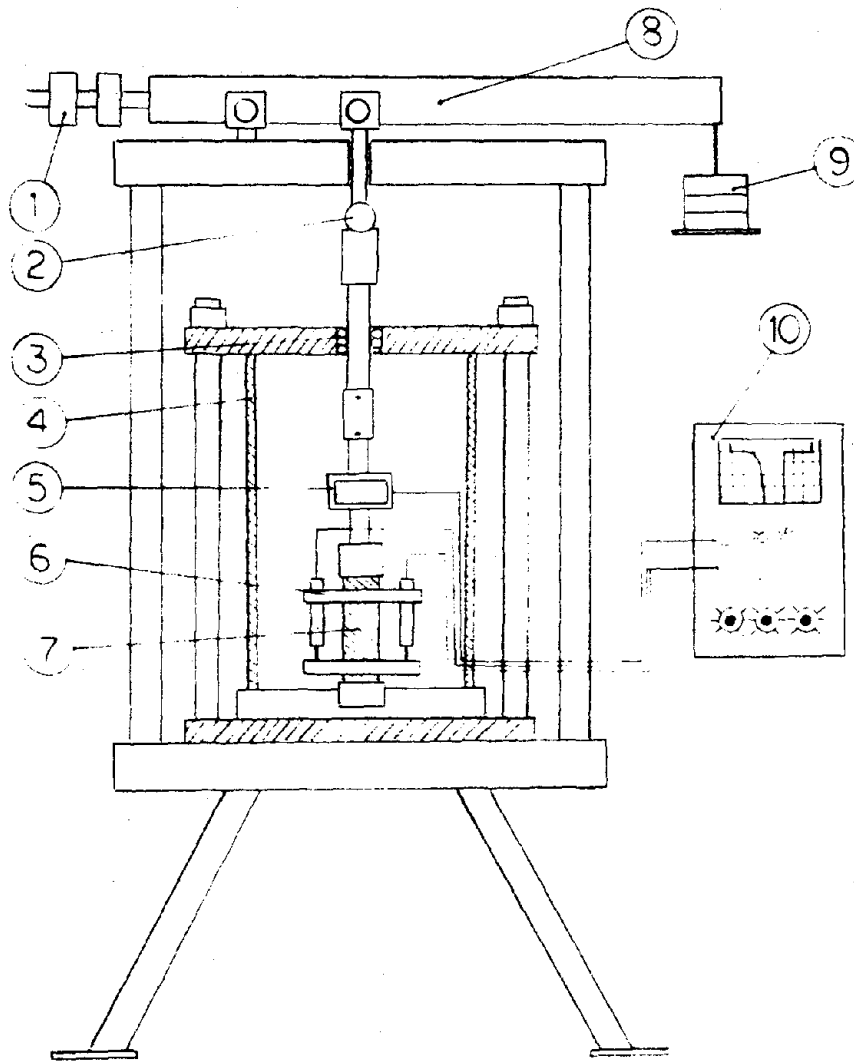
1. Balance Weight

2. A 3/4" Steel Ball

3. Slide Bearing

4. Plexi-Glass Cylinder

5. Load Cell

6. L V D T

7. Soil Specimen

8. Lever Arm

9. Dead Weight

10. Amplifier & Recorder

Figure 5. Schematic Diagram of the Experimental Setup for Single- and Multi-Step Loading
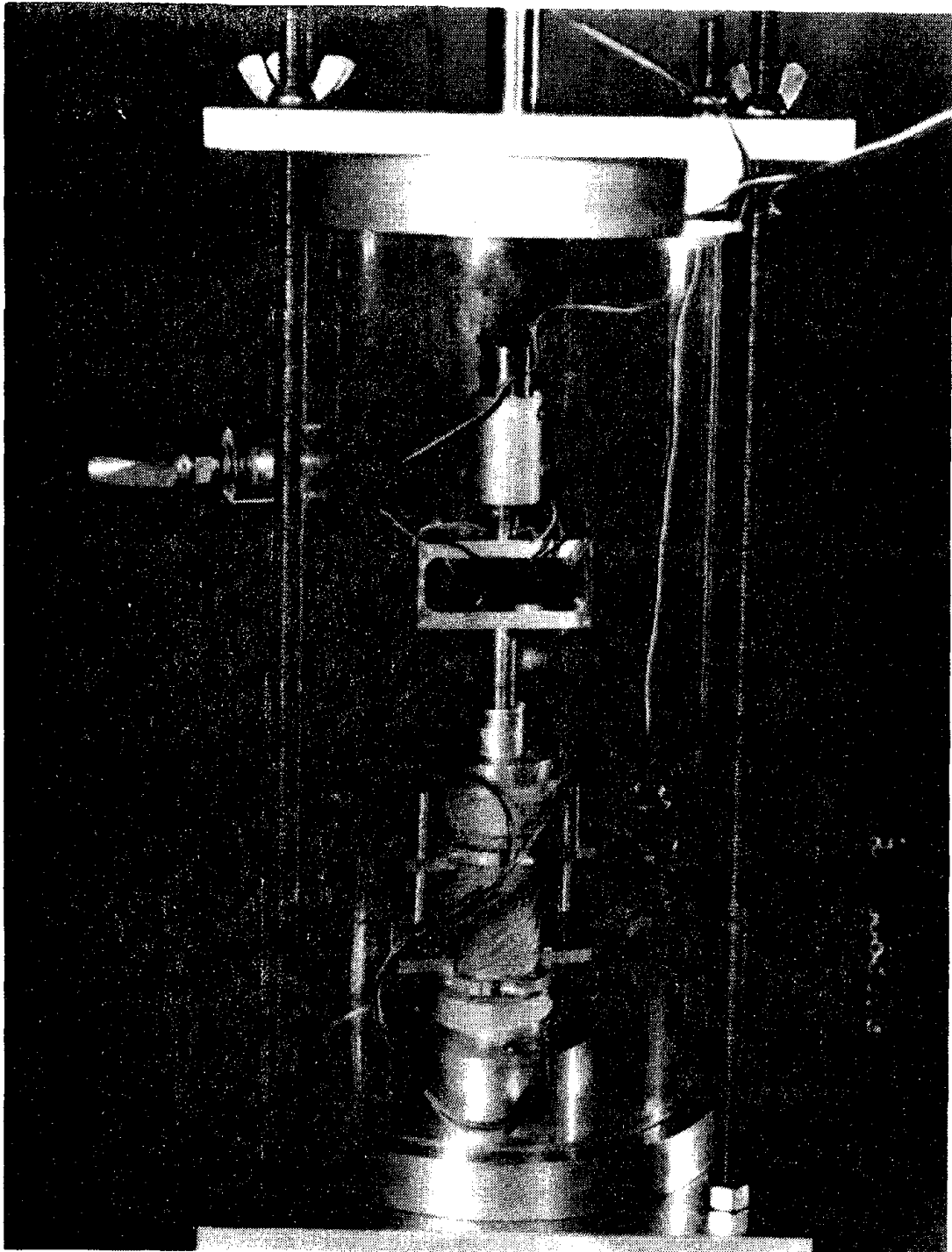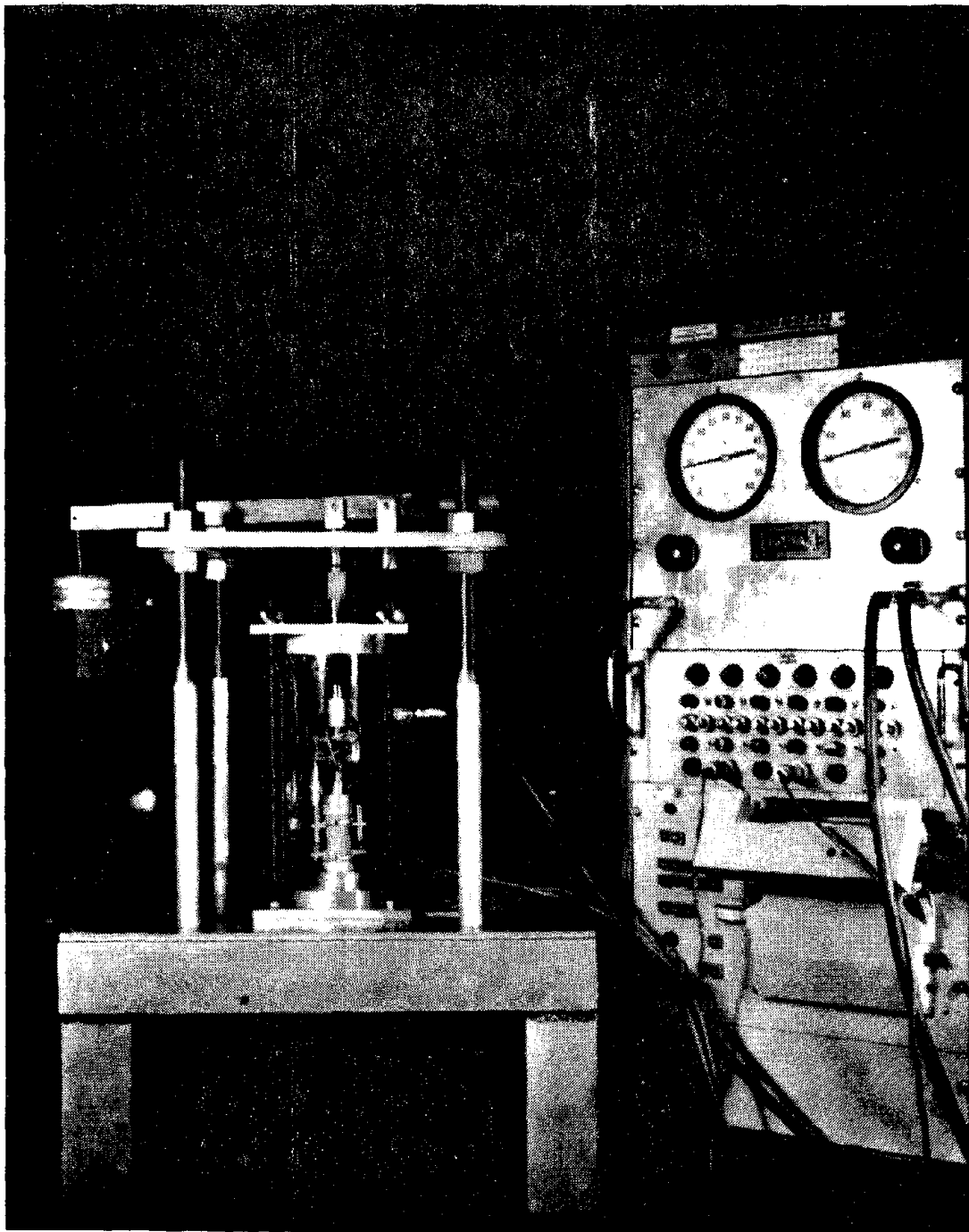
Figure 6. Close-Up Picture of Triaxial Cell

Figure 7. Picture of the Experimental Setup for Single-
and Multi-Step Loading

crookedness of specimens. Therefore, to eliminate this effect, the two LVDT's were connected in series, and the average deformation was measured for 1 7/8 in. of the length of specimen. The specially designed LVDT holder for measuring the soil deformation is shown in Figure 8.

The magnitude of applied load on specimens was obtained from a fabricated load cell. This load cell consists of a rectangular frame (see Figure 9) with a full-bridge circuit of four strain gauges. The strain gauges were selected from Micro-Measurements type CEA-06-250 UW-120, specially for higher fatigue life. The outputs of the LVDT's and load cell were fed into a six-channel electronic amplifier, Sanborn 656-1100, and a six-channel beam recorder, Sanborn 4500.

3.1.2 Dynamic Loading Test Apparatus

The dynamic loading test apparatus that is specially designed to produce sinusoidal stress on soil specimens is shown in Figure 10. The dynamic loading is applied by means of an eccentric system and a variable speed DC motor of 1/3 HP with variable range of rpm from 1 to 1725. The applied mean stress was imposed by a Bellofram with 4 in. square in area, that is controlled by a mac-valve. A schematic diagram of dynamic loading test apparatus is shown in Figure 11. The specimens were tested in the same triaxial cell used for single and multi-step loading tests.

3.2 Preparation of Specimens

The specimens used in this investigation were prepared from a soil that was obtained from the Test Track Area of the Pennsylvania Transportation Facility. The soil was passed through a #16 sieve, and was kept in an oven at $110°F$ for one week. To obtain a reasonably
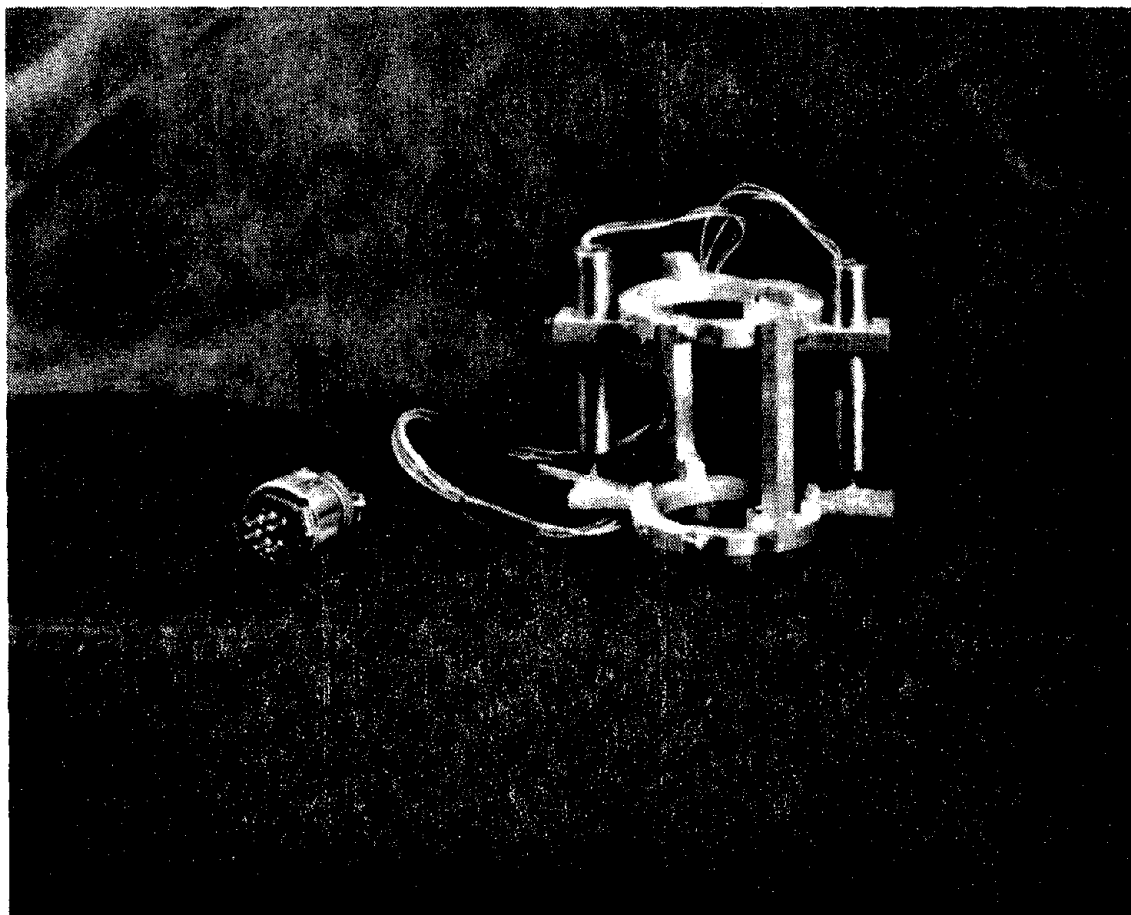
Figure 8. Detail View of L V D T Connection for
Measuring Axial Deformation of Soil
Specimen

strain gage

strain gage

strain gage

V_{in}

V_{out}

R   R

R   R
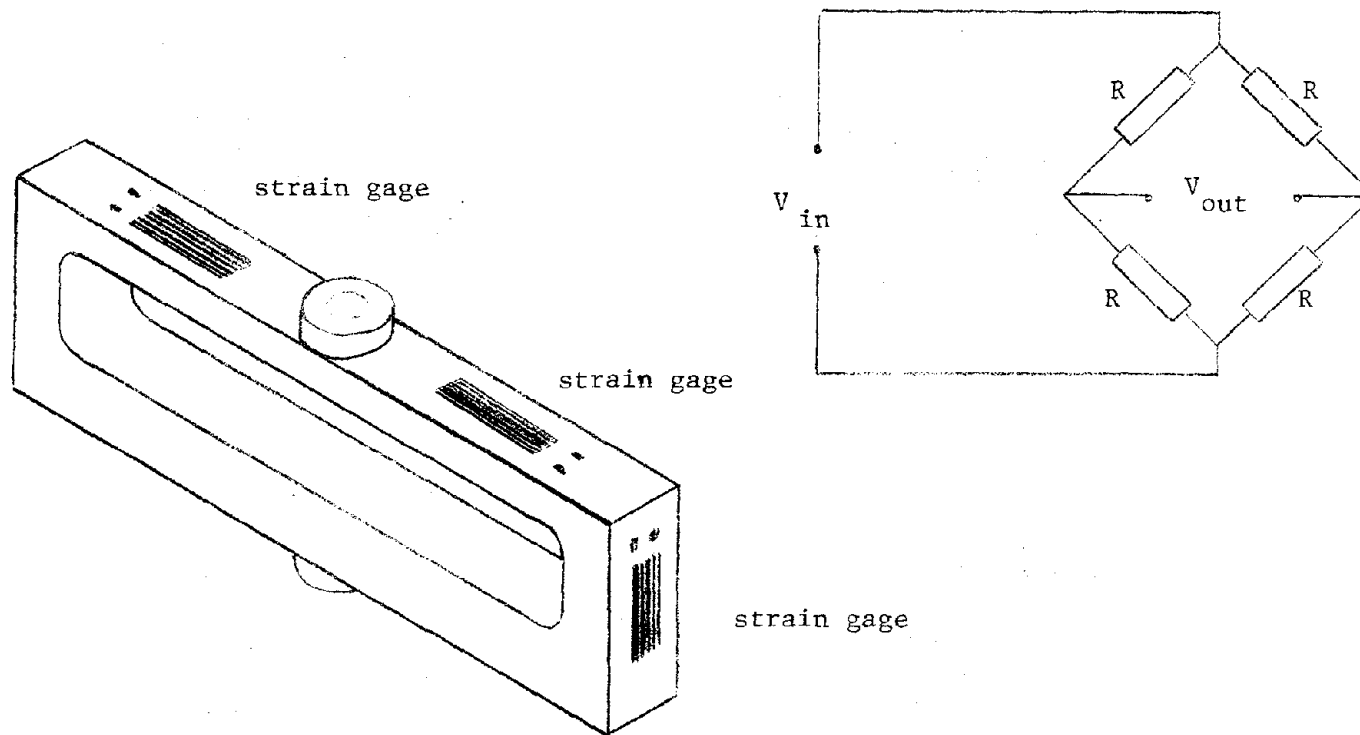
Figure 9.   Schematic Diagram of Spring Element and Full Bridge Circuit for
            Load Cell
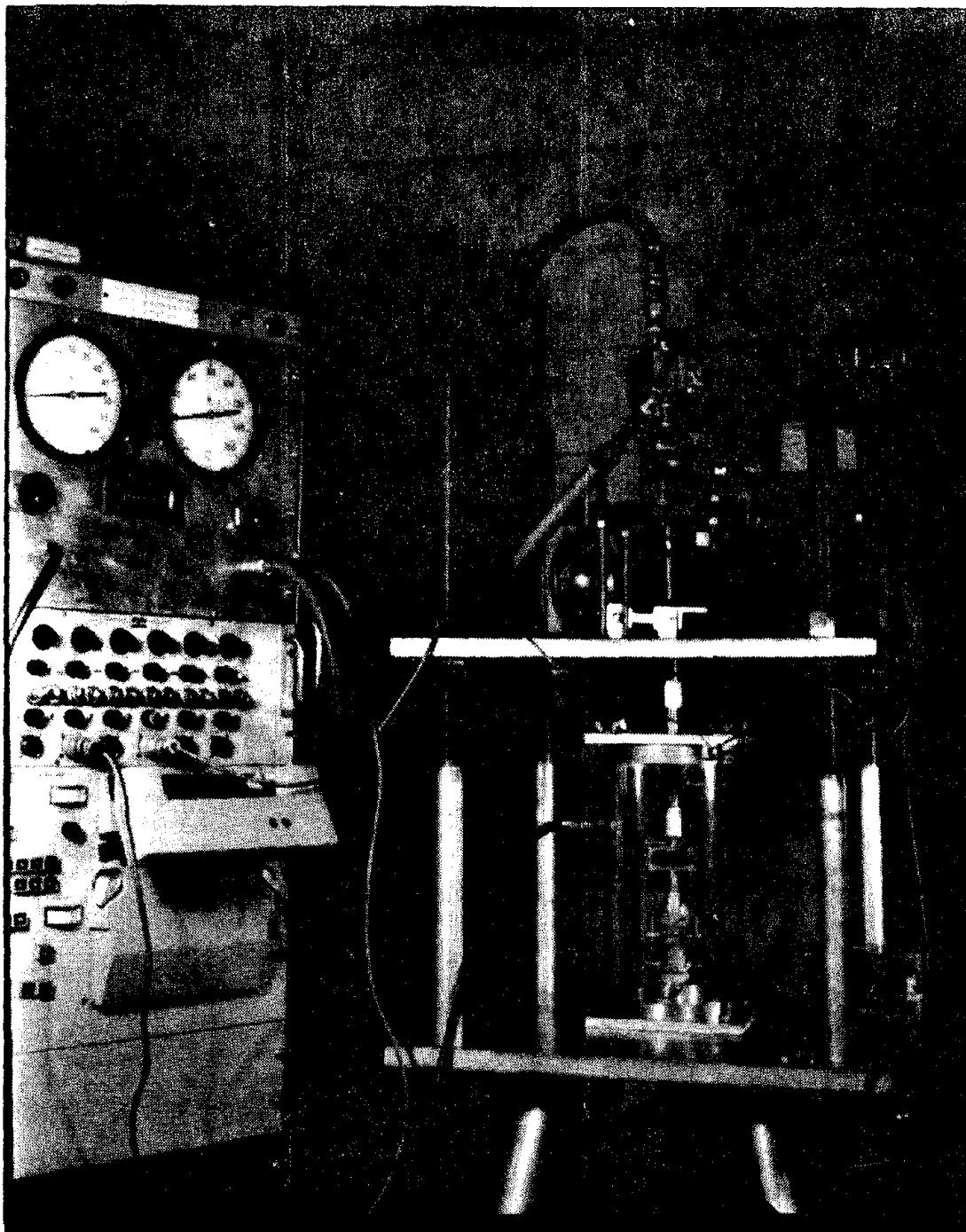
Figure 10. Picture of the Experimental Steup for Dynamic
Sinusoidal Loading
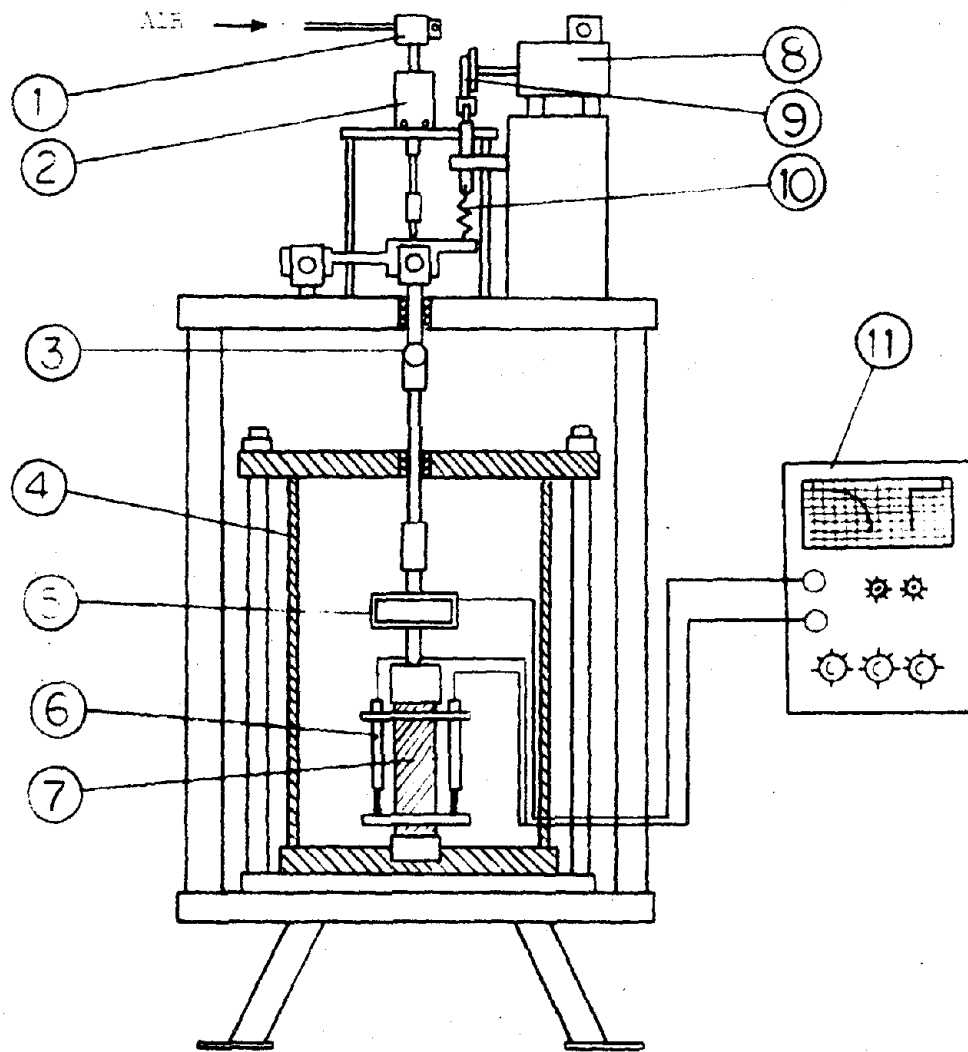
1. Mac-Valve

2. Bellofram

3. A 3/4" Steel Ball

4. Plexi-Glass Cylinder

5. Load Cell

6. L V D T

7. Soil Specimen

8. Variable Speed Motor

9. Eccentric System

10. Spring

11. Amplifier & Recorder

Figure 11. Schematic Diagram of the Experimental Set Up for Dynamic Sinusoidal Loading

reliable predetermined water content, 140 grams of oven dried soil

was thoroughly mixed with a 26.4 c.c. water in a completely sealed

plastic bag. The wet soil was compacted in a standard compaction

cylinder, 2.8 in. in overall length, 1.3 in. in diameter, and 3.78 cu.

in. in volume.

In soil engineering, compaction is any process by which the soil

particles are artifically rearranged and packed together into a closer

state of contact by mechanical means. During the compaction, the

porosity of the soil decreases, and thus the dry density increases.

The mechanical method of compaction can be accomplished by impact,

kneading action, vibration, and static or dynamic compression. The

compaction of soil for this investigation was done in a standard

compaction cylinder. The compaction was accomplished in three steps

by monotonically increasing compressive load from a Standard Tinius

Olsen Universal Testing Machine. Each layer received 200 lb. at the

rate of 1 in. per minute. The specimens were weighed and tested right

after extrusion from the compaction cylinder.

The degree of compaction of a soil which is characterized by its

dry density depends upon its moisture content, the amount of compaction

effort or energy expended on it, and the nature of the soil. The

moisture content of soil refers to the total amount of water contained

therein, either as free water or capillary water in the soil pores or

as absorbed water film around the solid particles. The moisture content

is determined by first weighing soil specimen in its wet state, drying

the specimen in an oven at a temperature $230^{o}F$, and then weighing the

dried specimen. The difference between the weights of the specimen

before and after drying represents the amount of water in the specimen,
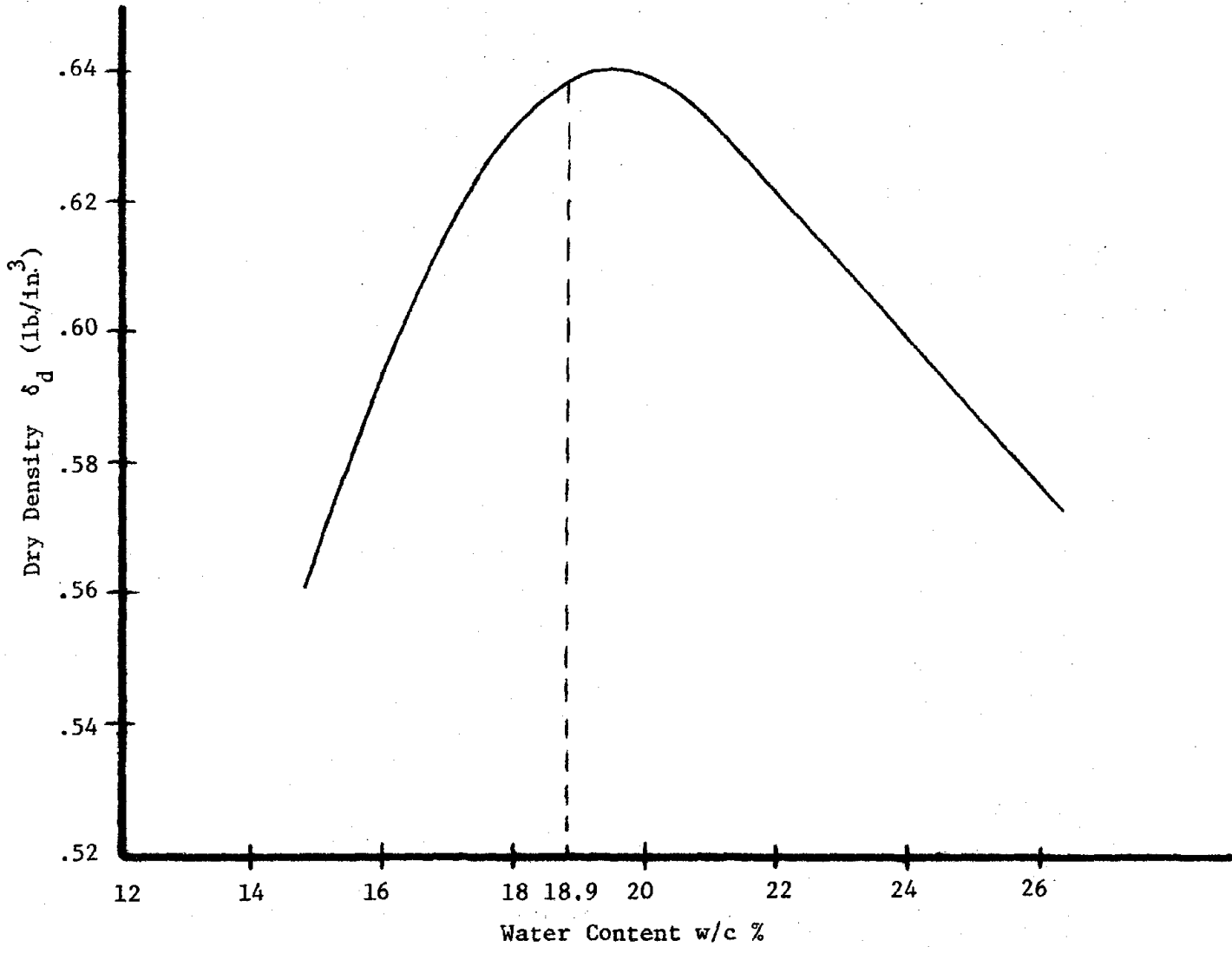
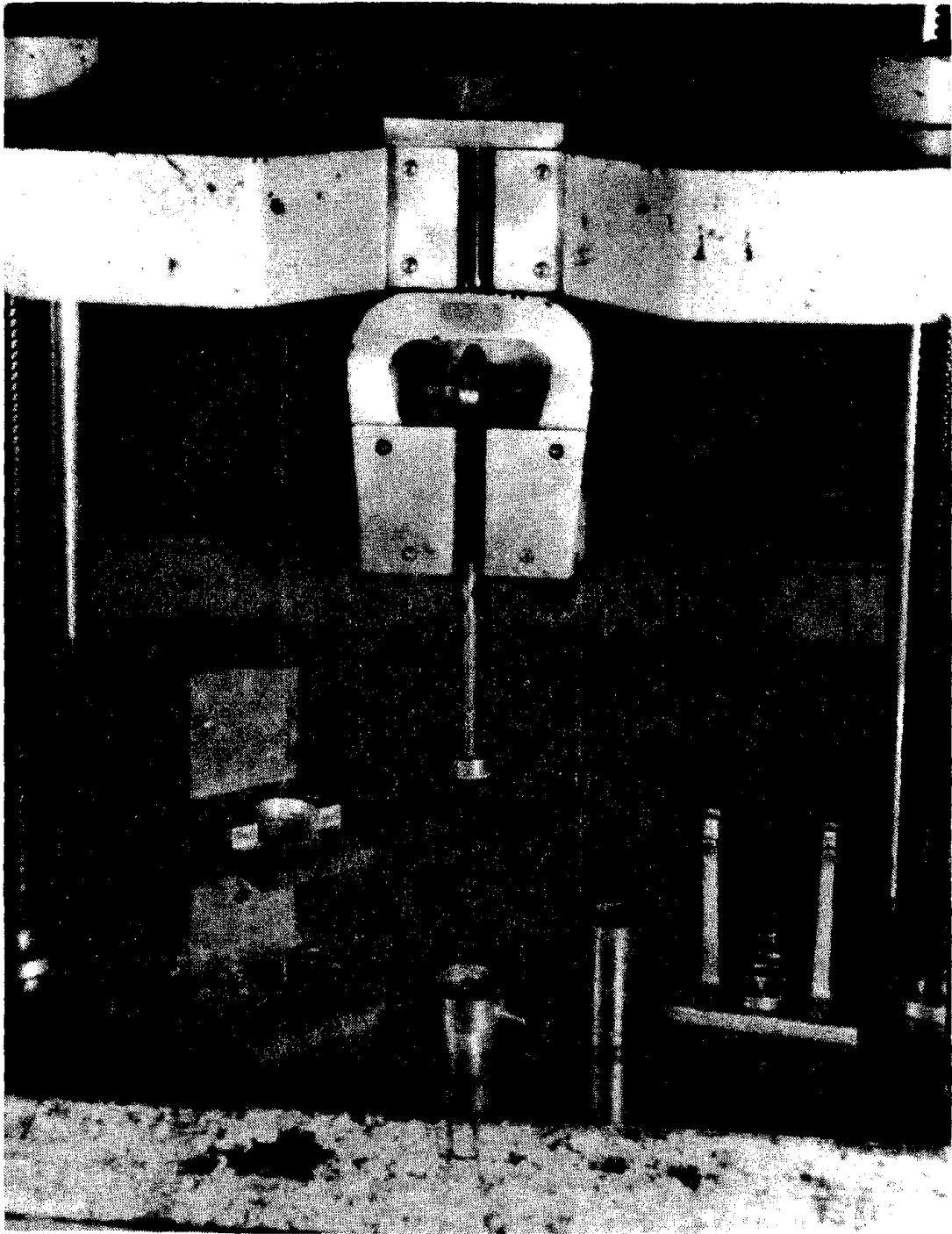Figure 12. Dry Density vs. Moisture Content for Testing Soil

Figure 13.   Picture of Soil Specimen Preparation Apparatus

and this weight, computated as a percentage of the weight of the dried specimen, is the moisture content of the soil.

$$\omega = \frac{W_\omega}{W_s} \times 100 \quad \text{Percent} \tag{25}$$

There exists a definite relationship between the soil moisture content and the degree of dry density to which a soil may be compacted. If a soil is compacted to such a degree that all voids are filled with water, then the soil is said to be saturated. The relationship between moisture content and dry density of the soil tested is shown in Figure 12. The soil specimen preparation apparatus is shown in Figure 13.

The soil specimens were covered with a rubber membrane during the test. This membrane protected the specimen against the moisture losses.

3.3 Experimental Procedures

3.3.1 Single and Multi-Step Loading Tests

The experimental program for single-step and multi-step creep loading conditions is presented in Table 1. In order to determine the single-step creep behavior, tests were conducted at six different stress magnitudes (4.58 psi, 9.54 psi, 14.1 psi, 19.1 psi, 28.6 psi, 38.0 psi). The deformation, as well as stress magnitudes were measured for 500 seconds from the application of the load. The deformation was recorded continuously for the first 100 seconds. After 500 seconds, the deformation was registered at four different time intervals (200 sec., 300 sec., 400 sec., 500 sec.). To provide a more accurate and reliable data, the deformation for each stress magnitude was obtained from the average value of identical tests.

Two-step creep loading tests were conducted for three different stress magnitudes (σ_1 = 14.1 psi, σ_2 = 9.54 psi/σ_1 = 19.1 psi, σ_2 =

4.58 psi/σ_1 = 19.1 psi, σ_2 = 9.54 psi), as shown in Figure 3. The second step loading was applied at five different time intervals (10 sec., 100 sec., 200 sec., 300 sec., 400 sec.), from the application of the first step. The deformation was registered for 500 sec. from the application of the first step loading. The continuous deformation record was obtained for the first 100 seconds from the application of load for each step.

Three-step loading tests were performed only for one of three stress values (σ_1 = 14.1 psi, σ_2 = 15.7 psi, σ_3 = 13.75 psi), as shown in Figure 4. The second and third step loading were applied for different time intervals. The following table shows the time intervals (t_1, t_2) used in three-step loading tests.

Table 2. Time Intervals (t_1 and t_2) Used in Three-Step Loading Tests.

$$
t_1(\text{sec.}) = \begin{cases} 10 & t_2(\text{sec.}) = \begin{bmatrix} 100 \\ 200 \\ 300 \\ 400 \end{bmatrix} \\ 100 & t_2(\text{sec.}) = \begin{bmatrix} 200 \\ 300 \\ 400 \end{bmatrix} \\ 200 & t_2(\text{sec.}) = \begin{bmatrix} 300 \\ 400 \end{bmatrix} \\ 300 & t_2(\text{sec.}) = \begin{bmatrix} 400 \end{bmatrix} \end{cases}
$$

where t_1 and t_2 are the time of application of second and third step

loading respectively. The time intervals were measured from the

application of first step loading. All specimens were tested at room

temperature (75°F).

3.3.2 Dynamic Loading Tests

In order to investigate the behavior of a cohesive soil under

uniaxial dynamic load, tests were performed for different frequencies

mean stresses, and dynamic stress magnitudes. The dynamic sinusoidal

load was superimposed after 500 seconds of the application of mean

load on soil specimens. The deformation was measured for three time

intervals after application of the dynamic load (100 sec., 300 sec.,

500 sec.). Tests were conducted for four different dynamic

sinusoidal stress amplitudes (5.2 spi, 7 psi, 10 psi, 13 psi), and

four mean stress values (11 psi, 17 psi, 24 psi, 28 psi). Each

dynamic test was performed for four different frequencies (9 Hz,

125 Hz, 22 Hz, 26 Hz). All tests were conducted at the room

temperature (75°F).

CHAPTER IV

EXPERIMENTAL RESULTS AND INTERPRETATION

4.1 Experimental Results

The results from the uniaxial creep tests for different stress

magnitudes are shown in the form of strain-time curves in Figure 14.

The creep deformation was measured for a wide range of stress mag-

nitudes up to the failure point. The results for two-step and

three-step loading conditions are presented in Figures 15 through

29. Each of these figures indicates different time interval. A

typical hysteresis loop obtained from dynamic sinusoidal loading

test for a specific frequency and three different total number of

cycles are shown in Figure 30. Figure 31 shows the variation of

the dynamic strain amplitude with frequency. The strain response

amplitude against the dynamic stress amplitude is shown in Figure 32.

4.2 Interpretation of the Result

4.2.1 Single-Step Creep

The creep compliance was defined as the ratio of the creep

strain to the applied stress at a certain time ($\frac{\varepsilon}{\sigma}$). For a linear

viscoelastic material, the creep compliance-stress curve is a hori-

zontal line at various constant time values. In order to determine

the linear range from creep test results, the creep compliance was

obtained and plotted against stress magnitude. These curves were

obtained for four different time intervals (10 sec., 100 sec., 300

sec., 500 sec.), as shown in Figure 33. This figure shows, for

stress levels higher than 10 psi, the behavior of soil is highly
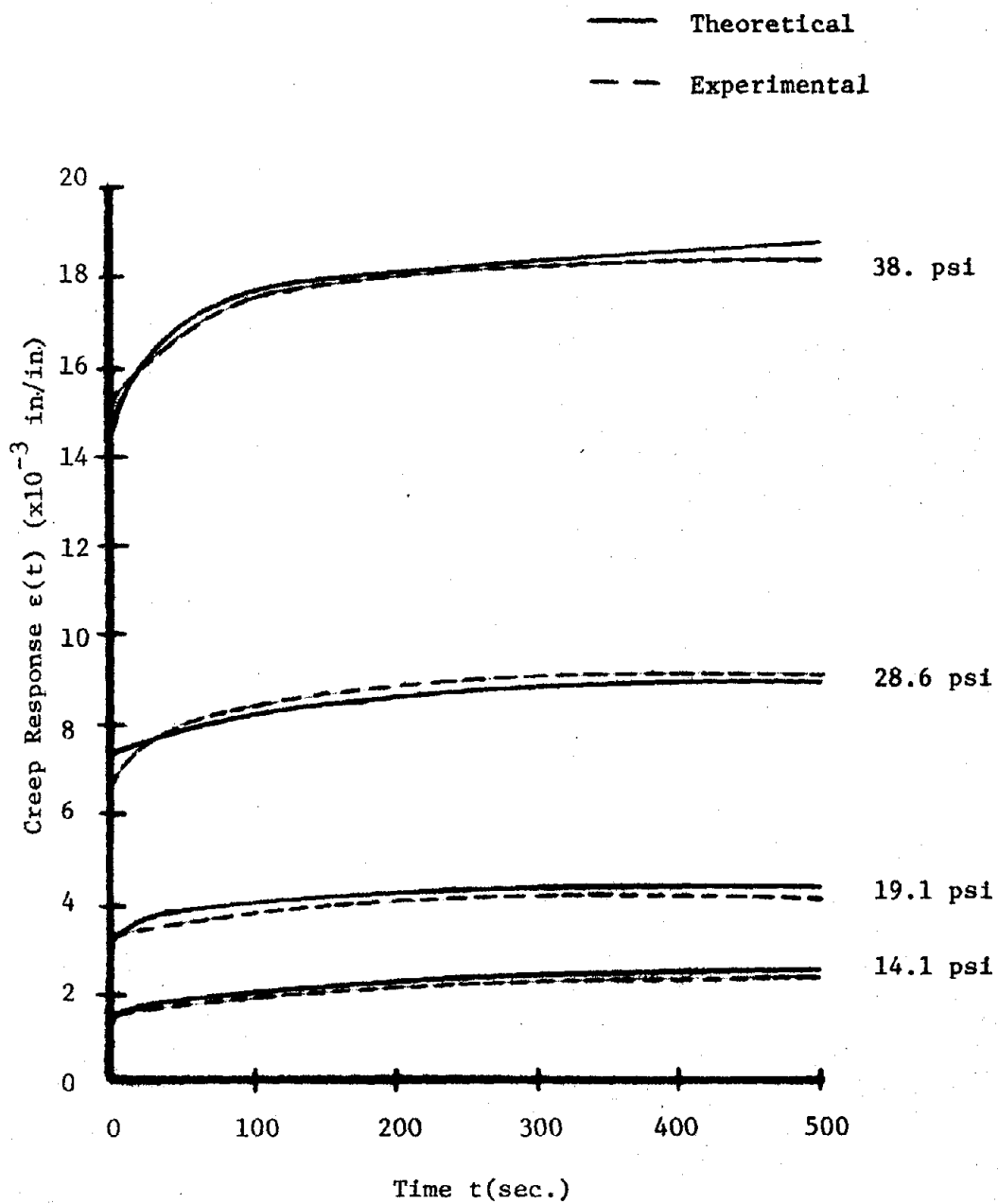
Figure 14. Theoretical and Experimental Creep
Response vs. Time for Different Stress
Levels
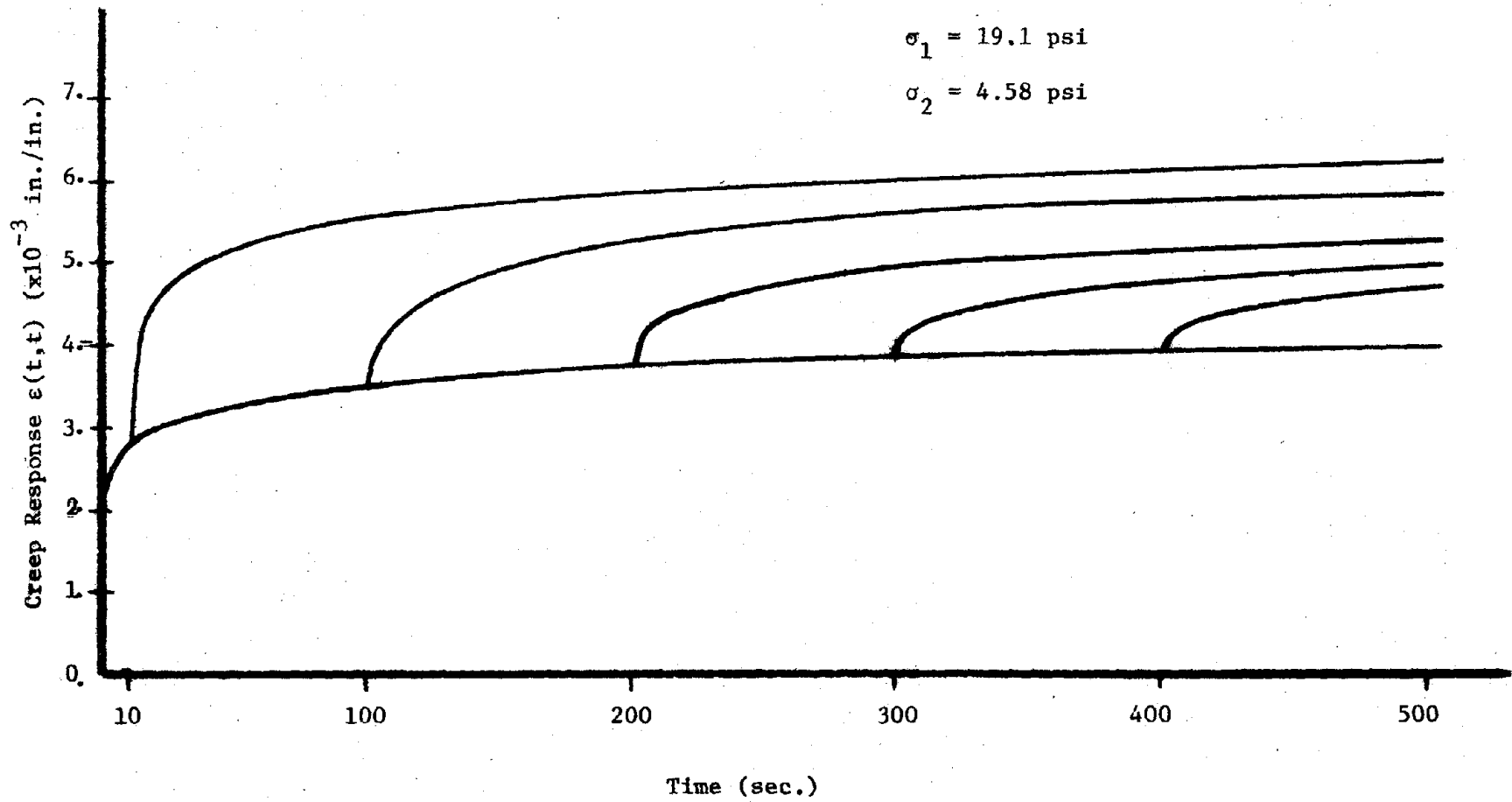
Figure 15. Experimental Creep Response for Two-Step Loading at Different Time Interval of the Second Step Loading
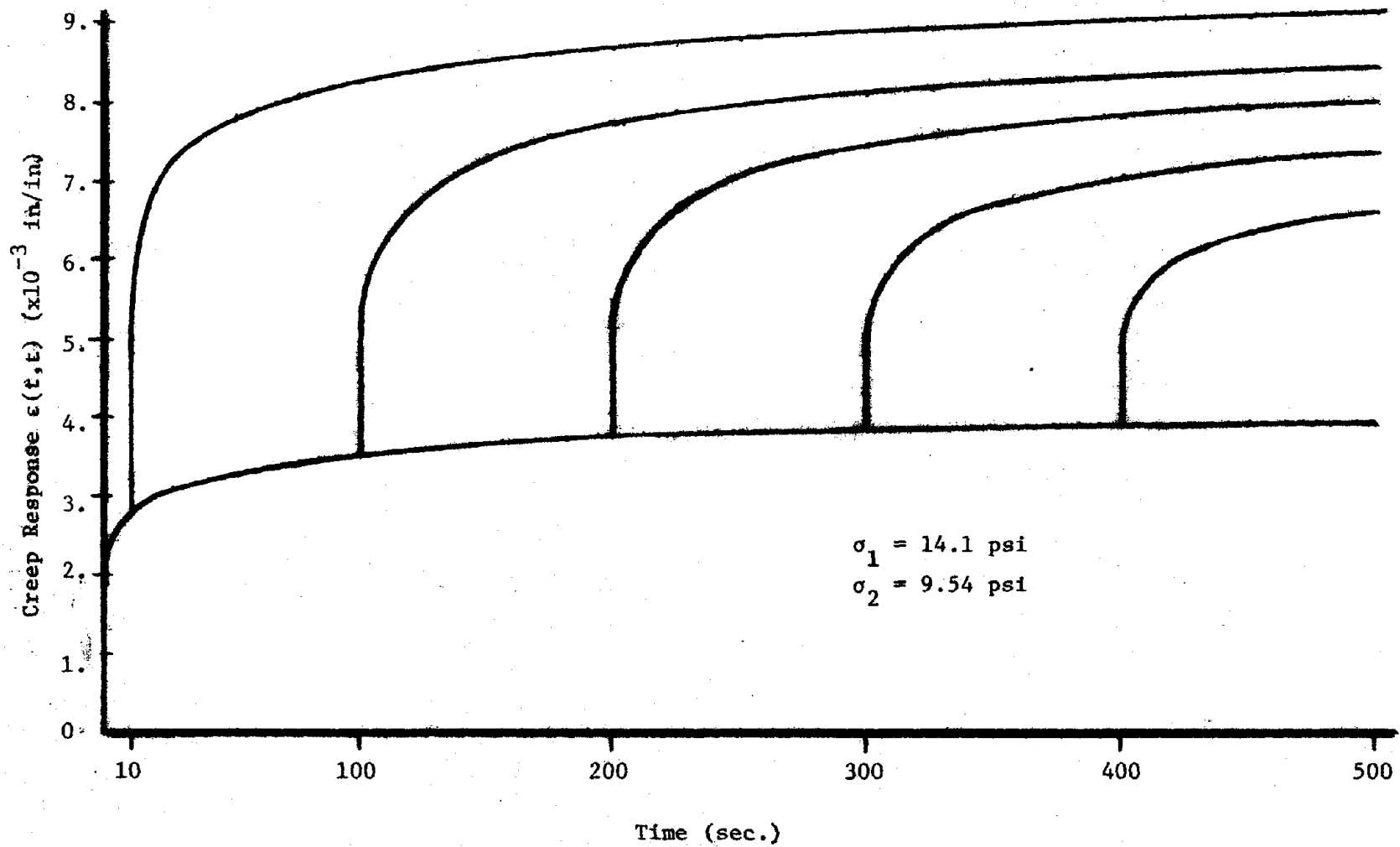
Figure 16. Experimental Creep Response for Two-Step Loading at Different Time Interval of the Second Step Loading

Figure 17. Experimental and Theoretical Creep Response for Two-Step Loading at $t_1=10$ sec.
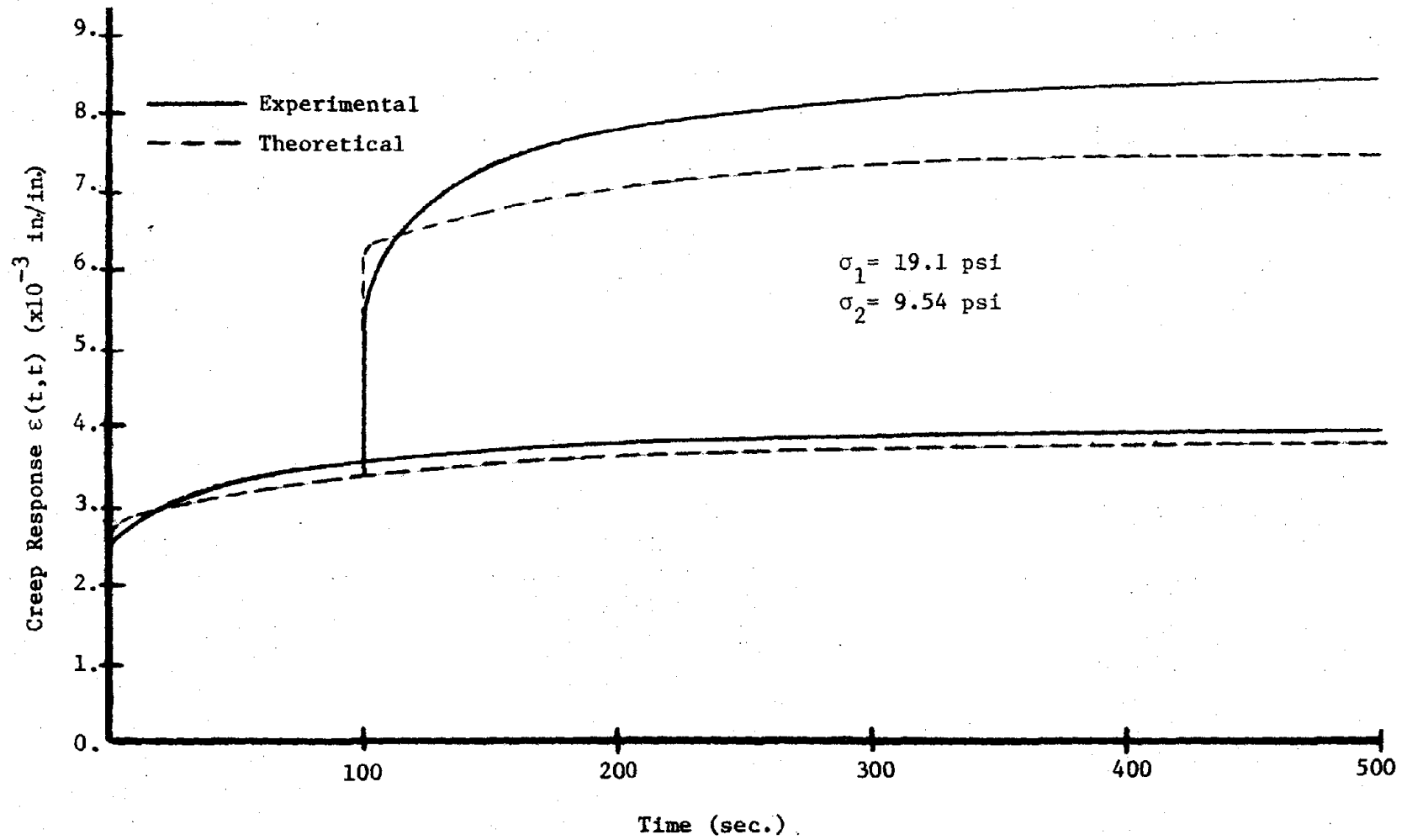
Figure 18. Experimental and Theoretical Creep Response for Two-Step Loading at $t_1 = 100$ sec.
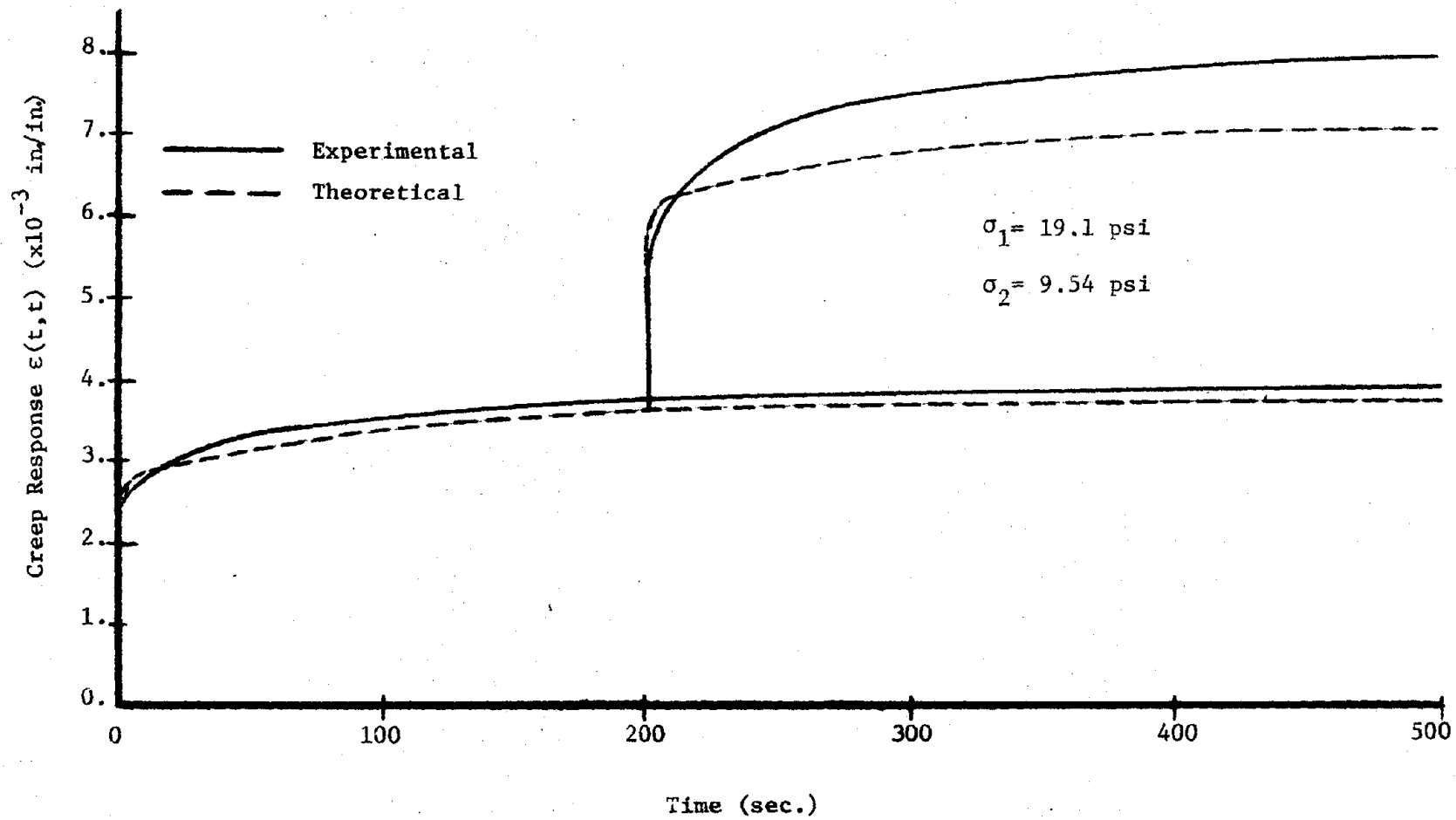
Figure 19. Experimental and Theoretical Creep Response for Two-Step Loading at $t_1 = 200$ sec.
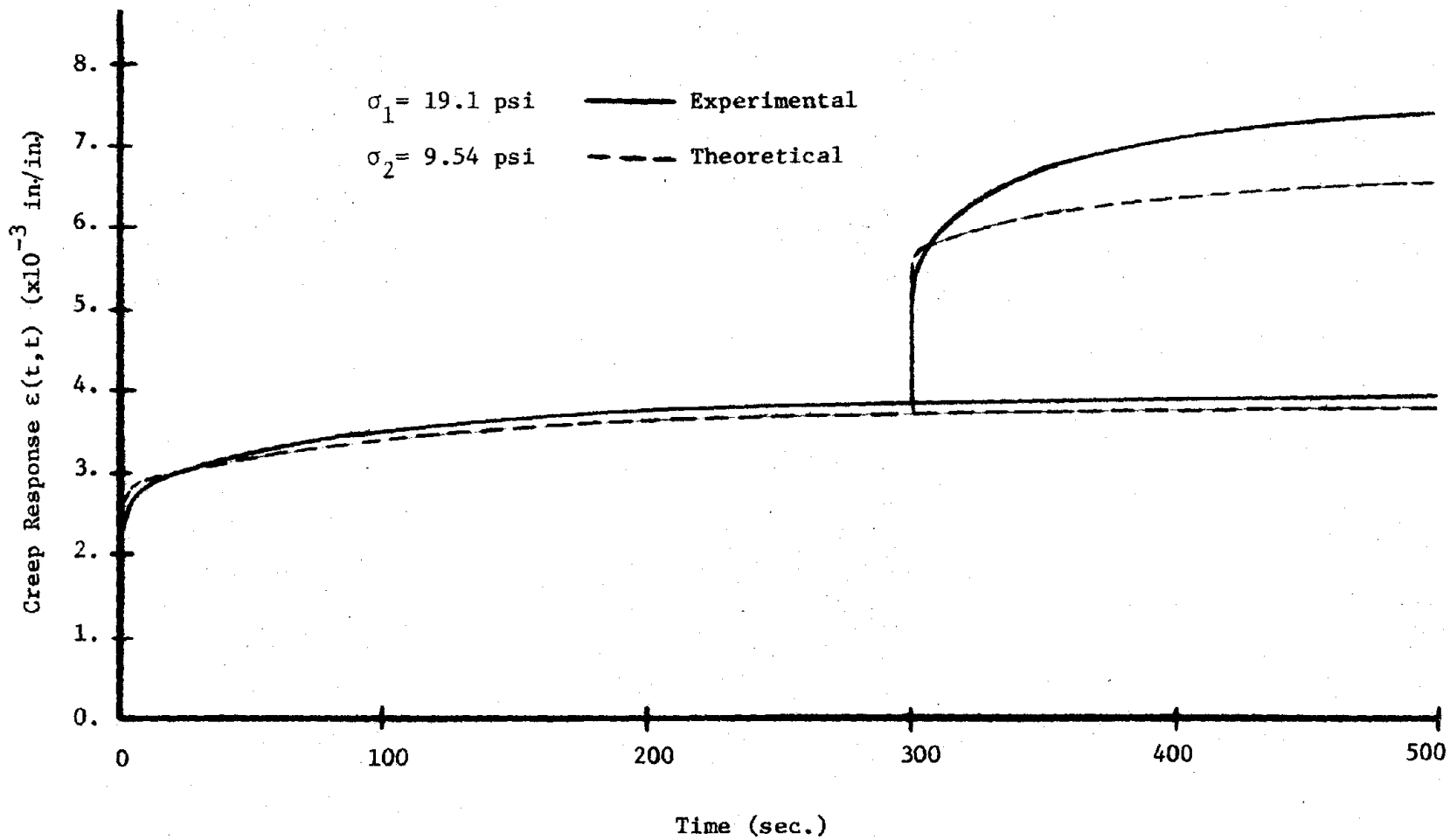
Figure 20. Experimental and Theoretical Creep Response for Two-Step Loading at t_1=300 sec.
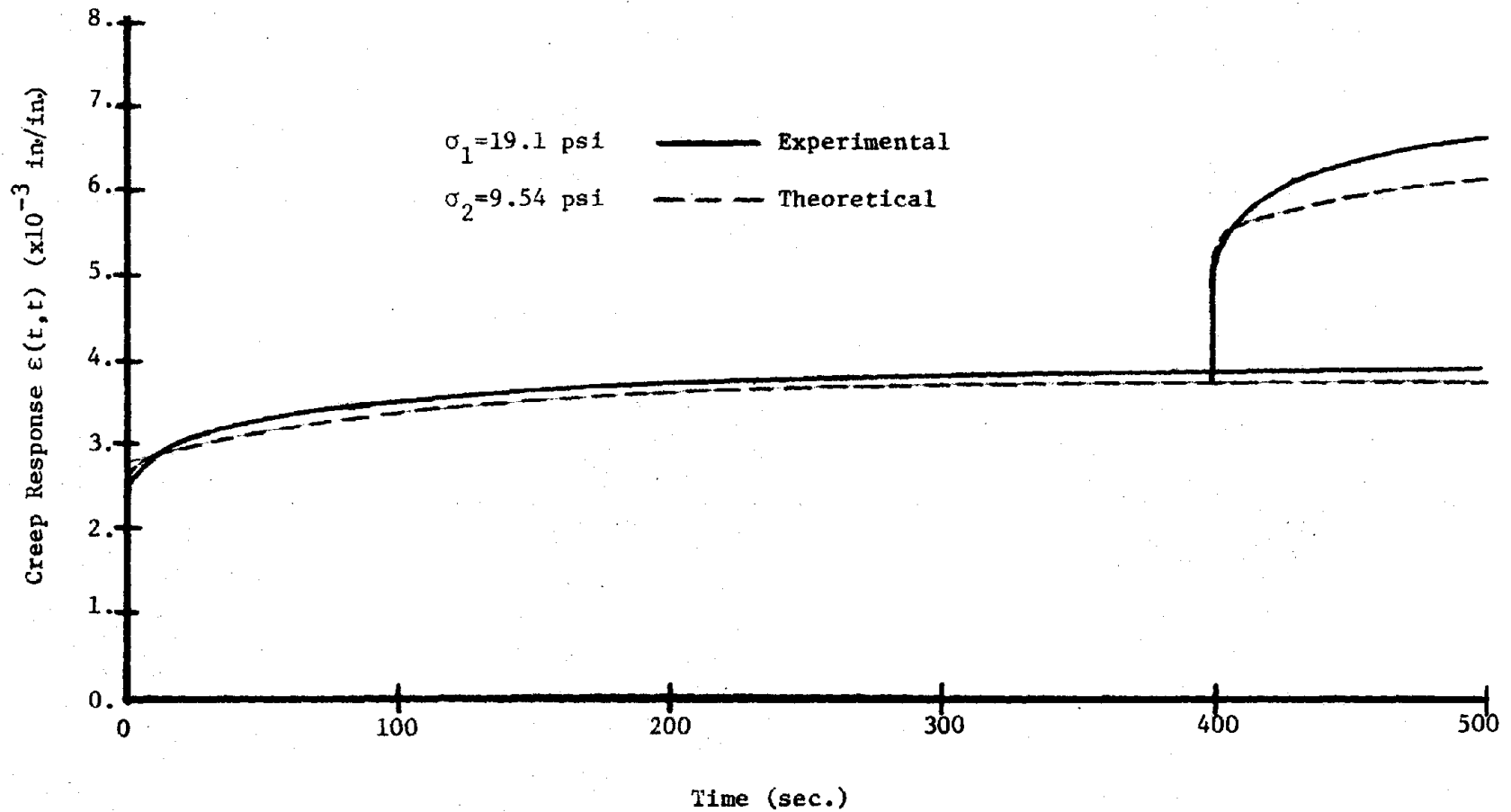
Figure 21. Experimental and Theoretical Creep Response for Two-Step Loading at $t_1 = 400$ sec.
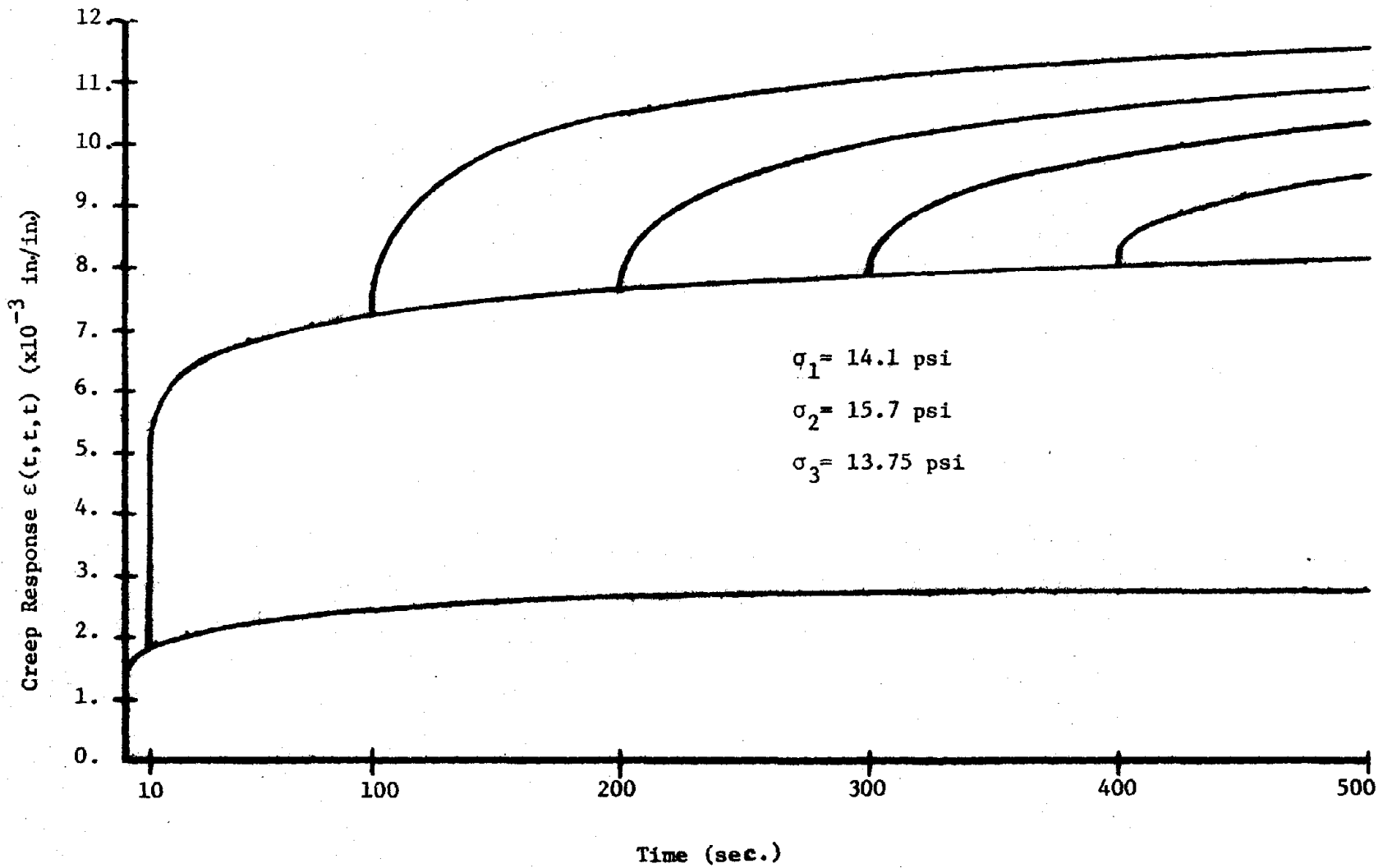
Figure 22. Experimental Creep Response for Three-Step Loading for t_1=10 sec., and Different t_2

The figure shows a plot with the following labels:

Y-axis: Creep Response $\epsilon(t,t,t)$ ($\times 10^{-3}$ in/in)

X-axis: Time (sec.)

σ_1= 14.1 psi

σ_2= 15.7 psi

σ_3= 13.75 psi
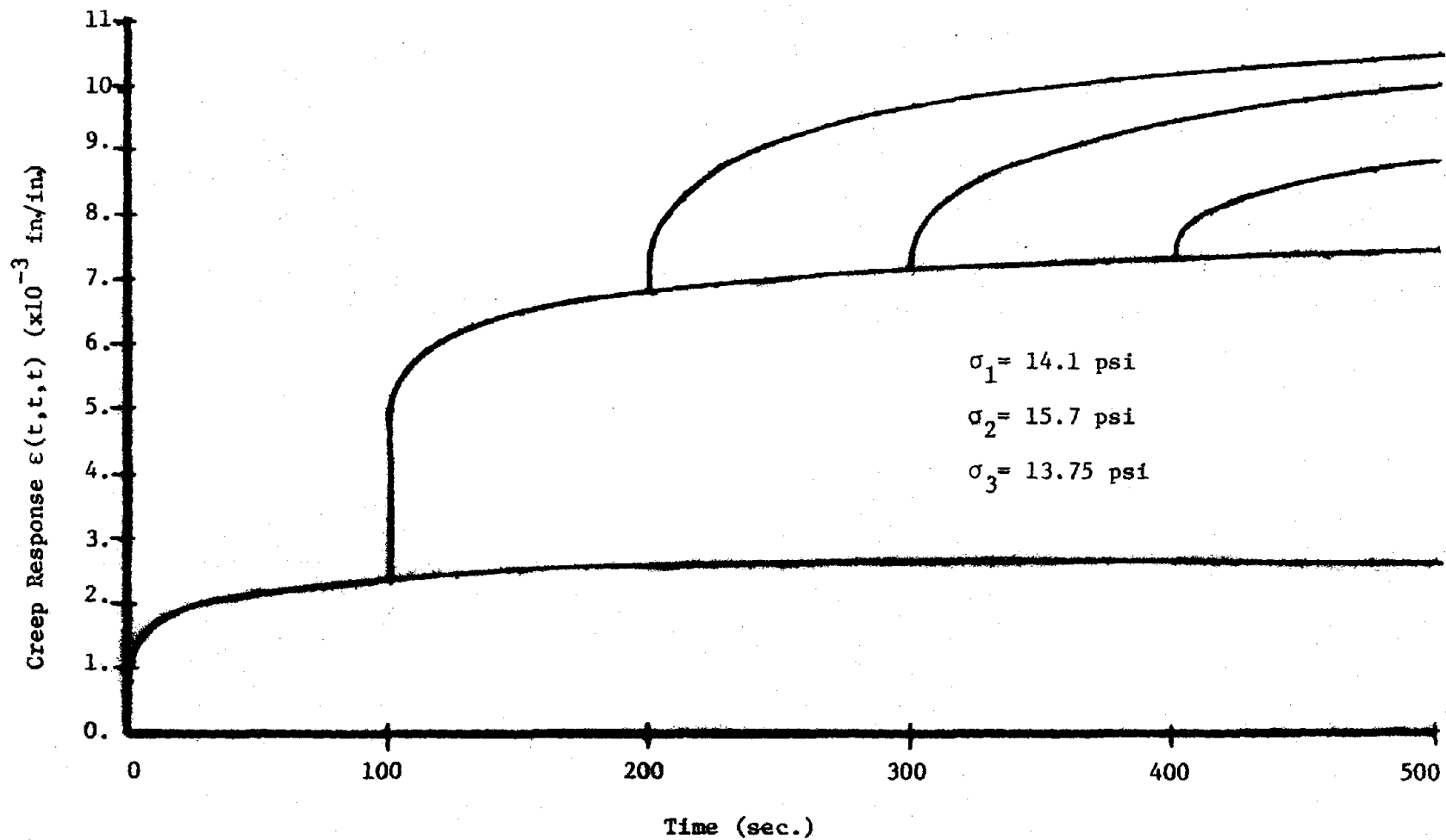
Figure 23. Experimental Creep Response for Three-Step Loading for t_1=100 sec., and Different t_2

The figure shows a plot of Creep Response $\epsilon(t,t,t)$ ($\times 10^{-3}$ in./in.) versus Time (sec.), with:
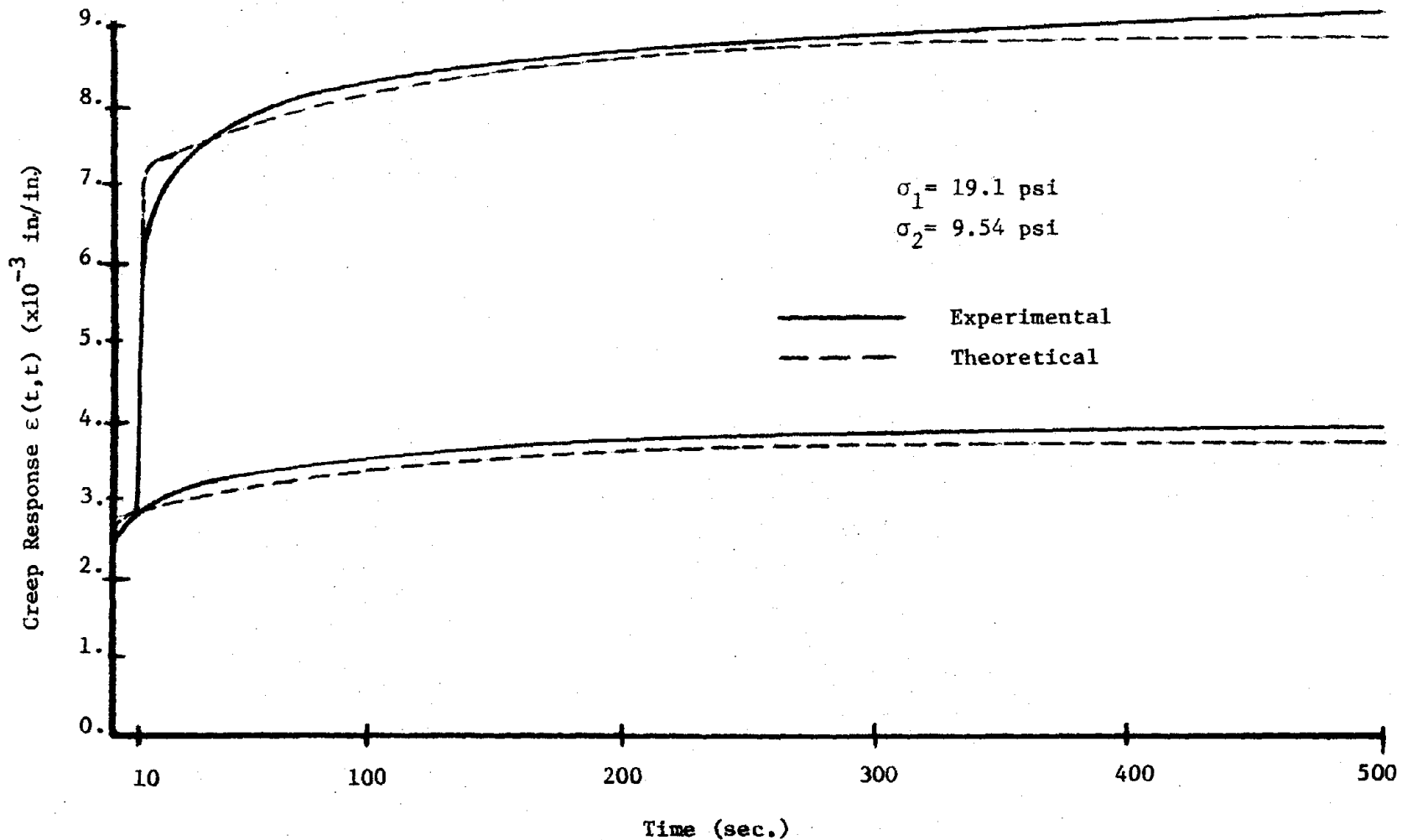
σ_1= 14.1 psi

σ_2= 15.7 psi

σ_3= 13.75 psi
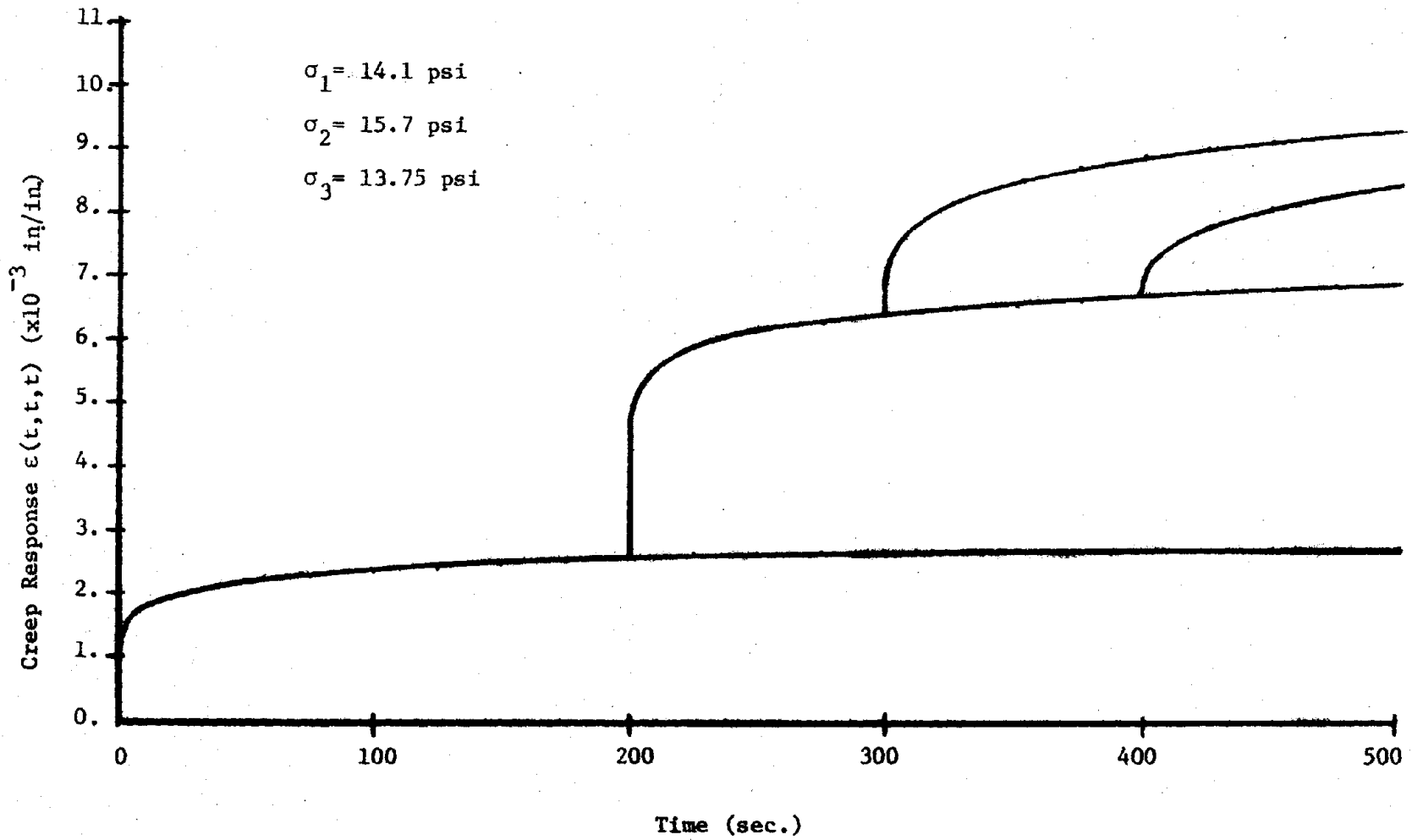
Figure 24. Experimental Creep Response for Three-Step Loading for $t_1=200$ sec., and Different t_2
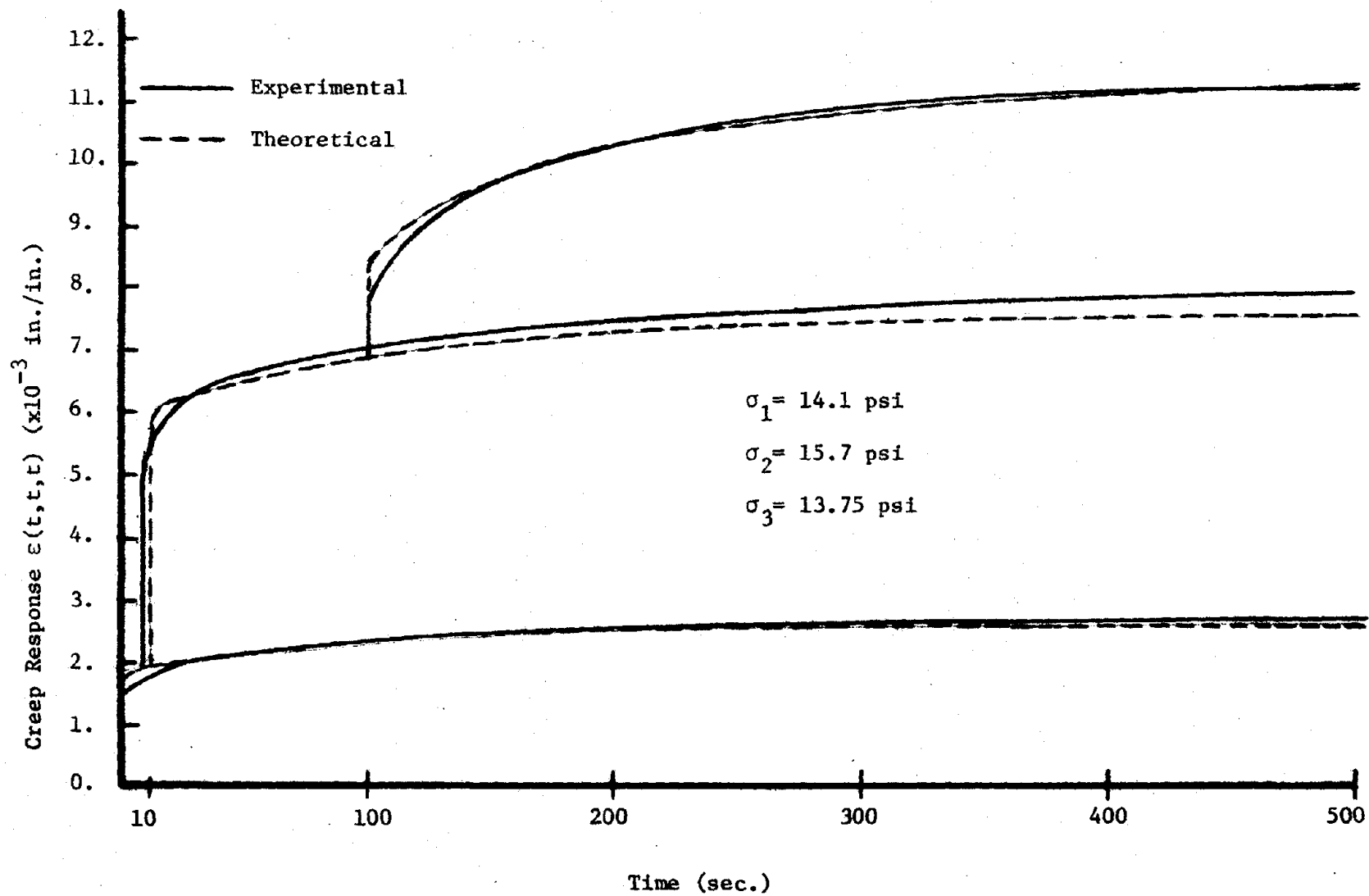
Figure 25. Experimental and Theoretical Creep Response for Three-Step Loading for t_1=10 sec., and t_2=100 sec.
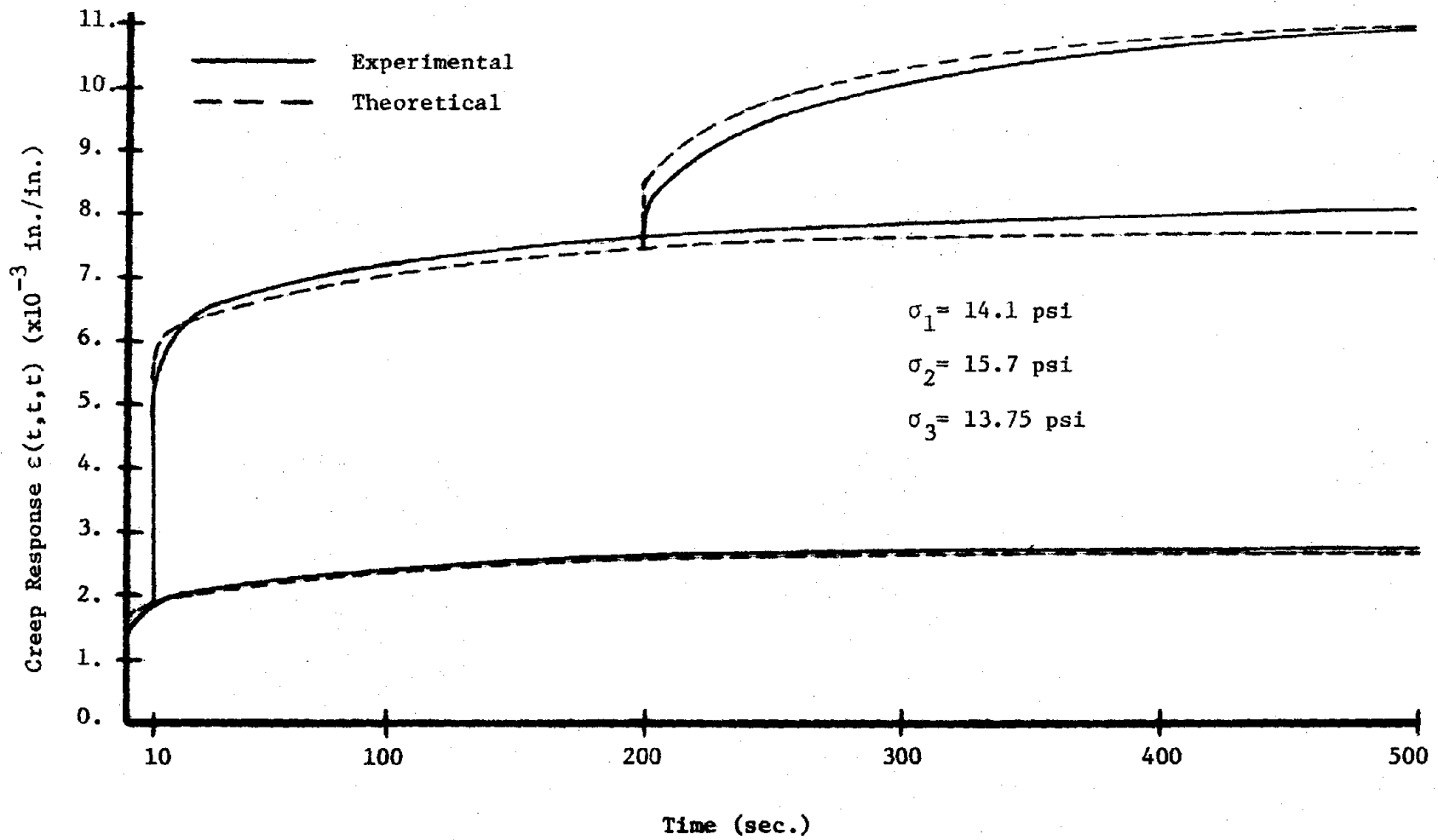
Figure 26. Experimental and Theoretical Creep Response for Three-Step Loading for t_1=10 sec., and t_2=200 sec.

Creep Response $\varepsilon(t,t,t)$ $(\times 10^{-3}$ in./in.)

Experimental

Theoretical

$\sigma_1 = 14.1$ psi

$\sigma_2 = 15.7$ psi

$\sigma_3 = 13.75$ psi

Time (sec.)
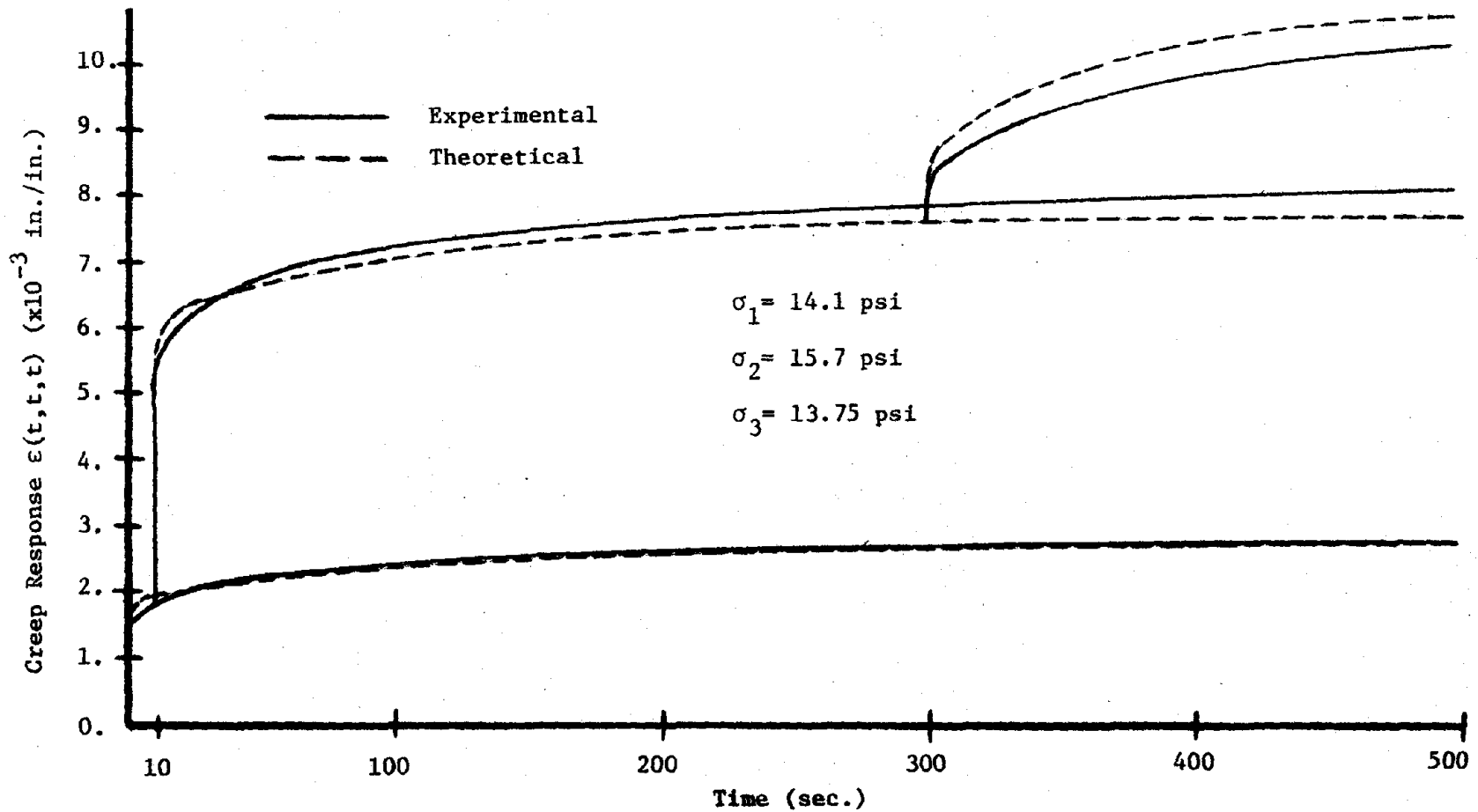
Figure 27. Experimental and Theoretical Creep Response for Three-Step Loading for $t_1 = 10$ sec., and $t_2 = 300$ sec.
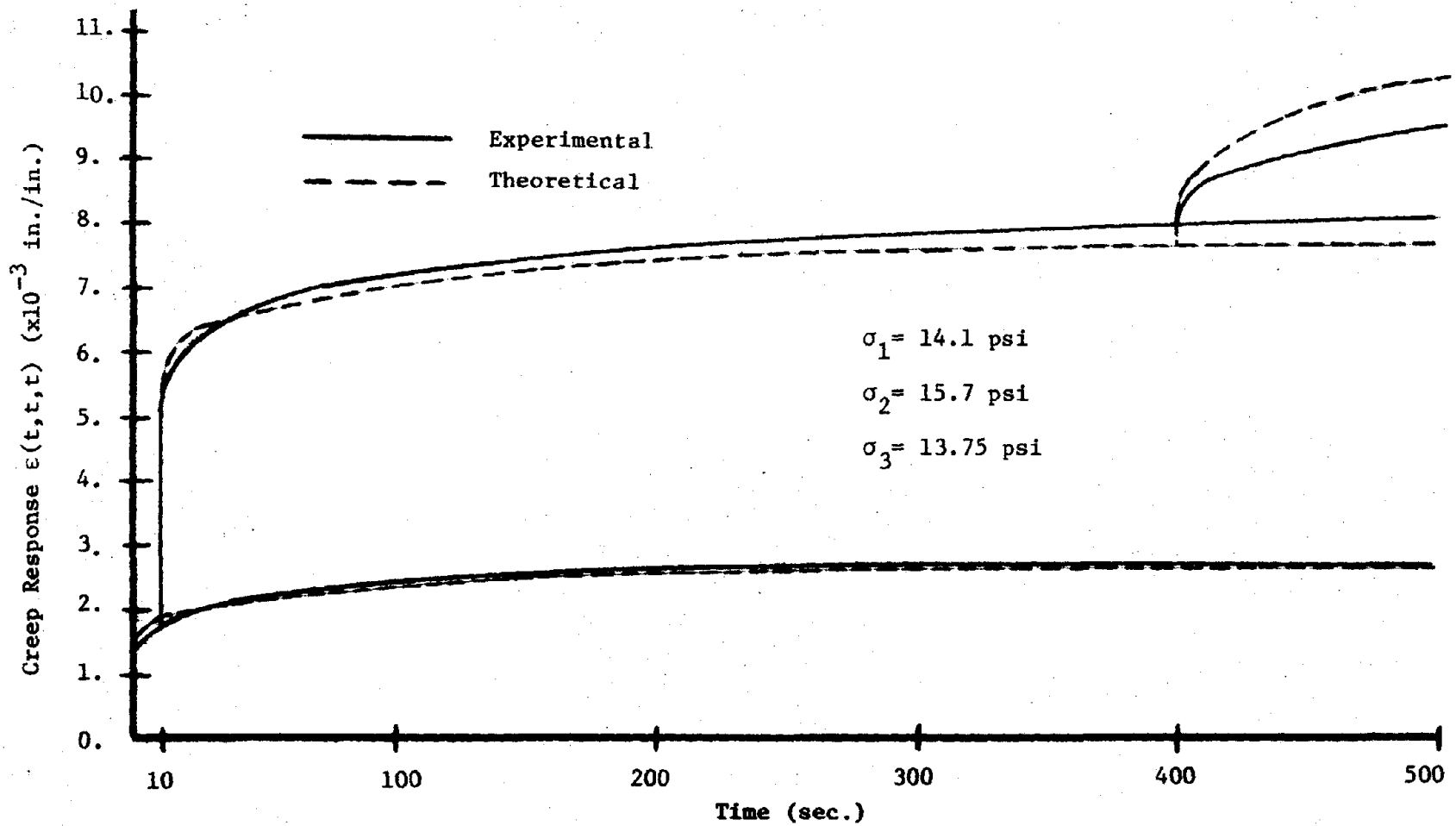
Figure 28. Experimental and Theoretical Creep Response for Three-Step Loading for t_1=10 sec., and t_2=400 sec.
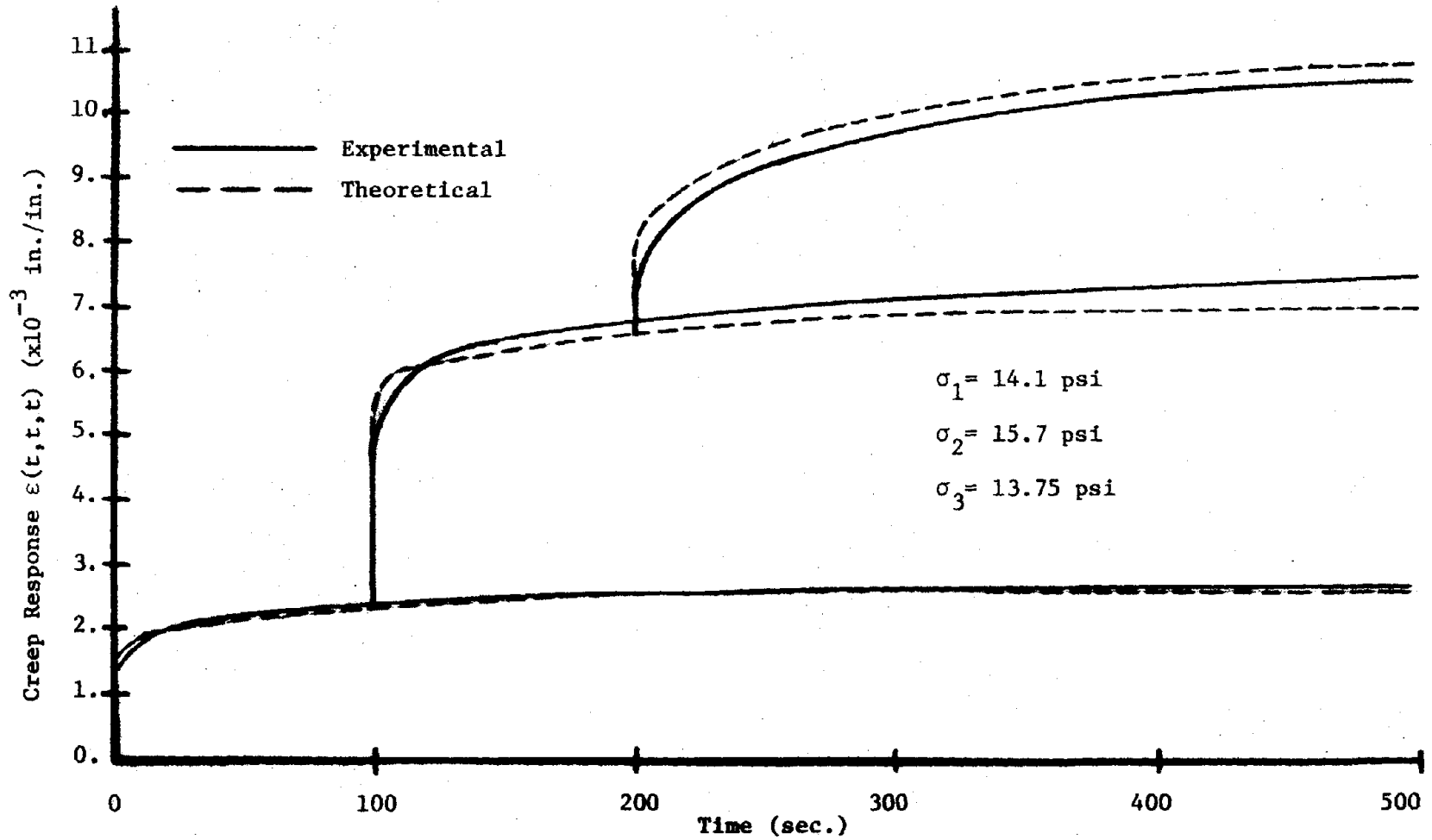
Figure 29. Experimental and Theoretical Creep Response for Three-Step Loading for t_1=100 sec., and t_2=200 sec.
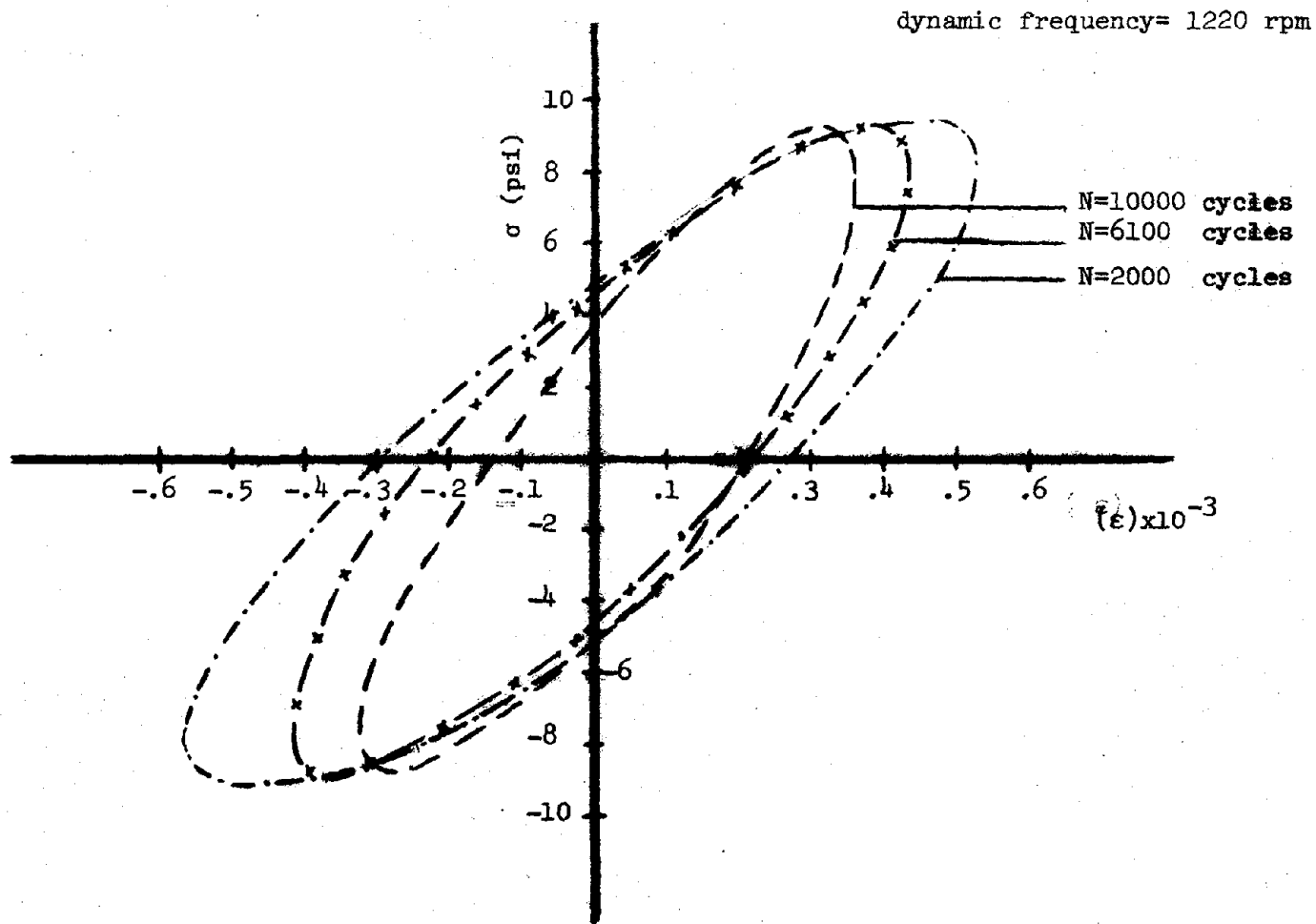
Figure 30. A Typical Dynamic Sinusoidal Stress-Strain Curve for Different
Total Number of Cycles (Hystersis Loop)
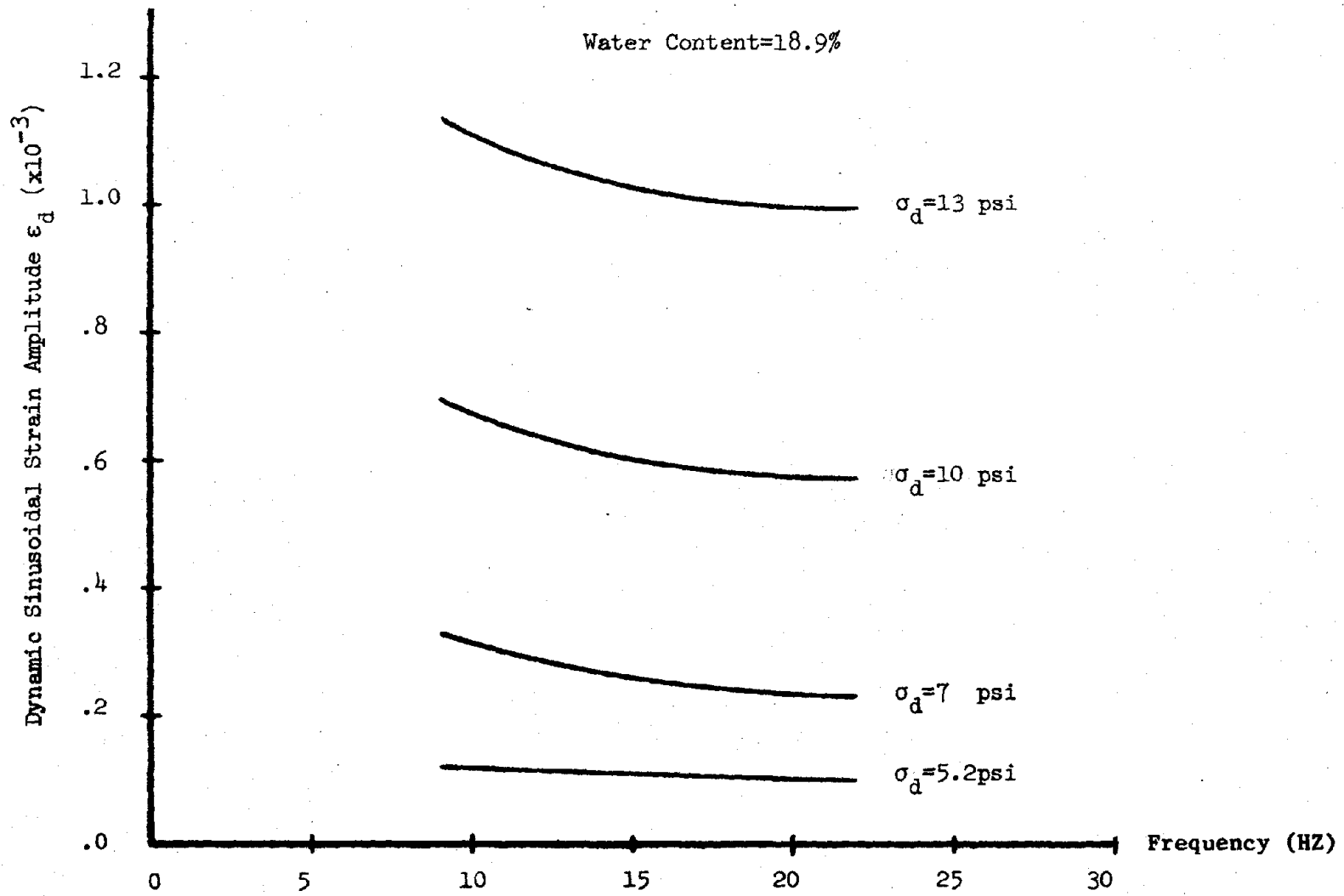
Figure 31. Variation of Dynamic Sinusoidal Strain Amplitude with Frequency for Different Dynamic Stress Amplitude
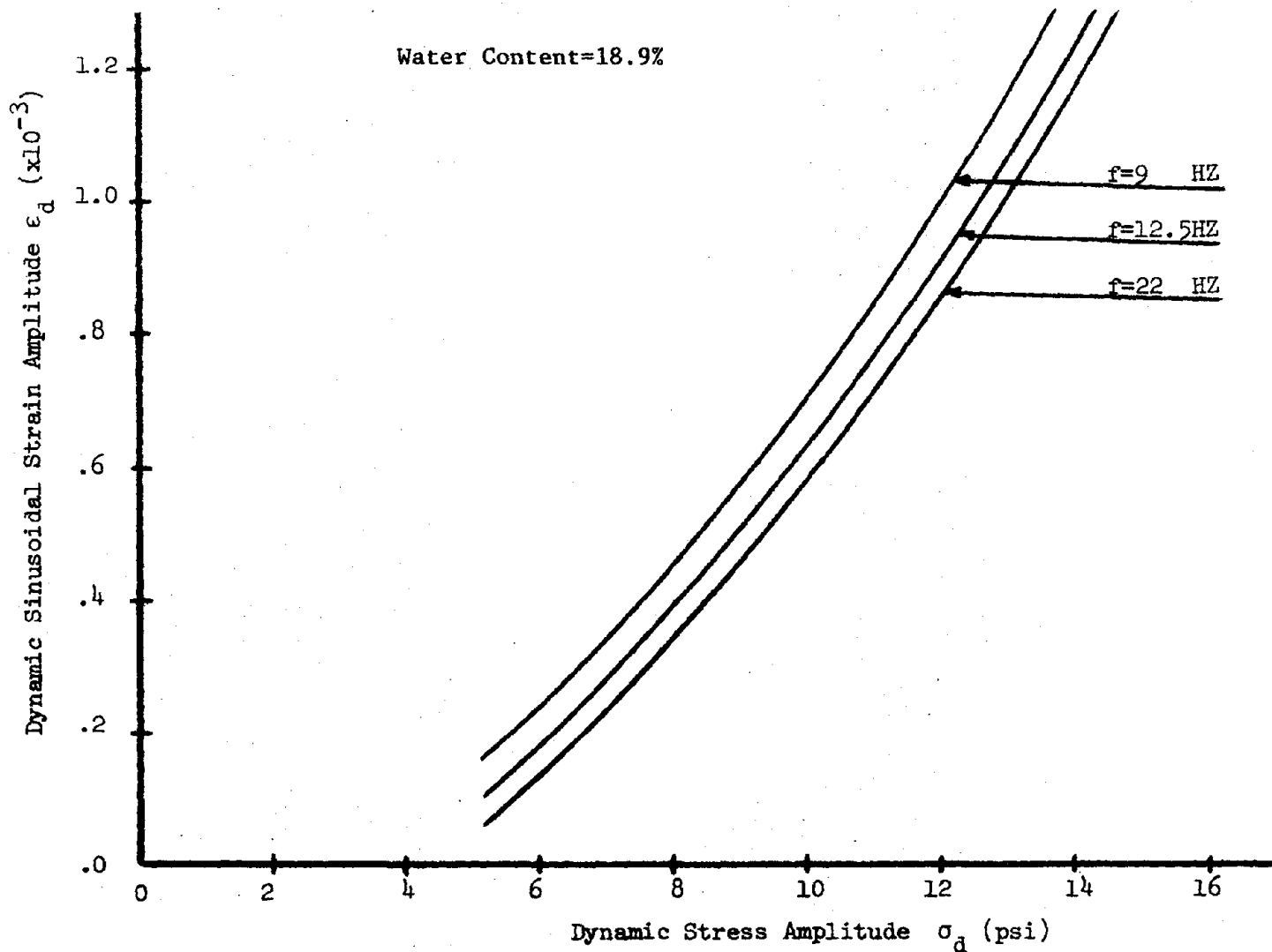
Figure 32. Variation of Dynamic Sinusoidal Strain Amplitude with Dynamic Sinusoidal Stress Amplitude for Different Frequencies
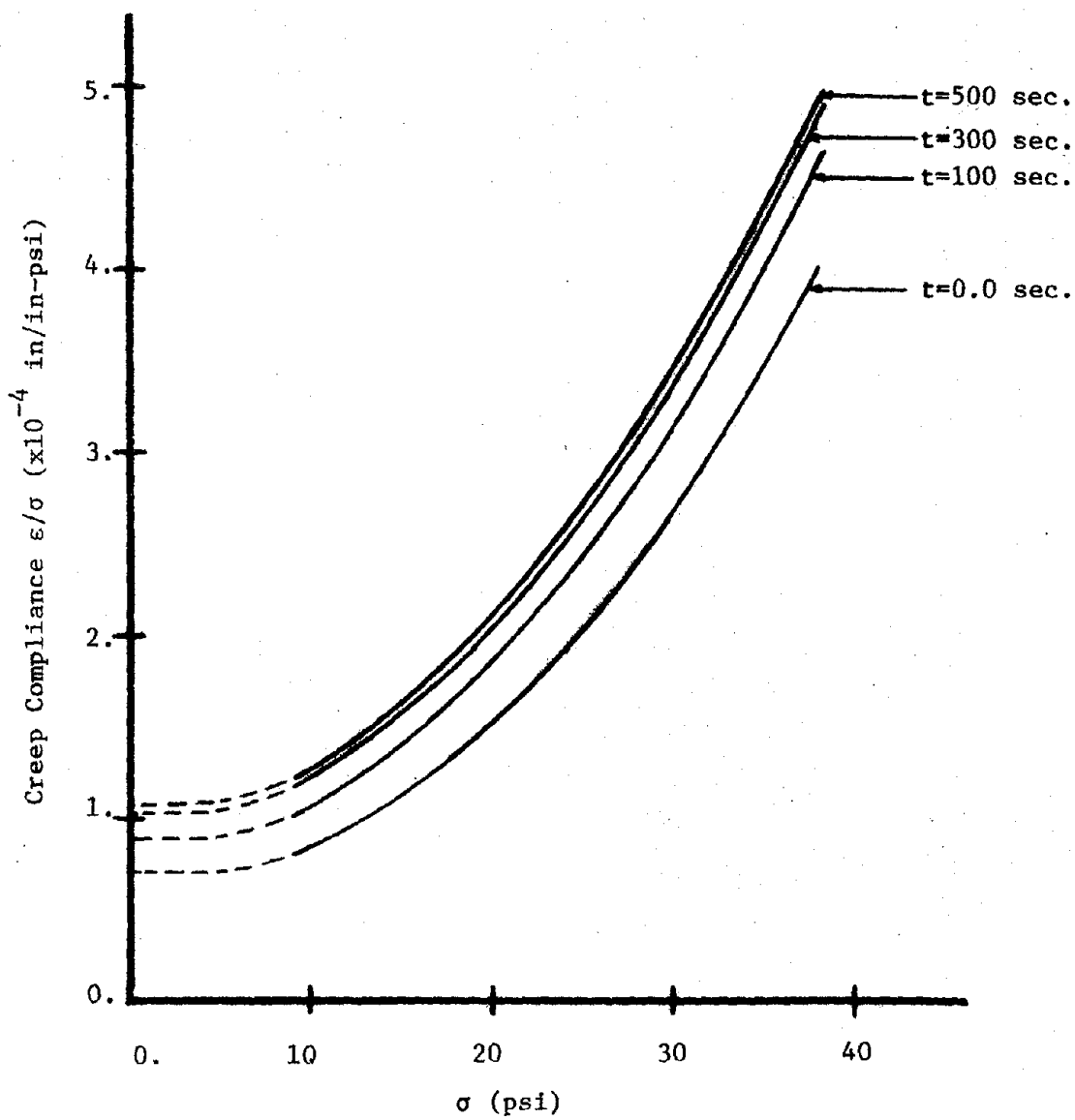
Figure 33. Variation of Creep Compliance for Single-Step Loading Condition with Stress for Different Time of Loading

nonlinear. The slope of this curve in this region increases with stress magnitude. The linear range was observed for stress level lower than 10 psi. In this region, the slope of creep compliance-stress curve is zero. As shown in Figure 33, the creep compliance rapidly increases with stress for each time value beyond the stress level of 10 psi.

The measured creep compliance function was found fit with an equation of a polynomial type with three terms as follows:

$$\frac{\varepsilon}{\sigma} = D_1 + D_2\sigma + D_3\sigma^2 \tag{26}$$

A computer program for curve fitting based upon the least square method was performed in APL language, as shown in Appendix A. This program is able to estimate the required terms for best fit. The curve fitting was done, for all four different time intervals discussed earlier. The kernel functions, $D_1(t)$, $D_2(t,t)$, and $D_3(t,t,t)$, as obtained by fitting the data, are shown in Figures 34, 35, and 36. Figures show that $D_1(t)$ and $D_3(t,t,t)$ increase with time, whereas, $D_2(t,t)$ decreases with time. For lower time interval, the influence of $D_2(t,t)$ on the total response is significant, and it decreases rapidly with the increment of time. As shown in Figure 35, for higher time interval, the second order kernel function in equation (26), is not very sensitive and very rapidly decreases in value.

In order to approximate the first order kernel function $D_1(t)$, a curve fitting program based upon the least square method was developed (see Appendix A). The slope of $D_1(t)$ for different time was plotted in a semi-log scale as shown in Figure 37. This figure shows,
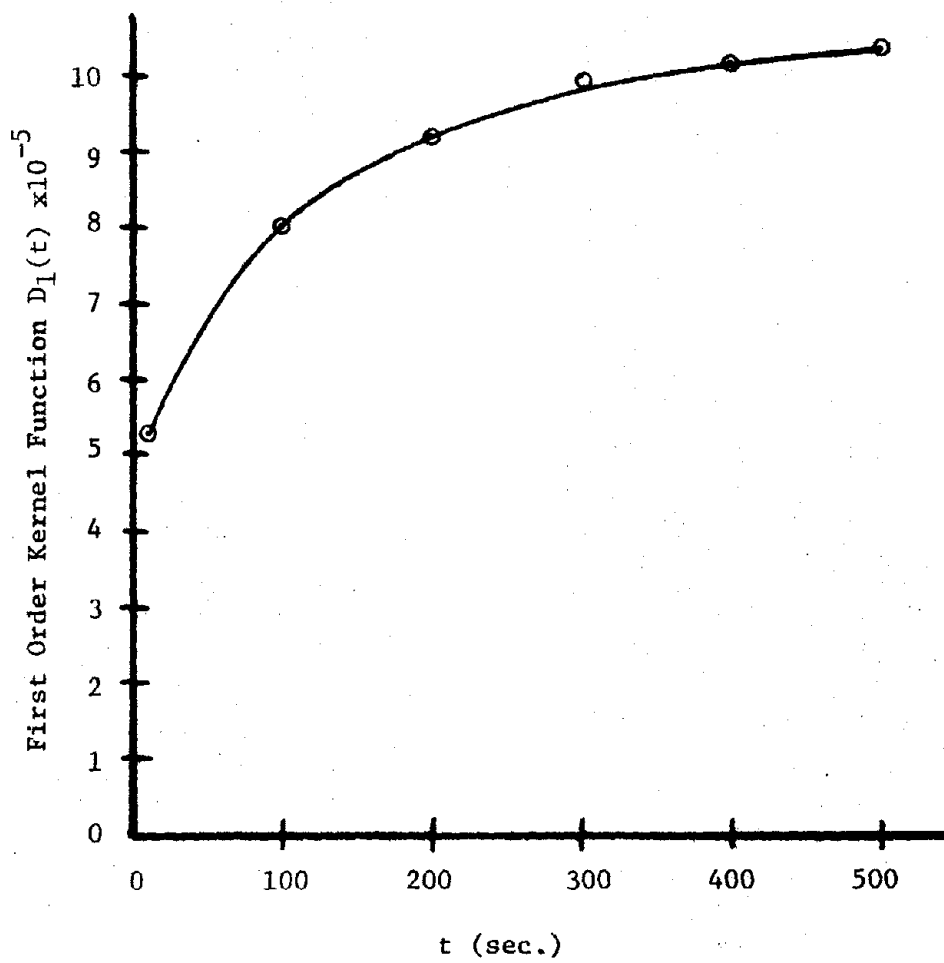
Figure 34. Variation of the First Order Kernel Function
with Time
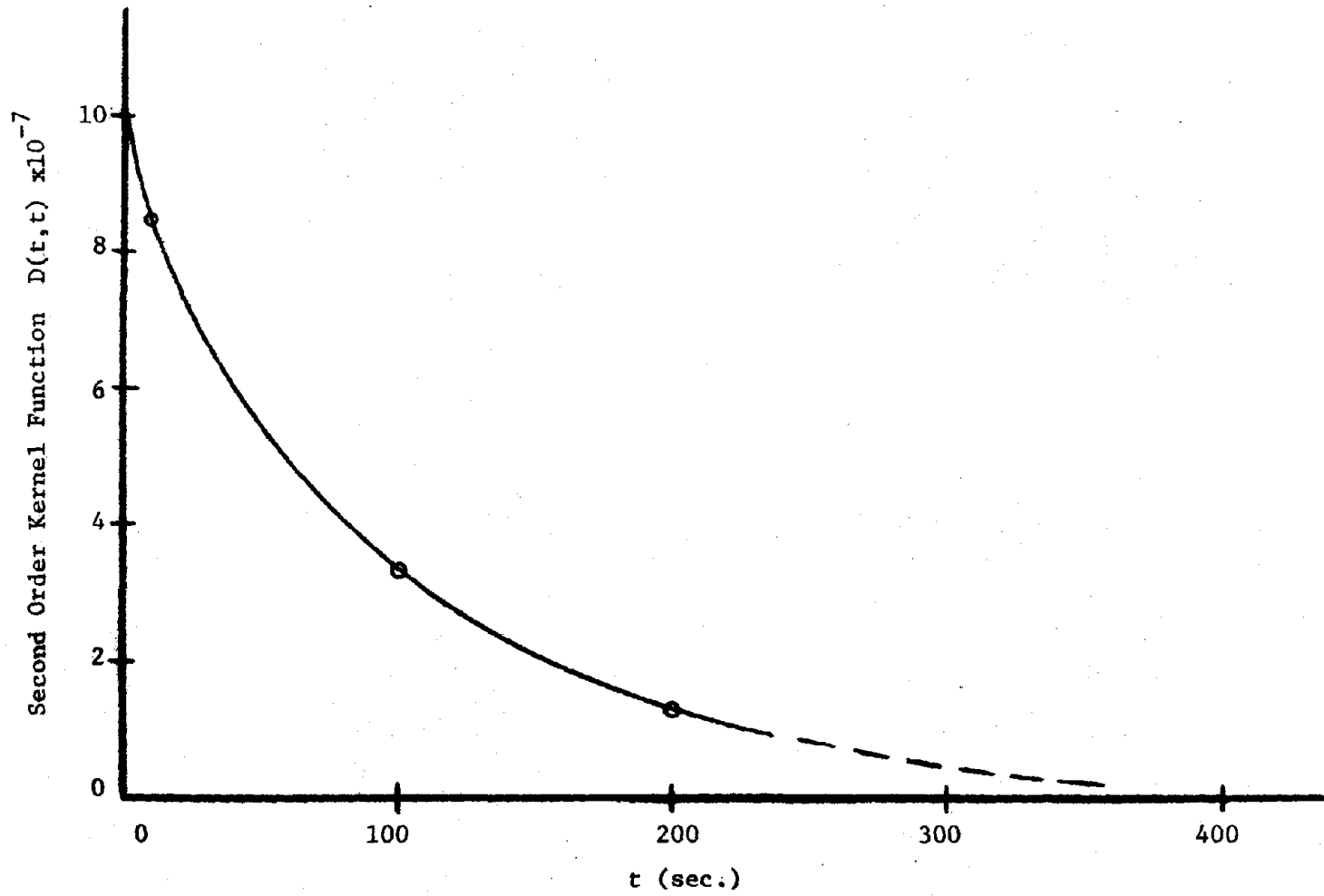
Figure 35. Variation of the Second Order Kernel Function with Time
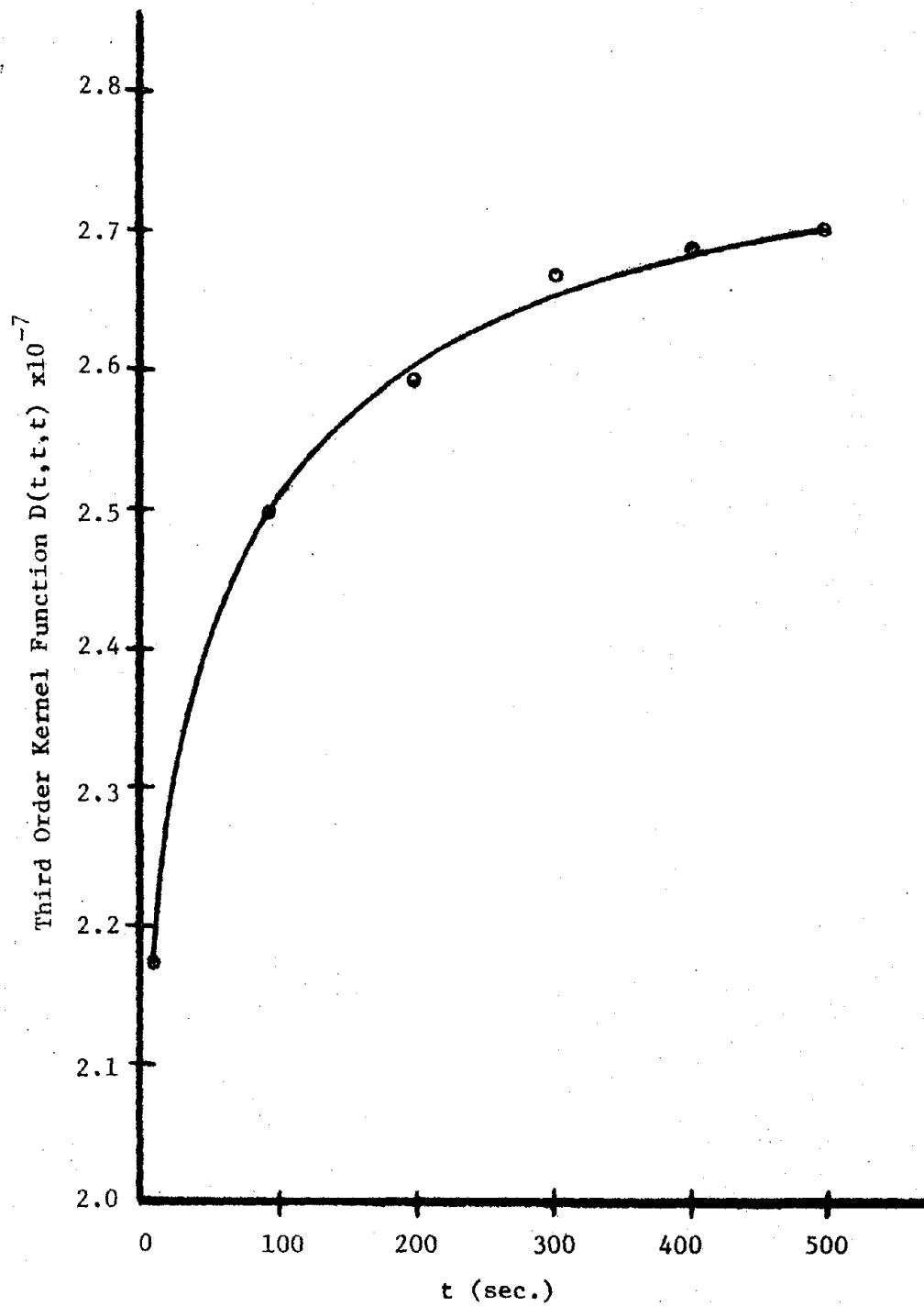
Figure 36.   Variation of the Third Order Kernel Function
with Time
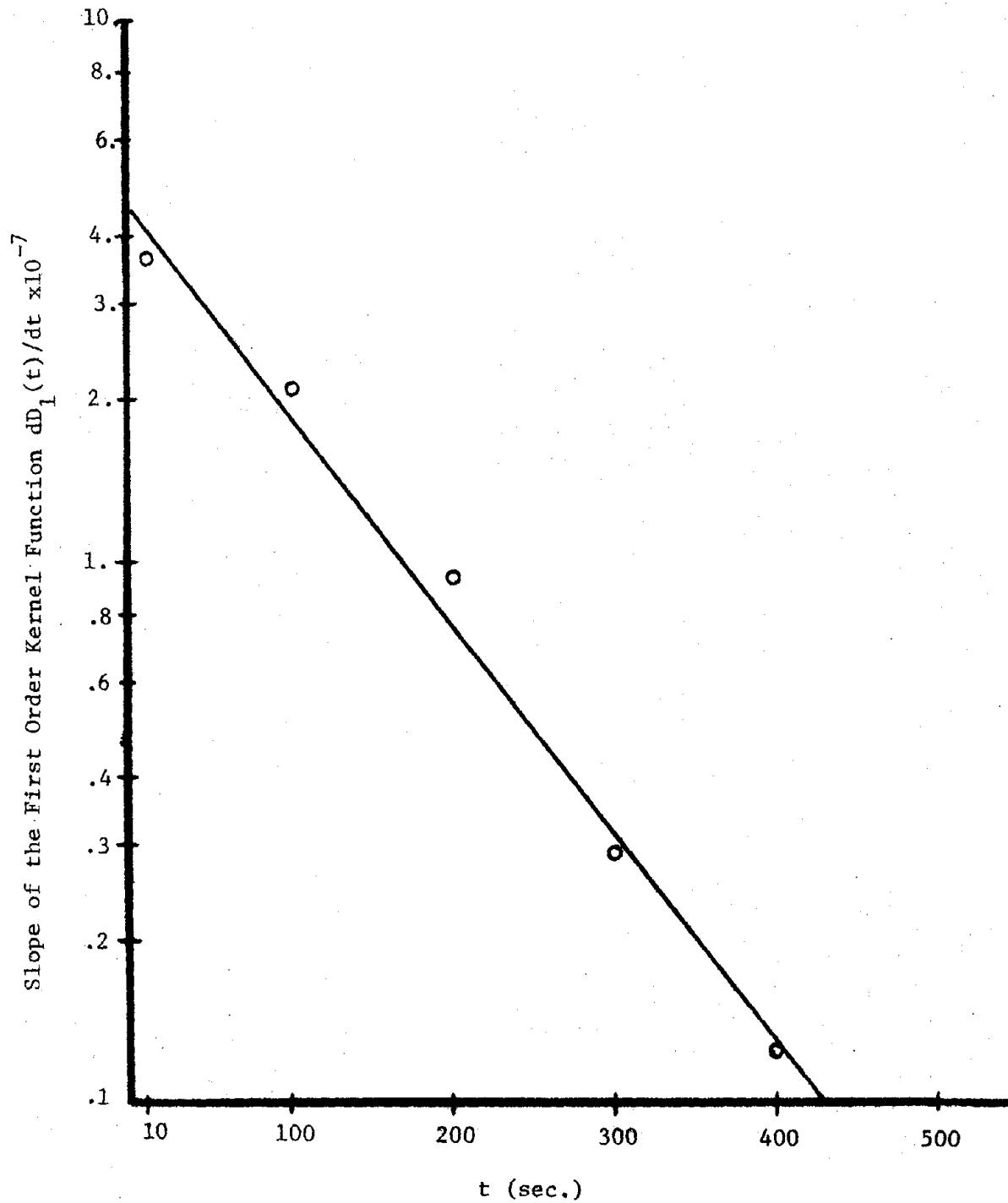
Figure 37. Variation of the Slope of the First Order Kernel
Function with Time (Semi-Log Scale)

$\dfrac{dD_1(t)}{dt}$ is linearly decreasing with time. Therefore, the first

order kernel function can be defined as the following equation:

$$D_1(t) = [4.99 + 5.09(1 - e^{-\frac{t}{110}})] \times 10^{-5} \qquad (27)$$

The second order kernel function $D_2(t,t)$, can be obtained by

plotting $D_2(t,t)$ against time in a semi-log scale, as shown in

Figure 38. The curve shows that the logarithm of D_2 decreases

linearly with time. The following equation is the second order

kernel function obtained from Figure 38.

$$D_2(t,t) = 9.25 \times 10^{-7} e^{-\frac{t}{100}} \qquad (28)$$

Figures 34 and 36 show that the third order kernel function has

the same type of curve as the first order. Therefore, the same

procedures were followed to determine the third order kernel func-

tion as was done for the first order. The slope of $D_3(t,t,t)$

versus time is shown in Figure 39. The figure indicates that the

third order kernel function can be represented by the following

relation:

$$D_3(t,t,t) = [2.2 + .47(1 - e^{-\frac{t}{100}})] \times 10^{-7} \qquad (29)$$

In view of equations 27-29, the uniaxial creep response of the

cohesive soil for a duration less than 500 seconds, can be given as:

$$\varepsilon(t,\sigma) = [4.99 + 5.09(1 - e^{-\frac{t}{100}})] \times 10^{-5}\, \sigma + 9.25 \times 10^{-7} e^{-\frac{t}{100}} \sigma^2 +$$

$$[2.2 + .47(1 - e^{-\frac{t}{100}})] \times 10^{-7} \sigma^3 \qquad (30)$$
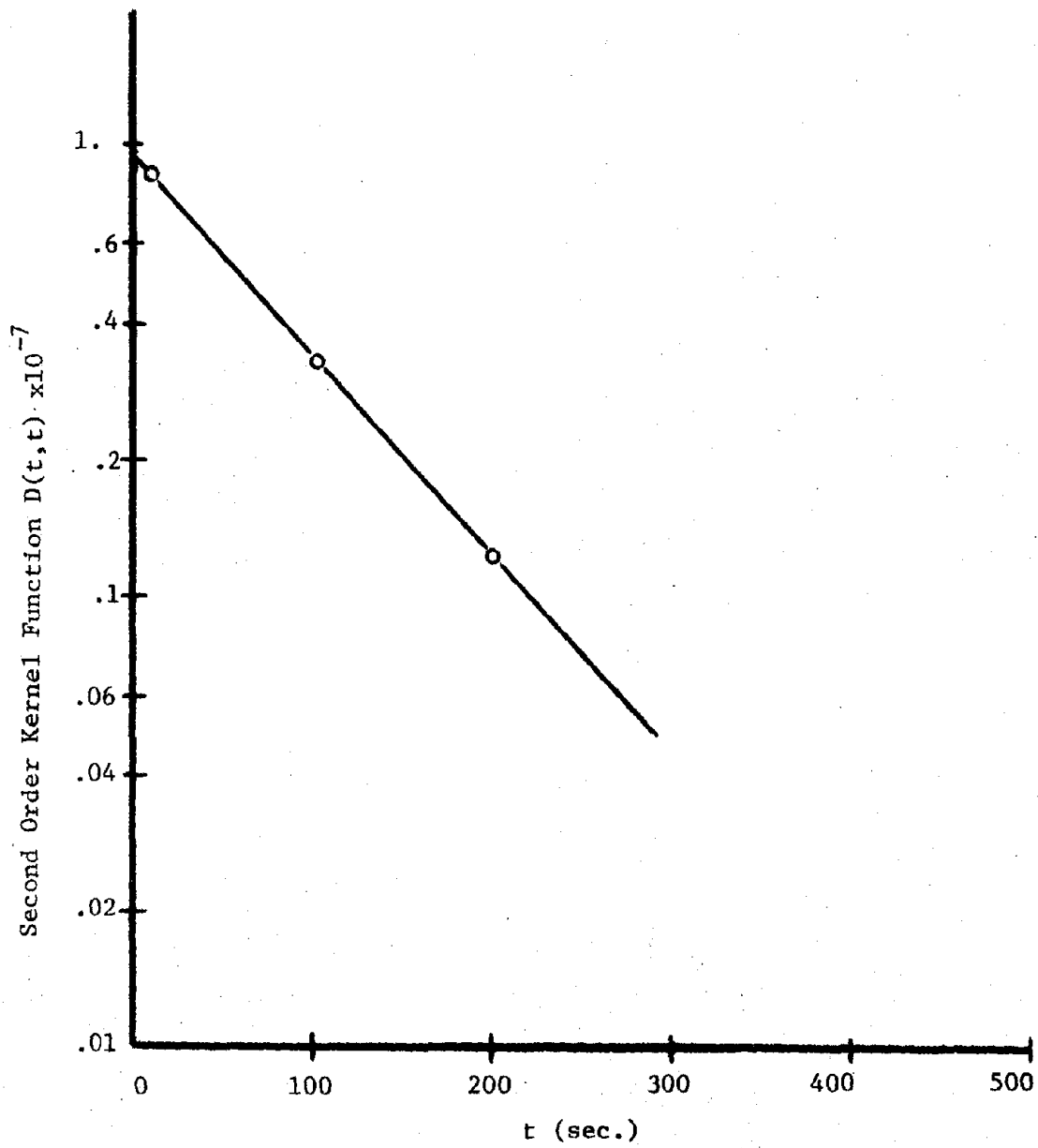
Figure 38. Variation of the Second Order Kernel Function with
Time (Semi-Log Scale)
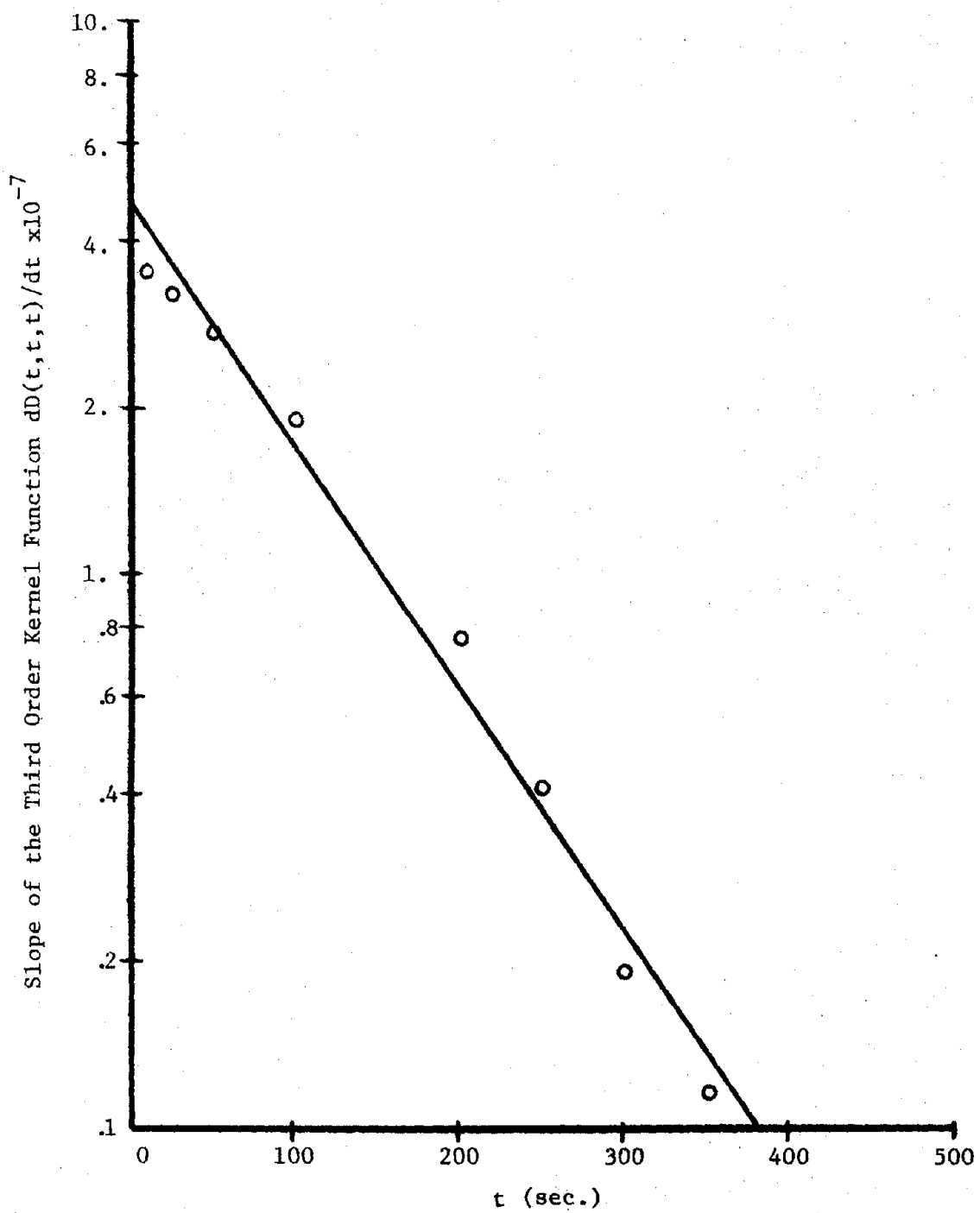
Figure 39. Variation of the Slope of the Third Order Kernel
Function with Time (Semi-Log Scale)

Figure 14 shows the comparison between the theoretical and experimental curves. This figure shows that equation (30) correlates with the experimental results closely with the error between the experimental and theoretical curves being less than five percent (see Appendix A).

4.2.2 Two-Step Loading

The response of soil under two-step loading condition was predicted by substituting equations (27), (28), and (29) in equation (13). A computer program in APL language was developed to facilitate the numerical computations (see Appendix A).

The experimental results show that the instantaneous time dependent creep response for the second step depends upon the stress magnitude, as well as the time at which the second step was imposed. The overall instantaneous time independent strain response which is, the summation of instantaneous strains for the first and second steps right after application of load, ε_{02} with respect to the time of the application of the second step loading t_1 is shown in Figure 40. This figure shows ε_{02} is decreasing with the increment of t_1. To obtain a relation for ε_{02} with respect to t_1, curves in Figure 40, were replotted on a log-log scale as shown in Figure 41. These curves show that the logarithm of ε_{02} is decreasing linearly with the logarithm of t_1, for a constant stress magnitude. As t_1 tends to one second, D_{02} tends to the instantaneous time independent strain value for a single-step creep, for a stress value equal to the sum of the stresses for two steps. Therefore, the overall instantaneous time independent strain for two-step loading condition can be
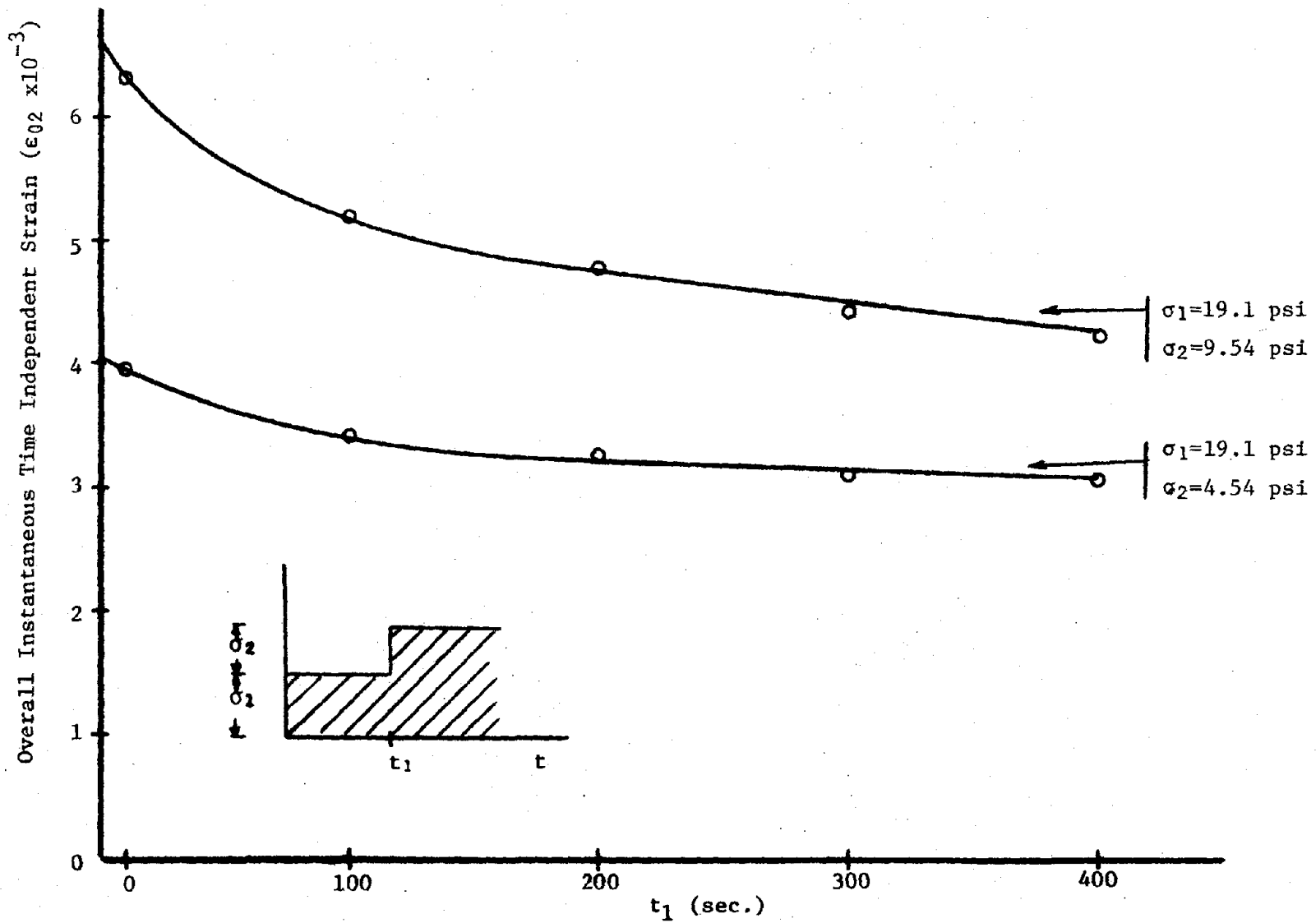
Figure 40. Overall Instantaneous Time Independent Strain for Two-Step Loading Tests vs. t_1
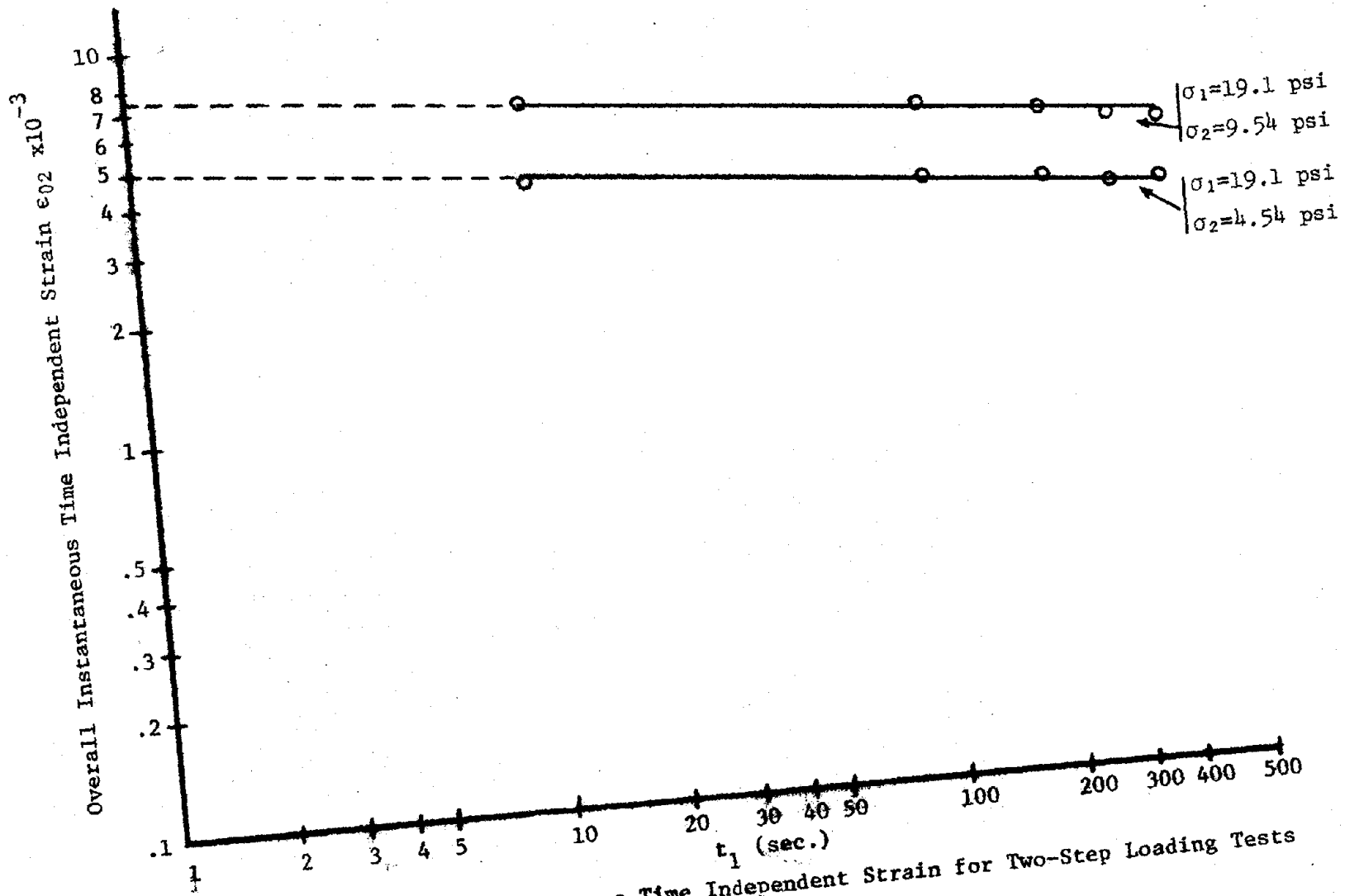
Figure 41. Overall Instantaneous Time Independent Strain for Two-Step Loading Tests vs. t_1 (log-log scale)

represented by the following equation:

$$\varepsilon_{02}(t_1) = \varepsilon_{oo}t_1^{-.1} \qquad t_1 > 1 \text{ sec.} \qquad (31)$$

where ε_{oo} is the instantaneous time independent strain from single-step creep response.

The theoretical and experimental results for two stress levels and different t_1 are shown in Figure 17 through Figure 21. The error between the experimental two-step creep response curves and that evaluated by equation (13), was less than 12 percent (see Appendix A).

4.2.3 Three-Step Loading

The response of a nonlinear viscoelastic material for three-step loading condition was described by equation (15). The kernel functions in this equation can be obtained by equations (27), (28), and (29). A computer program in APL was performed to represent the response of soil for different stress levels, as well as, different time of application of second and third step loading (see Appendix A).

The experimental results from three-step loading tests show that the overall instantaneous time independent strain, ε_{03}, varies with stress magnitudes, as well as the time of application of the second and third step loading. Figure 42 shows the variation of ε_{03} for different t_1 and t_2. The instantaneous time independent strain was obtained from the experimental results and used in the computer program to determine the approximate response of soil under uniaxial three-step loading conditions. In Figure 25 through Figure 29 are compared the theoretical and experimental results for three-
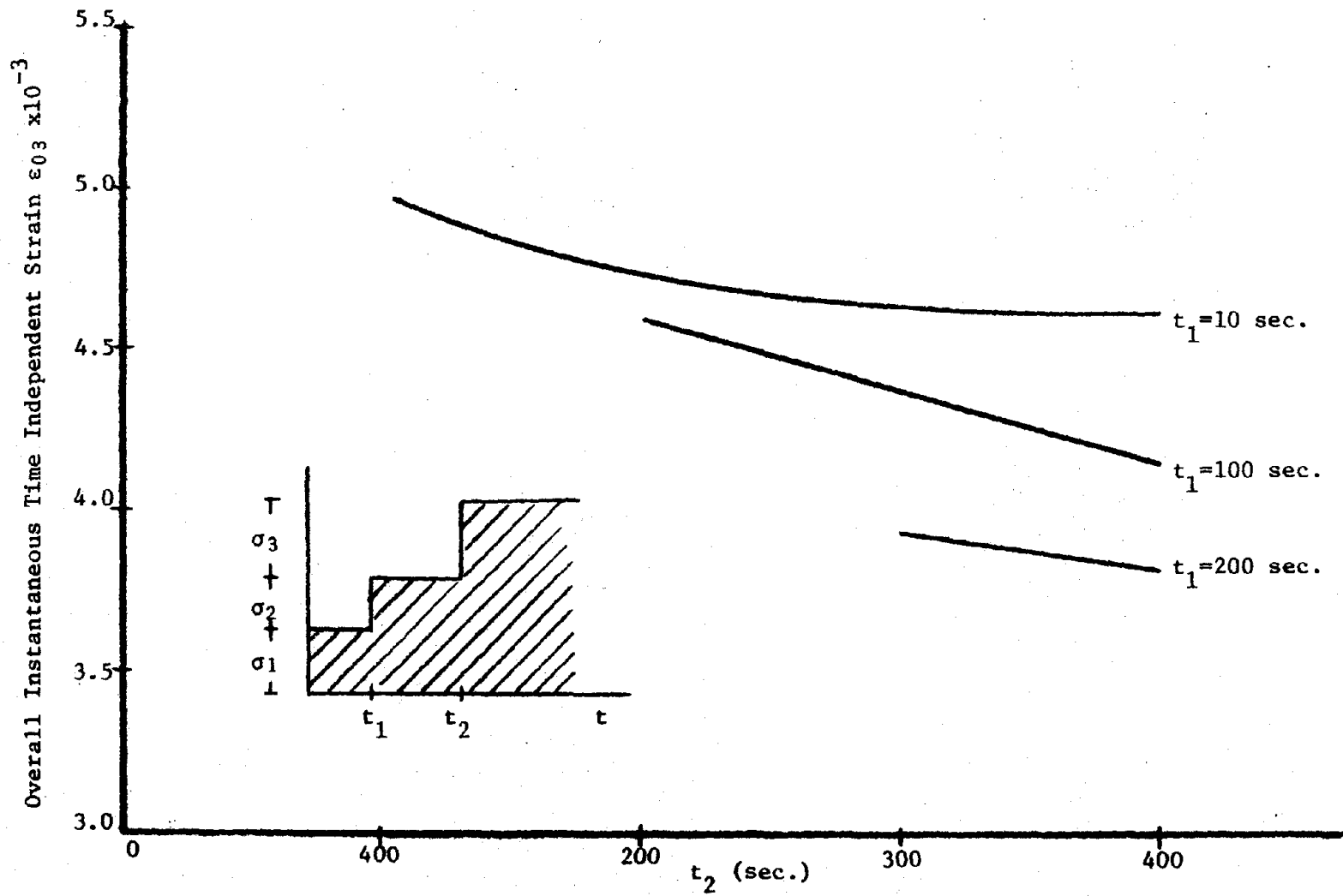
Figure 42. Overall Instantaneous Time Independent Strain for Three-Step Loading Tests vs. T_2 for Different T_1

step loading conditions on soil. The error between the experimental and theoretical curves for three-step loading tests has been found to be less than 10 percent (see Appendix A).

4.2.4 Dynamic Sinusoidal Loading

The results from the dynamic sinusoidal loading tests show that the response of the cohesive soil under dynamic loading condition is almost independent of mean stress amplitude. In other words, the dynamic strain does not vary with the mean stress, whereas, the overall strain response increases as a result of the creep effect from the mean stress on soil specimens. Figure 30 indicates that the dynamic sinusoidal strain amplitude decreases with the total number of cycles. Figures 31 and 32 show that the dynamic strain amplitude decreases with frequency, and increases rapidly with the stress amplitude. Figure 43 shows that the energy loss decreases with the frequency for a constant dynamic stress amplitude. The energy loss was obtained by evaluating area of hystersis loop.
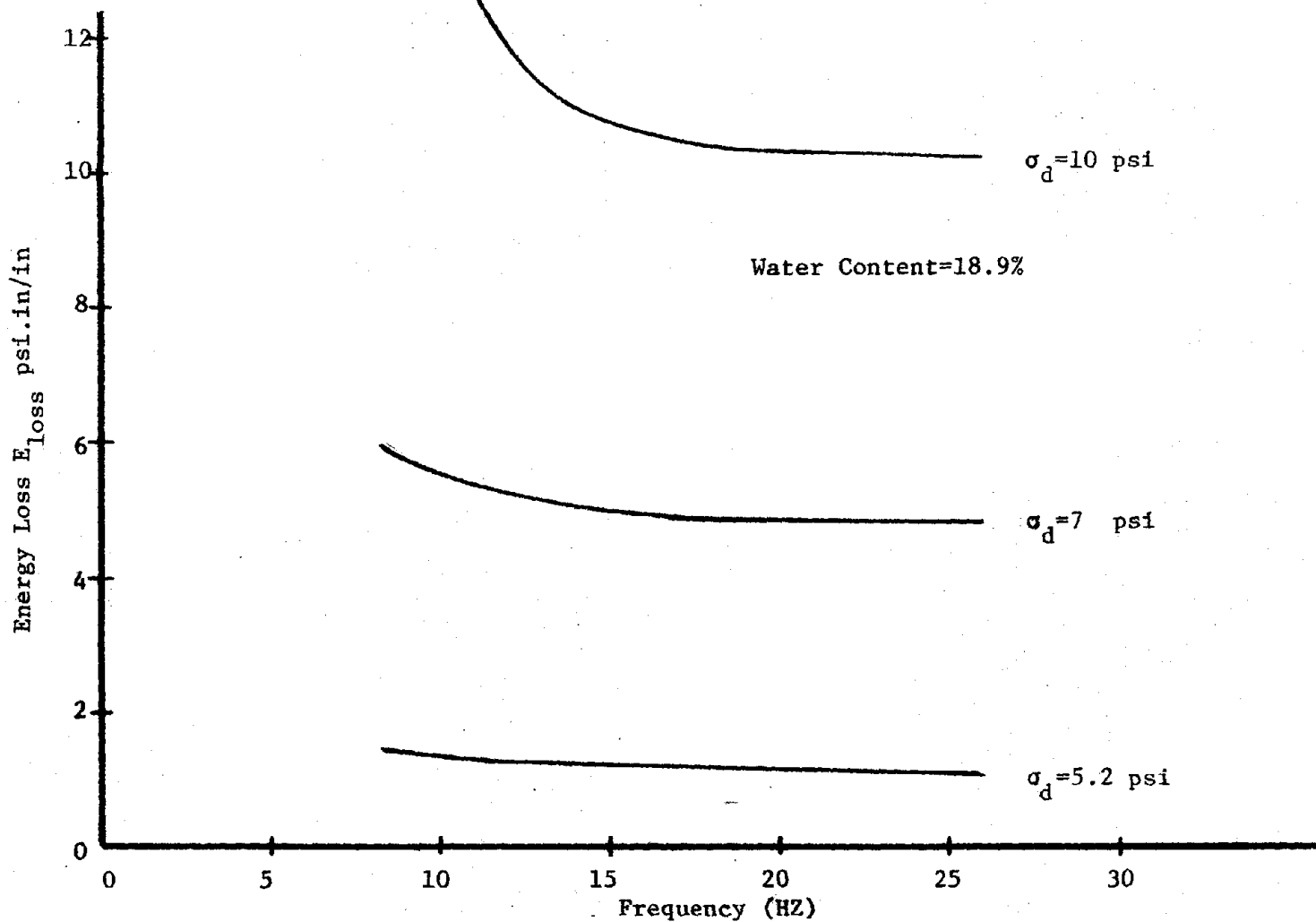
Figure 43. Variation of Energy Loss with Frequency for Different Dynamic Sinusoidal Stress Amplitude

CHAPTER V

SUMMARY AND CONCLUSIONS

5.1 Summary

The uniaxial creep behavior of a cohesive soil under single and multi-step loading has been studied in this thesis. A one-dimensional constitutive relationship based upon the multiple integral representation, has been developed to characterize the observed nonlinear viscoelastic behavior of the material. In order to obtain the constitutive relationship, various uniaxial single-step creep tests were performed using a specially developed test apparatus. These tests were performed for a short time (500 sec.), and for a wide range of stress amplitudes up to the failure. It has shown that the time-dependent kernel function can be expressed in the form of an exponential series. Experimental results from two- and three-step creep loading tests show that the creep response of soil under multi-step loading conditions can be predicted by the constitutive relationship that is obtained from the single-step creep tests. The dynamic behavior of soil has also been studied by performing dynamic sinusoidal loading tests on cylindrical samples of the test material using a specially designed apparatus

5.2 Conclusions

The following conclusions can be drawn from the results of the theoretical and experimental study:

(1) The behavior of cohesive soil under creep loading is linear for lower stress levels (less than 10 psi). The nonlinearity of the material which was studied in this thesis was observed for stress levels higher than 10 psi.

(2) The creep response function with respect to the stress amplitude can be represented by a polynomial series containing terms up to and including the third order. The coefficients of the polynomial are only time dependent and are defined as the kernel functions.

(3) The first and third order kernel functions increase with time, whereas, the second order kernel function decreases rapidly with time. The contribution of the second order kernel function to the creep behavior is significant for lower time intervals,whereas,for times higher than 300 seconds , its influence is minimal.

(4) The proposed constitutive relationship for single-step creep behavior can be generalized for two- and three-step loading conditions, as well as for dynamic creep behavior.

(5) The multiple integral representation of kernel functions obtained from single-step creep tests has been found to agree well with the experimental data from multi-step loading tests.

(6) The results from dynamic sinusoidal loading tests show that the dynamic strain amplitude decreases with frequency, and increases with dynamic stress amplitude. Also, the energy loss decreases with frequency for a constant dynamic stress amplitude.

5.3 Suggestions for Further Research

The author suggests the following topics for further research.

(1) Experimental and theoretical investigation of cohesive soils under multi-axial creep behavior must be studied and the results must be compared with in situ test results.

(2) Plastic and viscoplastic behavior of soils must be studied by performing the repeated loading, and creep-recovery tests.

(3) Nonlinear viscoelastic behavior of cohesive soils under other
dynamic loading conditions must be investigated,and the effect of confining
pressure on the dynamic mechanical behavior must be studied.

BIBLIOGRAPHY

1. Whitmann, R. V., Protonotarios, J. N. and M. F. Nelson, "Case Study of Dynamic Soil-Structure Interaction," Journal of Solid Mech. Found. Division, (ASCE), SM11, 1973, pp. 997-1009.

2. Parmalee, R. A., Perelman, D. S. and S. L. Lee, "Seismic Response of Multiple-Story Structures on Flexible Foundation," Bulletin Seismo., Soc. Am., Vol. 59, No. 3, 1969.

3. Veletsos, A. S. and B. Verbic, "Vibration of Viscoelastic Foundations," Earthquake Engineering and Structural Dynamics, Vol. 2, 1973, pp. 87-102.

4. Drescher, A., "Nonlinear Creep of Cohesive Soil," Archiuum Mechaniki Stosowanez, 5, 19, 1967.

5. Lockett, F. J., "Creep and Stress-Relaxation Experiments for Nonlinear Materials," Int. J. Engng. Sci., Vol. 3, Pergamon Press, Great Britain, 1965, pp. 59-75.

6. Wilson, S. D., and R. J. Dietrich, "Effect of Consolidation Pressure on Elastic and Strength Properties of Clay," Proc. American Society of Civil Engineering, Research Conference on Shear Strength of Cohesive Soils, 1960, pp. 419-435.

7. Mitchell, J. K. and J. R. McConnell, "Some Characteristic of the Elastic and Plastic Deformation of Clay on Initial Loading," Proceedings of the 6th International Conference on Soil Mechanics and Foundation Engineering, 1, Montreal, 1965.

8. Murayama, S. and T. Shibata, "Rheological Properties of Clays," Proc. 5th ICOSOMFE, 1, Paris, 1961, p. 269.

9. Vialov, S. S. and A. M. Skibitsky, "Problems of the Rheology of Soils," Proc. 5th ICOSOMFE, 1, Paris, 1961, p. 387.

10. Vialov, S. S. and A. M. Skibitsky, "Rheological Processes in Frozen Soils and Dense Clays," Proc. 4th ICOSOMFE, 1, London, 1957, p. 120.

11. Folque, J., "Rheological Properties of Compacted Unsaturated Soils," Proceedings of 5th ICOSOMFE, 1, Paris, 1961, p. 113.

12. Barden, L., "Consolidation of Clay With Nonlinear Viscosity," Geotechnique, 4, 15, 1965.

13. Kondner, R. L. and R. J. Krizek, "Creep Compliance Response of a Cohesive Soil," Journal of the Franklin Institute, Vol. 279, 1965, pp. 366-373.

14. Kondner, R. L., "Characteristic Periods of Cohesive Soil-Foundation Systems," Proceedings of the Third World Conference on Earthquake Engineering, Vol. 1, New Zealand, 1965.

15. Kondner, R. L., "Stress-Strain-Time Spectrum Response of a Cohesive Soil," Applied Polymer Symposia, No. 1. 1965, pp. 147-162.

16. Kondner, R. L. and R. J. Krizek, "Correlation of Creep and Dynamic Response of a Cohesive Soil," International Union of Theoretical and Applied Mechanics, Rheology and Soil Mechanics Symposium, Grenoble, 1964, pp. 333-342.

17. Krizek, R. J., "Application of the One-Sided Fourier Transform to Determine Soil Storage and Dissipation Characteristics," Proceedings of the Symposium on Soil-Structure Interaction, Tucson, Arizona, 1964, pp. 625-633.

18. Kondner, R. L., and M. M. K. Ho, "Viscoelastic Response of a Cohesive Soil in the Frequency Domain," Transaction of the Society of Rheology, 9:2, 1965, pp. 329-342.

19. Kondner, R. L. and R. J. Krizek, "Dynamic Response of Cohesive Soils for Earthquake Considerations," Proceedings of the Third World Conference on Earthquake Engineering, Vol. 1, New Zealand, 1965.

20. Krizek, R. J. and A. G. Franklin, "Energy Dissipation in a Soft Clay," Proceedings of the International Symposium on Wave Propagation and Dynamic Properties of Earth Material, 1967, pp. 797-807.

21. Kondner, R. L. and J. B. Forrest, "Dynamic Compression of Clay Under an Explosive Pulse," Transaction of the Society of Rheology, 10:1, 1966, pp. 253-273.

22. Klausner, Y., "Volumetric Stress-Strain Relationships in Soils," Proceedings of the 5th International Congress on Rheology, Vol. 2, 1970, pp. 591-602.

23. Drnevich, V. P., "Resonant-Column Testing Problems and Solutions," Dynamic Geotechnical Testing, ASTM, STP 654, Denver, Colorado, 1977.

24. Drnevich, V. P., Hardin, B. O. and D. J. Shippy, "Modulus and Damping of Soils by the Resonant-Column Method," Dynamic Geotechnical Testing, ASTM, STP 654, Denver, Colorado, 1977.

25. Green, A. E. and R. S. Rivlin, "The Mechanics of Nonlinear Materials With Memory, Part I," Archive for Rational Mechanics and Analysis, Vol. 1, 1957, p. 1.

26. Green, A. E., Rivlin, R. S. and A. J. M. Spencer, "The Mechanics of Nonlinear Materials With Memory, Part II," Archive for Rational Mechanics and Analysis, Vol. 3, 1959, p. 82.

27. Green, A. E., and R. S. Rivlin, "The Mechanics of Nonlinear Materials With Memory, Part III," _Archive for Rational Mechanics and Analysis_, Vol. $\underline{4}$, 1960, p. 387.

28. Pipkin, A. C., and T. G. Rogers, "A Nonlinear Integral Representation for Viscoelastic Behaviour," _J. Mech. Phys. Solids_, Pergamon Press, Great Britain, Vol. $\underline{16}$, 1968, pp. 59-72.

29. Nakada, O., "Theory of Nonlinear Response," _Journal of the Physical Society of Japan_, Vol. $\underline{15}$, No. 12, 1960, pp. 2280-2288.

APPENDIX A

COMPUTER PROGRAMS AND A TYPICAL OUTPUT DATA

```
     ∇ Z←Y FIT X
[1]    Z←Y⊞X∘.*0,ι2
     ∇
```

```
     ∇  Z←T CREEP S;L1;L3;Y;D10;D11;D30;D31;A;B;D2;L2
[1]      '******************************'
[2]      L1←115
[3]      L2←100
[4]      L3←100
[5]      D10←4.9892E¯5
[6]      D11←5.175E¯5
[7]      D2←9.25E¯7
[8]      D30←2.2E¯7
[9]      D31←4.7E¯8
[10]     Y←(D10+(D11×(1-*(-T÷L1))))×S
[11]     Y←Y+(D2×(*(-T÷L2))×S×S)
[12]     Y←Y+((D30+(D31×((1-*(-T÷L3)))))×S×S×S)
[13]     A← 16 1 ρT
[14]     B← 16 1 ρY
[15]     '        TIME               STRAIN'
[16]     '******************************'
[17]     '******************************'
[18]     Z←A,B
     ∇
```

T CREEP 14.1

```
* * * * * * * * * * * * * * * * * * * * * * * * * * * * * * *
      TIME                  STRAIN
* * * * * * * * * * * * * * * * * * * * * * * * * * * * * *
* * * * * * * * * * * * * * * * * * * * * * * * * * * * *
```

TIME	STRAIN
$0.000000000E0$	$1.504085070E^-3$
$1.000000000E1$	$1.559892103E^-3$
$2.000000000E1$	$1.611110308E^-3$
$3.000000000E1$	$1.658116248E^-3$
$4.000000000E1$	$1.701255656E^-3$
$5.000000000E1$	$1.740845955E^-3$
$6.000000000E1$	$1.777178571E^-3$
$7.000000000E1$	$1.810521052E^-3$
$8.000000000E1$	$1.841119024E^-3$
$9.000000000E1$	$1.869197978E^-3$
$1.000000000E2$	$1.894964921E^-3$
$1.500000000E2$	$1.995251062E^-3$
$2.000000000E2$	$2.060485388E^-3$
$3.000000000E2$	$2.130482146E^-3$
$4.000000000E2$	$2.160048802E^-3$
$5.000000000E2$	$2.172525302E^-3$

```
    ∇ Z←T TWO S;Y;L1;L3;D0;D00;D11;D31;A;P;D2;D2;C
[1]    L1←115
[2]    L2←100
[3]    L3←100
[4]    D00←D
[5]    D11←5.175E¯5
[6]    D2←9.25E¯7
[7]    D31←4.7E¯8
[8]    D0←D00+((4.9892E¯5)×S[1])+((2.20225E¯7)×((S[1]*3))
[9]    Y←D0+(D11×(1-*(-T÷L1))×S[1])
[10]   Y←Y+(D11×(1-*((S[3]-T)÷L1))×S[2])
[11]   Y←Y+(D2×(*(-T÷L2))×(S[1]*2))+(D2×(*(-(T-S[3])÷L2))×(S[2]*2))
[12]   Y←Y+(2×S[1]×S[2]×D2×(*(-T÷(2×L2)))×(*(-(T-S[3])÷(2×L2))))
[13]   Y←Y+((D31×(1-*(-T÷L3))×(S[1]*3)))
[14]   Y←Y+(D31×(1-*(-(T-S[3])÷L3))×(S[2]*3))
[15]   Y←Y+(3×(S[1]*2)×(S[2])×(D31×((1-*(-T÷L3))*(2÷3))×(1-*(-(T-S[3])÷L3))*(1÷3)))
[16]   Y←Y+(3×(S[1])×(S[2]*2)×(D31×((1-*(-T÷L3))*(1÷3))×((1-*(-(T-S[2])÷L3))*(2÷3))))
[17]   C←D
[18]   C←(Y-C)×100÷C
[19]   A← 30 1 ρT
[20]   P← 30 1 ρY
[21]   C← 30 1 ρC
[22]   '*******************************************'
[23]   '   TIME                STRAIN          ERROR'
[24]   '*******************************************'
[25]   Z←A,P,C
    ∇
```

T11 TWO 14.1 9.54 10

Γ:

3Γ⁻3

Γ:

Y11+1.4Γ⁻3

```
**************************************************
    TIME               STRAIN            ERROR
**************************************************
   1.500000000E1      4.953701227E⁻3     8.687665962E0
   2.000000000E1      5.007553785E⁻3     4.405821747E0
   2.500000000E1      5.058113631E⁻3     2.010592704E0
   3.000000000E1      5.106158624E⁻3     1.226708742E0
   3.500000000E1      5.151977040E⁻3     2.392569166E⁻1
   4.000000000E1      5.195736309E⁻3    ⁻2.277677035E⁻2
   5.000000000E1      5.277547740E⁻3    ⁻8.154999013E⁻1
   6.000000000E1      5.352372267E⁻3    ⁻1.006653353E0
   7.000000000E1      5.420844668E⁻3    ⁻1.307478189E0
   8.000000000E1      5.483521136E⁻3    ⁻1.025905611E0
   9.000000000E1      5.540900969E⁻3    ⁻1.516453879E0
   1.000000000E2      5.593 436742E⁻3   ⁻1.085853151E0
   1.100000000E2      5.641540487E⁻3    ⁻1.399595092E0
   1.300000000E2      5.725923232E⁻3    ⁻1.079344350E0
   1.500000000E2      5.796684748E⁻3    ⁻6.753697122E⁻1
   1.700000000E2      5.856029350E⁻3    ⁻6.330905466E⁻1
   1.900000000E2      5.905802742E⁻3    ⁻2.728363207E⁻1
   2.100000000E2      5.947551196E⁻3    ⁻8.457225012E⁻1
   2.500000000E2      6.011946844E⁻3    ⁻5.629055397E⁻1
   2.900000000E2      6.057265315E⁻3    ⁻1.062259044E0
   3.300000000E2      6.089163934E⁻3    ⁻1.462504757E0
   3.700000000E2      6.111620352E⁻3    ⁻2.006789148E0
   4.100000000E2      6.127431980E⁻3    ⁻2.498981931E0
   5.000000000E2      6.147976193E⁻3    ⁻3.345865575E0
```

```
      ∇ Z←T STEP3 S;Y;L1;L3;D00;D11;D31;D0;A;B;C;D;E;F;P;C;R;RR;V;D2;L2
[1]    L1←115
[2]    L2←100
[3]    L3←100
[4]    D11←5.175E¯5
[5]    D2←9.25E¯7
[6]    D31←4.7E¯8
[7]    D0←□
[8]    D00←□
[9]    R←□
[10]   A←(1-*(-T÷L1))
[11]   B←(1-*(-(T-S[4])÷L1))
[12]   C←(1-*(-(T-S[5])÷L1))
[13]   D←(1-*(-T÷L3))
[14]   E←(1-*(-(T-S[4])÷L3))
[15]   F←(1-*(-(T-S[5])÷L3))
[16]   Y←D0+D00+((4.9892E¯5)×S[1])+((2.20225E¯7)×((S[1])*3))
[17]   Y←Y+(D11×((A×S[1])+(B×S[2])+(C×S[3])))
[18]   Y←Y+((S[1]*2)×D2×(*(-T÷L2)))+((S[2]*2)×D2×(*(-(T-S[4])÷L2)))
[19]   Y←Y+((S[3]*2)×D2×(*(-(T-S[5])÷L2)))
[20]   Y←Y+(2×S[1]×S[2]×D2×(*(-T÷2×L2))×(*(-(T-S[4])÷2×L2)))
[21]   Y←Y+(2×S[1]×S[3]×D2×(*(-T÷2×L2))×(*(-(T-S[5])÷2×L2)))
[22]   Y←Y+(2×S[2]×S[3]×D2×(*(-(T-S[4])÷2×L2))×(*(-T-S[5])÷2×L2)))
[23]   Y←Y+(D31×((D×(S[1]*3))+(E×(S[2]*3))+(F×(S[3]*3))))
[24]   Y←Y+(3×(S[1]*2)×D31×(D*(2÷3))×((S[2]×(F*(1÷3)))+(S[3]×(F*(1÷3)))))
[25]   Y←Y+(3×S[1]×D31×(D*(1÷3))×(((S[2]*2)×(E*(2÷3)))+((S[3]*2)×(F*(2÷3)))))
[26]   Y←Y+(3×S[2]×S[3]×D31×(E*(1÷3))×(F*(1÷3))×((S[2]×(F*(1÷3)))+(S[3]×(F*(1÷3)))))
[27]   Y←Y+(6×S[1]×S[2]×S[3]×D31×(D*(1÷3))×(E*(1÷3))×(F*(1÷3)))
[28]   RR←(Y-R)×100÷R
[29]   P← 30 1 ρT
[30]   C← 30 1 ρY
[31]   FF← 30 1 ρRR
[32]   '*********************************************************'
[33]   '  TINT              STRAIN              ERROR'
[34]   '*********************************************************'
[35]   Z←P,C,FF
      ∇
```

T16 STEP3 14.1 9.54 13.75 10 100

□:

   3E⁻3

□:

   .48E⁻3

□:

   X16+5.78E⁻3

```
* * * * * * * * * * * * * * * * * * * * * * * * * * * * * * * * * * * * * * * * *
   TIME                STRAIN              ERROR
* * * * * * * * * * * * * * * * * * * * * * * * * * * * * * * * * * * * * * * * *
   1.025000000E2       6.914361113E⁻3       8.511630775E0
   1.050000000E2       7.018496679E⁻3       6.803139971E0
   1.100000000E2       7.173734076E⁻3       4.451573621E0
   1.150000000E2       7.297141197E⁻3       2.660962260E0
   1.200000000E2       7.404217562E⁻3       1.650433306E0
   1.250000000E2       7.500354148E⁻3       9.740730685E⁻1
   1.300000000E2       7.588263638E⁻3       6.401012956E⁻1
   1.400000000E2       7.745264948E⁻3      ⁻3.530010660E⁻2
   1.500000000E2       7.882765256E⁻3      ⁻3.191039945E⁻1
   1.600000000E2       8.004816483E⁻3      ⁻3.880477509E⁻1
   1.700000000E2       8.114008175E⁻3      ⁻3.193098847E⁻1
   1.800000000E2       8.212184309E⁻3      ⁻1.922179299E⁻1
   1.900000000E2       8.300754731E⁻3      ⁻8.720834299E⁻2
   2.000000000E2       8.380850506E⁻3       2.014648858E⁻1
   2.200000000E2       8.519228664E⁻3       5.100125549E⁻1
   2.400000000E2       8.633309058E⁻3       8.093070807E⁻1
   2.600000000E2       8.727640344E⁻3       1.154848684E0
   2.800000000E2       8.805796796E⁻3       9.376065519E⁻1
   3.000000000E2       8.870642409E⁻3       8.485949213E⁻1
   3.400000000E2       8.969264719E⁻3       4.172046486E⁻1
   3.800000000E2       9.037476993E⁻3       2.827007613E⁻1
   4.200000000E2       9.084744215E⁻3      ⁻7.080405574E⁻2
   4.600000000E2       9.117541355E⁻3      ⁻3.329541395E⁻1
   5.000000000E2       9.140321625E⁻3      ⁻6.918554457E⁻1
```